論文 / 著書情報
Article / Book Information

題目(和文)	
Title(English)	Radio Resource Management for mmWave V2V Communications
著者(和文)	殷越
Author(English)	Yue Yin
出典(和文)	学位:博士(学術), 学位授与機関:東京工業大学, 報告番号:甲第11844号, 授与年月日:2022年3月26日, 学位の種別:課程博士, 審査員:阪口 啓,廣川 二郎,TRAN GIA KHANH,西尾 理志,藤井 輝也,藤井 威生
Citation(English)	Degree:Doctor (Academic), Conferring organization: Tokyo Institute of Technology, Report number:甲第11844号, Conferred date:2022/3/26, Degree Type:Course doctor, Examiner:,,,,,
学位種別(和文)	博士論文
Type(English)	Doctoral Thesis

Doctoral Dissertation

Radio Resource Management for mmWave V2V Communications

Supervisor Professor Kei Sakaguchi

Department of Electrical and Electronic Engineering
School of Engineering
Tokyo Institute of Technology

Yue Yin

Contents

List of Figures

List of Tables

Abstract

Millimeter-wave (mmWave) vehicle-to-vehicle (V2V) communications have drawn wide attention as a critical technology to extend the restricted perception of onboard sensors and upgrade the level of vehicular safeness that requires a high data rate. However, mmWave V2V communications confront intractable scalability challenges due to the co-channel inter-link interference.

In this dissertation, efficient radio resource management solutions suitable for co-channel inter-link interference mitigation in multi-hop mmWave V2V communications are developed. To better quantify the co-channel inter-link interference, a ray-tracing channel model is created. Based on that, the features of co-channel inter-link interference and the impacts of co-channel inter-link interference on the signal-to-interference-plus-noise ratio (SINR) and end-to-end (E2E) throughput in three typical road scenarios are investigated theoretically.

In the light of the above analysis, an efficient spatial resource control method called ZigZag antenna configuration is proposed. This novel antenna configuration can significantly suppress the destructive inter-link interference in the case of reusing a single channel, and ensure an E2E throughput over 1 Gbps comparing to the conventional antenna configuration at mmWave band. The author further conducts outdoor experiments on a single straight road to demonstrate the effectiveness of ZigZag antenna configuration in practical use.

Finally, this dissertation proposes a distributed radio resource management scheme that integrates spatial, frequency, and power domains to enhance mmWave V2V communications performance. In spatial domain, ZigZag antenna configuration is utilized to mitigate the co-channel inter-link interference, which plays a decisive role for short inter-vehicle distance. In frequency and power domains, two resource blocks are allocated alternately and transmit power is controlled to suppress the co-channel inter-link interference, which have a decisive impact for long inter-vehicle distance. Simulation results reveal that the achievable E2E throughput always maintains higher than the required data rate for all vehicles in mmWave V2V relay

communications. More remarkably, this scheme works effectively in scalable mmWave V2V topology.

Acknowledgments

First and foremost, I am highly grateful to my supervisor, Prof. Kei Sakaguchi, for his invaluable advice, continuous support, and patience during my study. Besides the technical guidance, I have also learned a great deal from him, including attitude toward research, writing, and presentation, which will be the greatest asset to my career. His support gives me the opportunity and confidence to join the Tokyo Tech Academy for Super Smart Society (WISE-SSS) program. Through the WISE-SSS program, I am lucky to follow Prof. Sakaguchi to attend the collaborative research with DENSO. It is my precious experience. I also appreciate Dr. Maruta Kazuki's commitment to fast and precise feedback on my research and collaborative research problems. I would also like to thank Dr. Yu Tao for his valuable guidance throughout my studies. I am grateful to Associate Prof. Tran and emeritus Prof. Araki for their valuable advice during my seminar presentations. I would like to thank Ms. Minani and Ms. Funabashi. Their kind help and support have made my study and life in Japan a wonderful time. I would like to thank all my lab mates for a cherished time spent together in the lab and social settings. I would like to thank Mr. Haoze Chen from Rice University and Mr. Zongdian Li in our lab for their contributions to the outdoor experiment of my research. I would like to thank Mr. Amr Amrallah for his encouragement when I was confused. Finally, my appreciation also goes out to my family, boyfriend, and friends for their encouragement and support throughout my studies.

Chapter1

Introduction

In the last decade, intelligent transport system (ITS) has developed rapidly. Vehicle-to-everything (V2X) communications are an integral part of the ITS framework, which refers to particular mobile network communication exchanging data between one vehicle and the others. V2X communications include four types: vehicle-to-infrastructure (V2I), vehicle-to-pedestrian (V2P), vehicle-to-vehicle (V2V), and vehicle-to-network (V2N) communications. These V2X communications can enhance traffic efficiency, road safety and provide entertainment services. This dissertation focuses on one of the V2X communications types, which is V2V communications. This chapter overviews the mmWave V2V communications, motivates the research problem addressed in this dissertation and summarizes our contributions.

1.1 V2V Use Cases

Based on the 3rd Generation Partnership Project (3GPP) standard, the V2V use cases are divided into basic V2V use cases and enhanced V2V use cases. TR22.885 describes the basic V2V use cases, including warning applications for road safety and cooperative adaptive cruise control for road safety and traffic efficiency [2, 3]. Specifically, the warning applications include forward collision warning, control loss warning, emergency vehicle warning, emergency stop warning, queue warning, wrong way driving warning, pre-crash sensing warning; Cooperative adaptive cruise control describes the scenario that a group of vehicles controls the speed by V2V communications [2]. To support these basic V2V use cases, based on the requirements of different uses cases, European Telecommunications Standards Institute (ETSI) specified some types of messages such as periodic broadcast-based cooperative awareness mes-

V2V use case group	Latency (ms)	Reliability (%)	Required data rate (Mbps)	Communication range (m)
Vehicle platooning	10-25	90-99.99	50-65	80-350
Advanced driving	3-100	99.99-99.999	10-50	360-500
Extended Sensors	3-100	90-99.999	10-1000	50-1000

Table 1.1: QoS requirements of enhanced V2V use cases [1]

sage (CAM) [4] and event-triggered broadcast-based decentralized environmental notification message (DENM) [5]. Society of Automotive Engineers (SAE) also specified the basic safety messages (BSMs). Typically, the required data rate of basic V2V use cases is 50-300 bytes per 100 ms, latency should be lower than 100 ms, and reliability needs to be higher than 99 % [2, 3].

TR22.886 specified four enhanced V2X use case groups: vehicle platooning, advanced driving, extended sensors, and remote driving [1]. The former three groups involve V2V use cases. To support enhanced use cases, on the basis of message transmission for basic V2V use cases, larger messages containing processed sensor data (e.g., Collective Perception Messages (CPM) [6]), raw sensor data, vehicles intention data, coordination, confirmation of future maneuver, etc. are required. A summary of Quality of Service (QoS) requirements for those enhanced V2V use cases is shown in Table 1.1 based on 3GPP Release 14/15. As shown in Table 1.1, the maximum required data rate reaches 1000 Mbps, the minimum latency is 3 ms, and the highest reliability needs to be 99.999 % [1]. The requirements of these enhanced V2V use cases on data rate, latency, and reliability are much higher than basic V2V use cases.

1.2 Existing V2V Communications Standards

There are two main technologies to support the basic V2V use cases. IEEE (Institute of Electrical and Electronics Engineers) 802.11p [7] is The first V2V technology and is the basis of the Dedicated Short Range Communications (DSRC) in America, ITS-G5 in Europe, and ITS-Connect in Japan. For DSRC and ITS-G5, the operation frequency is 5.9 GHz. For ITS-Connect, the operation frequency is 760 MHz. The 3GPP standardized a competing standard under Release 14 and Release 15 based on an adaptation of Long Term Evolution (LTE) for vehicular scenarios [8, 9]. The technology is known as LTE-V2X or Cellular V2X

Features	IEEE 802.11p			Cellular communications	
	DSRC [10] America	ITS-G5 [11] Europe	ITS-Connect Japan [13]	LTE-V2X [8, 9] (PC5 interface)	NR-V2X [12] (PC5 interface)
Frequency band	5.9 GHz	5.9 GHz	760 MHz	5.9 GHz	2.5 GHz, 5.9 GHz
Bandwidth	10 MHz	10 MHz	9 MHz	10, 20 MHz	10, 20, 30, 40 MHz
Support data rate	3-27 Mbps	3-27 Mbps	$\leq$ 18 Mbps	R14:$\leq$ 31.7 Mbps R15:$\leq$ 73.5 Mbps	$\leq$ 400 Mbps
Range	15-1000 m	15-1000 m	224 m	freeway: 320 m urban: 150 m	freeway: 320 m urban: 150 m
Message type	CAM, BSM etc.	CAM, BSM etc.	CAM, BSM etc.	CAM, BSM etc.	CAM, BSM etc.
Coverage	Ubiquitous	Ubiquitous	Ubiquitous	Ubiquitous	Ubiquitous
Mobility support	High speed	High speed	High speed	High speed	High speed

Table 1.2: A summary of existing V2V standards

(C-V2X) and is based on the PC5 or sidelink LTE radio interface. The PC5 interface allows direct V2V communications without transferring the data over the cellular network. Table 1.2 summarizes important features of existing technologies. The supported data rate of IEEE 802.11p is up to 27 Mbps. The LTE-V2X and NR-V2X (FR1: 410 MHz - 7.125 GHz) target higher data rates than IEEE 802.11p but lower than 1 Gbps. The existing V2V technologies are enough for the basic V2V use cases, but they cannot support the enhanced V2V use cases like extended sensors. The new communications standards are strongly called for to satisfy the high requirements of enhanced use cases.

1.3 Characteristics of mmWave Propagation

Having large continuous spectrum resources, millimeter-wave (mmWave) becomes a promising frequency band to support ultra-high data rate V2V communications. MmWave spectrum

refers to radio frequencies in the range of 30-300 GHz (corresponding wavelength between 10 and 1 mm). In practice, those adjacent to 30 GHz bands are also recognized as mmWave, like the 28 GHz bands. Now IEEE is specifying IEEE 802.11bd to adapt to advanced V2X applications, assuring backward compatibility with IEEE 802.11p (5.9 GHz) [7] and IEEE 802.11ad (60 GHz) [14]. Its peak data rate will be higher than 6.75 Gbps. 3GPP is also specifying NR-V2X (FR2: 24.25 GHz - 52.6 GHz) [12, 15] with the peak data rate of 20 Gbps. Except for those two millimeter-wave bands, Europe has allocated 63-64 GHz band for Intelligent Transportation System (ITS) applications. 28 GHz and 39 GHz also have high possibilities for V2X communications since these two mmWave frequency bands are selected for 5G deployment in the US, South Korea, and Japan. Especially, the 28 GHz band is being deployed for 5G in Japan, so it is easily adopted into the preliminary V2V/V2X tests.

However, it is not straightforward to unlock these bands for V2V communications due to the propagation challenge of mmWave. The main challenges of mmWave include the high path loss under isotropic communication and the susceptibility to blockage.

1.3.1 Path Loss

Here, the free-space path loss is introduced. A sample scenario is considered that a signal transmitted through free space to a receiver located at a distance d from the transmitter. Assume there are no obstacles along a straight line between the transmitter and receiver. Besides, the signal is assumed to propagate along a straight line between the transmitter and the receiver. This signal is called a line-of-sight (LOS) signal. The transmitter is assumed to be an isotropic antenna; thus, the power is radiated uniformly in all directions. The free-space path loss (P_L) is defined as

$$P_{\mathrm{L}} = \frac{P_{\mathrm{t}}}{P_{\mathrm{r}}} = \frac{(4\pi d)^2}{G_{\mathrm{t}} G_{\mathrm{r}} \lambda^2}, \tag{1.1}$$

where P_{t} and P_{r} are transmit power and received power respectively, G_{t} and G_{r} are the antenna gains in LOS direction at transmitter and receiver sides respectively, $\lambda = \frac{c}{f}$ is wavelength. c is the light speed that equals to 3×10^8 m/s. f is the carrier frequency. As the operating frequency is shifted to higher mmWave frequencies, λ becomes smaller and thus path loss will increase provided that G_{t}, G_{r} and d are fixed. For example, if the carrier frequency is increased from 5.9 GHz to 60 GHz with the fixed G_{t}, G_{r} and d, the increase in path loss can be computed as

$$10\log_{10}\frac{P_{\mathrm{L}}(5.9)}{P_{\mathrm{L}}(60)} = 10\log_{10}\frac{\lambda_{60}^2}{\lambda_{5.9}^2} = 20.1 \text{ dB}. \tag{1.2}$$

In microwave systems, transmission loss is accounted for principally by the free-space loss. However, additional loss factors come into play in the millimeter-wave bands, such as gaseous losses and rain in the transmission medium. For example, the average atmospheric absorption at 60 GHz is 15 dB/km [16]. High-gain directional antennas can be deployed to compensate for the increased path loss in the case of highly accurate beam alignment.

1.3.2 Blockage

MmWave is easily blocked for two reasons. One reason is that the radius of the first-order Fresnel zone is inversely related to the frequency band. Therefore, as the frequency increases to the mmWave band, the radius of the first-order Fresnel zone will decrease. This results in the LOS signal being easily blocked by obstacles. The specific analysis is as follows. The same scenario is considered that a signal transmitted to a receiver located at a distance d from the transmitter as shown in Fig. 1.1. In this figure, r_1 is the radius of the first Fresnel zone, which is described as

$$r_1 = \sqrt{\frac{cd_1d_2}{f(d_1+d_2)}}, \tag{1.3}$$

where d_1 and d_2 are the distances from the current position to the transmitter and receiver, respectively. When $d_1 = d_2 = \frac{d}{2}$, the maximum radius $r_{1\max} = \frac{1}{2}\sqrt{\frac{cd}{f}}$ appears. As the operating frequency is shifted to higher mmWave frequencies, the radius of the first Fresnel zone will decrease if d is fixed. For instance, if the carrier frequency is increased from 5.9 GHz to 60 GHz with the fixed d, the maximum radius of the first-order Fresnel zone in the 5.9 GHz frequency band is three times that in the 60 GHz frequency band. Besides, When d changes from 1 m to 100 m, $r_{1\max}$ varies from 0.07 m to 0.7 m at 60 GHz. If the transmitter and receiver are imagined as the antennas installed on the vehicles in the mmWave V2V communications scenario, then d represents inter-vehicle distance. Suppose there is another vehicle driving between the transmitter and the receiver. In the case of short inter-vehicle distance, because the maximum cross-sectional area of the first Fresnel zone at mmWave band is far less than the cross-sectional area of a vehicle, the connection between the transmitter and the receiver is blocked off. In the case of long inter-vehicle distances, the signal may not

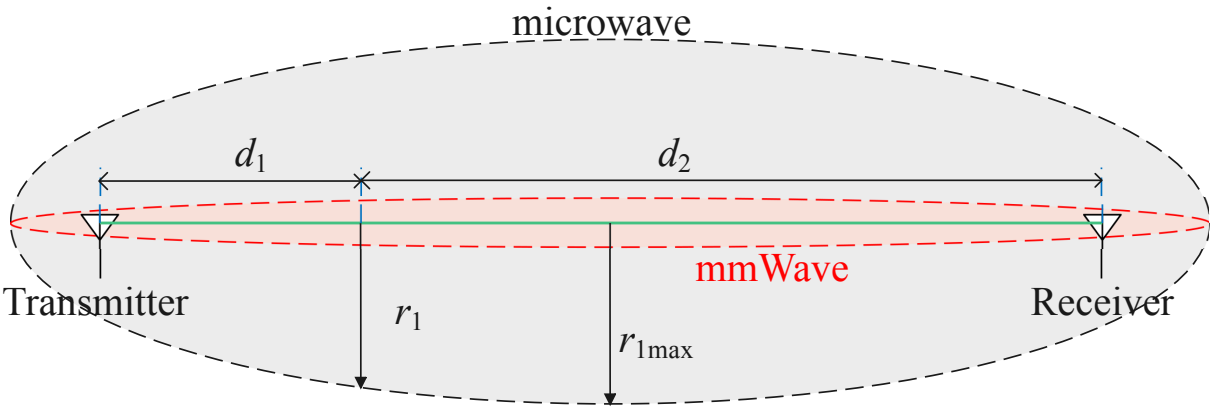

Figure 1.1: First Fresnel zone at microwave and mmWave frequency band

be blocked. However, due to the huge transmission loss in the mmWave frequency band, the connection between the transmitter and the receiver will also be unstable in this case.

The second reason for the easy blockage of mmWave frequency bands come from its distinguishing features involving poor diffraction capability and high penetration loss. For example, the average measurement diffraction loss of the outdoor marble corner is as much as 50 dB [17]. The outdoor penetration losses of tinted glass and brick at 28 GHz are 40.1 and 28 dB, respectively [18]. The human blockage at 73 GHz in an indoor environment is 30-40 dB [19].

For the preceding reasons, the mmWave frequency band has a severe blockage problem.

1.4 Challenges of mmWave V2V Communications

In mmWave V2V communications scenarios, the high-gain directional antennas can be used to compensate for significant path loss. Multi-hop relay topology is supposed to be deployed to cope with the problem of blockage. However, these kinds of solutions also introduce numerous additional challenges such as antenna placement, co-channel interference control, beam alignment, and scalability, as shown in Fig. 1.2.

Although a rooftop position for vehicle antennas was observed to provide the optimal coverage [20], and most simulations and measurements for V2V communications adopt the rooftop position [21,22], the direct co-channel interference caused by other links bring a strong negative effect, and thus how to select an optimal antenna position to balance the coverage and co-channel interference is one of the essential issues for V2V communications.

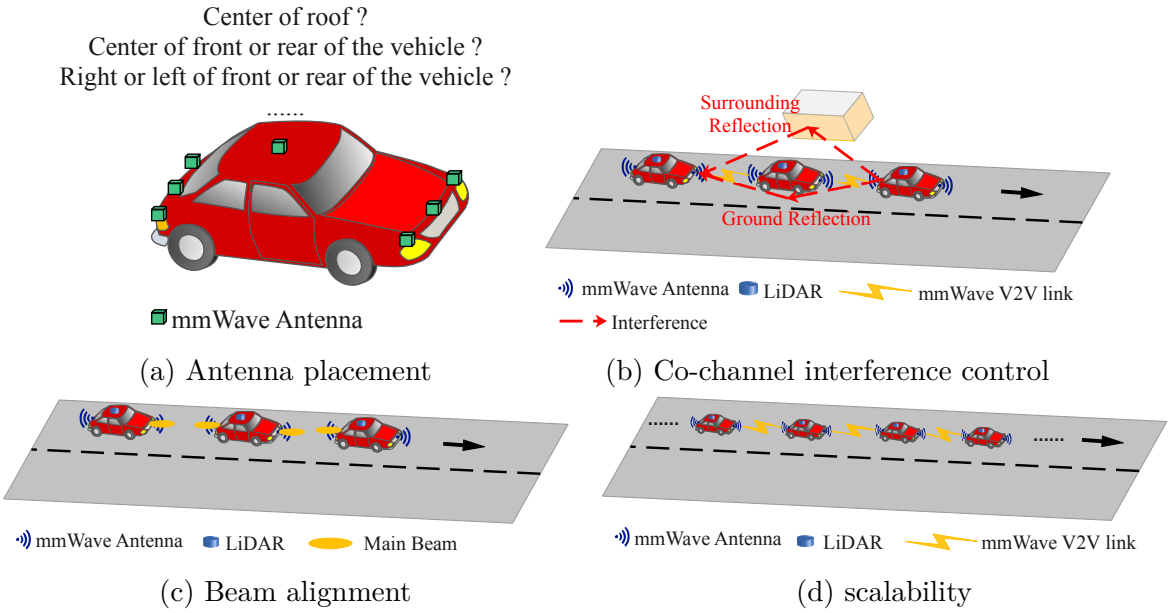

(a) Antenna placement (b) Co-channel interference control

(c) Beam alignment (d) scalability

Figure 1.2: Challenges of mmWave V2V communications

In the multi-hop relay scenario as shown in Fig. 1.2 (b), the interference including direct and reflected interference occur when the bandwidth is reused for multiple V2V links. To satisfy the high requirements of enhanced V2V use cases such as extended sensors, mitigating this co-channel interference in the scenario of mmWave V2V relays by radio resource management is also a vital issue.

To compensate for the high path loss at mmWave band, high gain directional antennas are employed in mmWave V2V communications systems. However, the narrow antenna main beam and motor-caused fluctuation require high accuracy of beam alignment. On the other hand, high-speed vehicular mobility requires the fast reaction of beam alignment. Therefore, improving the accuracy and efficiency of beam alignment is a critical challenge for mmWave V2V communications.

In practice, most road scenarios contain more than two vehicles, so multiple mmWave V2V links are usually established at the same time, as shown in Fig. 1.2 (d). An efficient radio resource management scheme to ensure the high quality of all V2V links in a scalable mmWave V2V topology is strongly called for.

Many researchers and groups are devoted to these four typical challenges, and the related works are classified as shown in Table 1.3.

Two central problems have been summarized through these related works. One of the

Challenge	Reference	Contribution
Antenna placement	[23]	Investigated the effect of antenna positions on a vehicle on path loss at 28 GHz by measurement
	[21]	Built an outdoor testbed using WiGig devices (60 GHz, located at rooftop) to measure inter-vehicle connectivity with different permitted vehicle speeds
Interference control	[24]	Analyzed the impact of interference from side lanes
Beam alignment	[25, 26]	25% performance gain in reliability and delay for ultra-dense vehicular scenarios (straight road, junction)
	[27]	Developed a vehicular-position-based overhead-free beam alignment scheme (throughput $>$ 1 Gbps)
	[28]	Optimized beamwidth by considering the number of disconnected links and probability of misalignment
	[29]	Proposed sensor aided beam tracking; latency is low due to without frequent realignment
Scalability	[30]	Proposed mmWave based sensor data broadcasting; 30% decrease in broadcasting delay compared with FIFO scheme
	[31]	Selected a relay node by random beamforming; increase E2E throughput, reduce the delay and mitigate direct interference

Table 1.3: Related works of mmWave V2V communications

problems is related to co-channel interference. On the one hand, co-channel interference is not comprehensively analyzed in two aspects: considered co-channel interference types and road scenarios. When multiple V2V links reuse the same bandwidth, interference will occur. Some related works assumed that the co-channel interference is small and negligible, or only the direct co-channel interference link is considered. The co-channel interference caused by ground reflection and surrounding reflection lacks for evaluation. The scenarios in these related works are mainly straight roads and junctions. Nevertheless, the channel characteristics of mmWave V2V fluctuate dramatically according to the environments where vehicles are driving. It is necessary to analyze the channel model of mmWave V2V relay communications in the typical

road scenarios and compare their channel characteristics. On the other hand, no efficient method of co-channel interference control has been proposed. Therefore, it is necessary to analyze co-channel interference comprehensively and design an effective method to mitigate such interference.

Another problem is the scalability of mmWave V2V communications. Most approaches focus on one V2V link or multiple pairing connections instead of a multi-hop relay scenario. For example, the approaches for beam alignment mainly considered a mmWave V2V link [26, 25]. However, they are not scalable enough to adapt to more complex V2V topology. It becomes one of the critical issues to design scalable radio resource management for mmWave V2V communications with relays.

In addition to the above problems, a dynamic V2V topology formed by high mobility vehicles requires a fast resource management mechanism. Resource management mechanisms can be divided into two types: centralized and distributed radio resource controls. The centralized one is more reliable. For instance, Mei *et al.* and Ashraf *et al.* proposed the centralized resource allocation schemes for Long Term Evolution V2V (LTE-V2V) communications systems to guarantee reliability requirement [32, 33]. Gao *et al.* targeted the energy efficiency and proposed a centralized power control and resource allocation for V2V communications [34]. However, these centralized radio resource management schemes have high control latency, high uplink transmission overhead, and cannot work out of coverage of the central node. By contrast, distributed radio resource control can reduce the control latency and work even out of coverage. Existing distributed schemes mainly adopt IEEE 802.11p for the access layer, which cannot support services that require data rate over 1 Gbps [35, 36]. Crucially, the collision of resource utilization becomes inevitable as the traditional carrier sense multiple access with collision avoidance (CSMA/CA) strategy suffers from its low efficiency. Therefore, it is essential to design better distributed radio resource management in dynamic vehicular scenarios to reduce the control latency and avoid the collision of resource utilization.

1.5 Summary of Contributions

This dissertation develops new radio resource management schemes for scalable mmWave V2V relays systems by coping with the mentioned three problems: (1) co-channel inter-link interference; (2) scalability of mmWave V2V communications; (3) efficient radio resource management mechanism. While the main focus is on overtaking traffic situations, some ideas are

also applicable for other traffic situations like safe driving at crossroads. We start by creating the ray-tracing based channel model and evaluating the impact of co-channel interference in typical road scenarios. The co-channel interference include direct co-channel interference, co-channel interference caused by ground reflection, and co-channel interference caused by surrounding reflection. This lays the foundation for designing radio resource management schemes to mitigate co-channel interference and support scalable mmWave V2V topology. We then develop a new spatial resource control method called ZigZag antenna configuration to mitigate this interference and maintain an over 1 Gbps throughput for mmWave V2V with relay. Furthermore, outdoor experiments demonstrate the effectiveness of a novel ZigZag antenna configuration on a single straight road. In addition to the radio resource management in the spatial domain, we also develop a distributed radio resource management scheme that integrates spatial, frequency, and power domains, for two transmission ranges (short/long). ZigZag antenna configuration is utilized to mitigate the co-channel interference in the spatial domain, which plays a decisive role in the short inter-vehicle distance. In frequency and power domains, two resource blocks are allocated alternately, and transmit power is controlled to suppress the co-channel interference, which has a decisive impact on co-channel interference mitigation for the long inter-vehicle distance. Simulation results reveal that the achievable end-to-end throughput maintains consistently higher than the required data rate for all vehicles. Most importantly, it works effectively in scalable mmWave V2V topology.

It is noted that the definition of scalability in this study is one-dimensional. The scalability means that for all vehicles in a single-lane two-sides scenario, the E2E throughput is always higher than the required data rate in multi-hop relay systems. The propagation direction of the signal is opposite to the driving direction of the vehicles. We summarize our contributions as follows:

- Chapter 2: Impact of co-channel interference for mmWave V2V relay communications

    1. Introduce basic and general mmWave V2V relay scenarios on the basis of scenario complexity; Introduce single straight road, horizontal curve, and slope on the basis of road scenarios.

    2. Establish ray-tracing channel models of mmWave V2V communications in three typical road scenarios and summarize the characteristics of these typical road scenarios; Evaluate co-channel interference in different scenarios and point out the features of co-channel interference in basic mmWave V2V relay communications.

The impact of antenna heights on co-channel interference mitigation, SINR and throughput is analyzed, and an optimal antenna height is found.

  * This work is published in
    - Y. Yin, H. Chen, Z. Li, T. Yu and K. Sakaguchi. "ZigZag Antenna Configuration for MmWave V2V with Relay in Typical Road Scenarios: Design, Analysis and Experiment," *IEICE Transactions on Communications*, 2021, Volume E104.B, Issue 10, Pages 1307-1317.

- Chapter 3: ZigZag antenna configuration for basic mmWave V2V relay communications

  1. Mitigate co-channel interference by ZigZag antenna configuration for basic mmWave V2V relay communications. The features of the ZigZag antenna configuration are described and then the principle of co-channel interference mitigation with this novel antenna configuration is explained. Next, we compare the performance of the proposed method with that of conventional antenna configuration by the simulation based on standard IEEE 802.11ad and show the superiority of the proposed method on co-channel interference mitigation and E2E throughput improvement.
  2. Implement an outdoor experiment that verifies the effectiveness of ZigZag antenna configuration. The worst interference case, i.e., three vehicles driving in a single straight road with equal inter-vehicle distance, is selected as an experimental scenario. The throughputs are measured in field trials and are consistent with the simulation results.

  * These works are published in
    - Y. Yin, H. Chen, Z. Li, R. Fukatsu, T. Yu and K. Sakaguchi, "Design of Antenna Configuration for Interference Control in MmWave V2V Communication Systems." *2020 IEEE 92nd Vehicular Technology Conference (VTC2020-Fall)*, 2020, pp. 1-5, doi: 10.1109/VTC2020-Fall49728.2020.9348872.
    - Y. Yin, H. Chen, Z. Li, T. Yu and K. Sakaguchi. "ZigZag Antenna Configuration for MmWave V2V with Relay in Typical Road Scenarios: Design, Analysis and Experiment," *IEICE Transactions on Communications*, 2021, Volume E104.B, Issue 10, Pages 1307-1317.

- Chapter 4: Distributed radio resource management scheme for scalable mmWave V2V topology

1. The required data rate considering driving safety is analyzed in mmWave V2V communications with multiple relays at different inter-vehicle distances and vehicle speeds in an overtaking traffic situation, which is the basis for radio resource management.

2. A distributed radio resource management scheme is proposed to ensure scalability for mmWave V2V relaying topology. First, ZigZag antenna configuration is employed in the spatial domain to mitigate the inter-link co-channel interference impact caused by the reuse of resource blocks (RBs). Further, in frequency and power domains, two transmission modes (Mode 1 and Mode 2) are defined according to the inter-vehicle distance and are switched based on the required data rate for each V2V link. The full available bandwidth is divided into two RBs, called $\{RB_1, RB_2\}$ respectively. In mode 1, all bandwidth is used for the current V2V link. In mode 2, one of RB_1 and RB_2 is selected for the current V2V link. If continuous V2V links are in the same mode, RB_1 and RB_2 are alternately allocated for each V2V link in a ZigZag manner.

* The contribution of this chapter is presented in

  - Y. Yin, T. Yu and K. Sakaguchi, "Required-Data-Rate-Based Distributed Resource Allocation Scheme for MmWave V2V with Relay," *IEEE CCNC*, Jan, 2022.
  - Y. Yin, T. Yu, K. Maruta, K. Sakaguchi. "Distributed and Scalable Radio Resource Management for mmWave V2V Relays towards Safe Automated Driving," *Sensors* 22.1 (2022): 93.
  - Y. Yin, T. Yu, K. Maruta, K. Sakaguchi, "Distributed and Scalable Radio Resource Management for mmWave V2V Relays towards Safe Automated Driving," *IEICE Mobile Communication Research Workshop*, Mar. 2022.

1.6 Organization

The rest of the dissertation is organized as follows, as shown in Fig. 1.3. We describe the channel model of mmWave V2V relay communications and evaluate the features of co-channel interference in Chapter 2. We develop a ZigZag antenna configuration method that leverages spatial resource control to reduce the co-channel interference in Chapter 3. Chapter 4 proposes

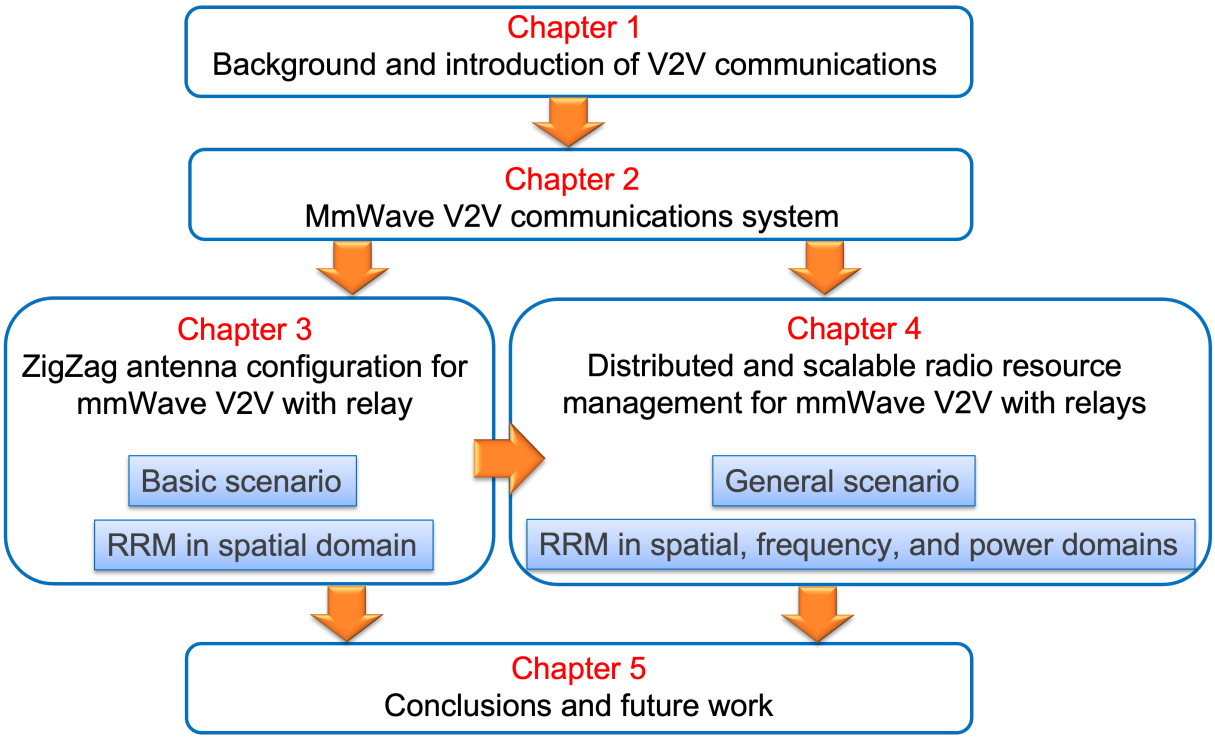

Figure 1.3: Organization of dissertation

a distributed radio resource management scheme that integrates spatial, frequency, and power domains for two transmission ranges (short/long). Finally, we conclude the dissertation and describe some potential future research venues in Chapter 5.

Chapter2

mmWave V2V Communications System

This chapter introduces basic and general mmWave V2V relay scenarios based on scenario complexity; introduce single straight road, horizontal curve, and slope based on different road scenarios. Then, the ray-tracing channel models of mmWave V2V communications in three typical road scenarios are established. The characteristics of these typical road scenarios are summarized. Finally, co-channel interference in different scenarios is evaluated by simulation. It is shown that ground reflection is the main interference compared with direct interference and the interference caused by surrounding reflection in all scenarios under conventional antenna configuration. Besides, the received powers of ground reflection in all road scenarios are strongest in the case of equal inter-vehicle distance.

2.1 Scenario Introduction

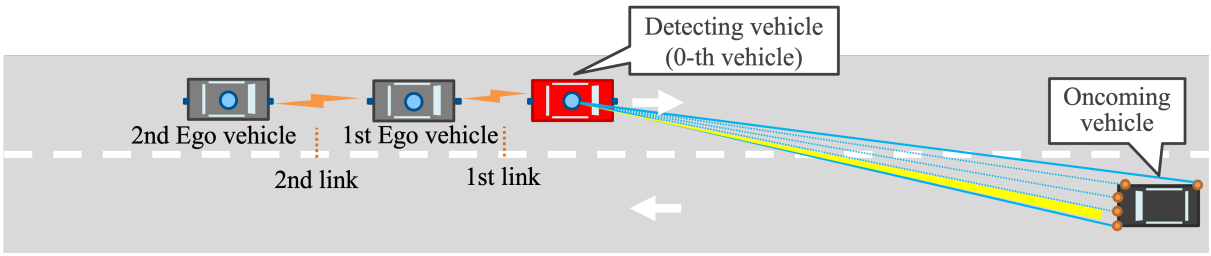

Figure 2.1: Basic scenario of mmWave V2V communications with relay

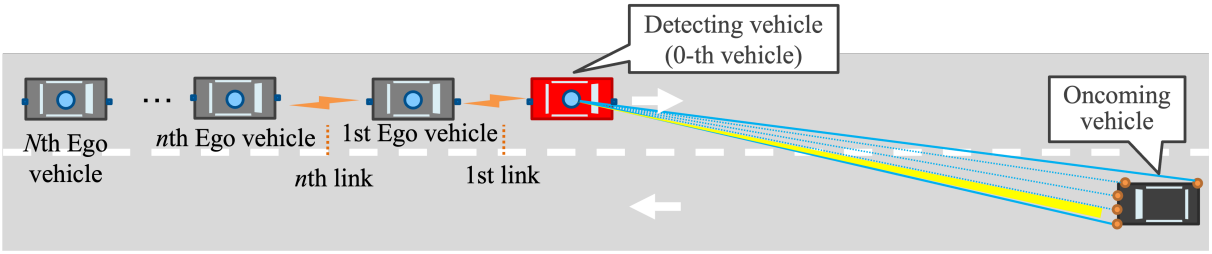

Figure 2.2: General scenario of mmWave V2V communications with relays

2.1.1 Basic and General mmWave V2V Relays Scenarios

To evaluate the impact of co-channel interference in the mmWave V2V relay topology, the general scenario is simplified to the most basic scenario where only one V2V link suffers from co-channel inter-link interference. This scenario is called the basic scenario as shown in Fig. 2.1. This dissertation considers the overtaking traffic situation in a straight two-lane road with width w_{lane}. Vehicles equipped with a light detection and ranging (LiDAR) are running in the middle of their lanes. Let the 0-th vehicle be the Detecting vehicle, and the following two Ego vehicles are trying to achieve safe overtaking by avoiding collision with the Oncoming vehicle. Since the perception of each Ego vehicle is blocked by its front vehicles, the Ego vehicle requests the LiDAR data on the Detecting vehicle to perform cooperative perception. The rate of exchanging raw sensor data for safe overtaking is defined as the required data rate. During the information transmission, the 1st and the 2nd V2V links are established at the same time in the basic scenario. If the 1st and the 2nd V2V links use the same bandwidth, the 2nd V2V link will suffer from interference from the 1st V2V link. Because the first V2V link cannot suffer from strong interference from the front, it is regarded as a particular case. The co-channel interference, including direct and reflected interference, are analyzed in the basic scenario to prepare for analyzing co-channel interference effects in more complex general mmWave V2V topology scenarios.

In practical traffic scenarios, there are usually multiple vehicles on the road. The scenario where multiple mmWave V2V links are connected at the same time has a high probability. To make our proposed methods more applicable to actual scenarios, a multi-vehicle multi-link scenario is also considered, called the general scenario as shown in Fig. 2.2. In this figure, there are N Ego vehicles. The difference from the basic scenario is that if the V2V links before the nth V2V link reuse the same bandwidth with that of the nth link, the nth link will suffer interference from all links in front of it.

2.1.2 Three Typical Road Scenarios

The channel modeling of mmWave V2V communications varies in road scenarios. Most studies focus on a single mmWave V2V link on the single straight road scenario to the author's knowledge. Kato *et al.* analyzed the propagation characteristics of 60-GHz mmWave in inter-vehicle communications for Intelligent Transport Systems on a single straight road [37], and Fukatsu *et al.* described a fundamental cooperative perception also on a single straight road [38]. Cristina Perfecto *et al.* proposed a distributed association and beam alignment framework for mmWave V2V on a two-lane straight road [25], and they also extended their framework on an urban junction. Vitaly Petrov *et al.* analyzed the interference of mmWave/THz band V2V communications systems on a three-lane straight road [24]. Tomotaka Wada *et al.* analyzed the mmWave channel model on horizontal curve road scenario [39]. However, these studies only focus on a single mmWave V2V link. In reality, the situation of multiple mmWave V2V links established simultaneously is more common because most road scenarios will contain more than two vehicles. In addition, the channel characteristics of mmWave V2V fluctuate dramatically according to the environments where vehicles are driving. It is necessary to summarize typical road scenarios and analyze the channel models of mmWave V2V communications with relay in these typical road scenarios and compare their channel characteristics. This subsection will introduce three typical road scenarios: straight road, horizontal curve, and slope. Their channel characteristics will be analyzed in Sect. 2.3.

Safe and reasonable roadway horizontal curves should be designed based on an appropriate relationship between design speed and curvature and their collaborative relationships with superelevation and side friction. The minimum horizontal curve radius is given by

$$R_{\min} = \frac{v_{\text{limit}}^2}{g(e + f_s)}, \tag{2.1}$$

where v_{limit} is the road speed limit, g is the gravitational acceleration (9.8 m/s^2). e is the superelevation. For example, in areas where ice and snow are expected, a superelevation rate of 8% seems to be a conservative maximum value. In areas that are not plagued by ice and snow, a maximum superelevation rate of 10-12% seems to be a practical limit. Both modern construction techniques and driver comfort limit the maximum superelevation rate to 12% [40]. f_s is the side-friction factor that depends on v_{limit}. For instance, some comfortable side-friction factors are tabulated in Table 2.1 [40]. This study sets the parameters of the horizontal curve based on these theories.

For the slope scenario, the maximum grades for freeways depend on the road speed limit

v_{limit} (km/h)	f_s
40	0.21
50	0.18
55-80	0.15
>110	<0.1

Table 2.1: Comfortable side-friction factors for the road speed limit

and terrain type. Based on the American Association of State Highway and Transportation Officials (AASHTO) specified geometric design of highways and streets, if the road speed limit is 80 km/h, the maximum grade is 4% [41].

2.2 Propagation Models and Assumptions

In a typical outdoor environment, a radio signal transmitted from a fixed source will encounter multiple objects in the environment, and these objects produce reflected, diffracted, or scattered copies of the transmitted signal. The most general ray-tracing model includes all attenuated, diffracted, and scattered multipath components. It uses geometrical optics to trace the propagation of the LOS and reflected signal components and signal components from object diffraction and diffuse scattering. However, in general, the LOS and reflected paths provide the dominant components of the received signal since diffraction and scattering losses are high. Theoretically, an infinite number of rays can be reflected off the building fronts to arrive at the receiver in an outdoor road scenario; in addition, rays may also be back-reflected from buildings behind the transmitter or receiver. However, since signal energy is dissipated with each reflection, signal paths corresponding to more than two or three reflections can generally be ignored. When the street layout is relatively straight, back reflections are usually negligible also. The multi-ray model incorporates the LOS path and all first-order reflection paths: specifically, there are the ground-reflected and the surrounding reflected. In the ray-tracing channel model, we assume a finite number of reflectors with known location and dielectric properties.

Based on the above analysis, a multi-ray reflection channel model of mmWave V2V communications with relay in the basic scenario is analyzed under three typical road scenarios to evaluate the impact of reflected interference shown in Fig.2.3. In these figures, d_{EF}^{1} and

d^2_{EF} are the straight line distance between the first/second Ego vehicle and its front vehicle, respectively. d_l is the distance of the obstacles (buildings, vehicles on the side lane, etc.) to

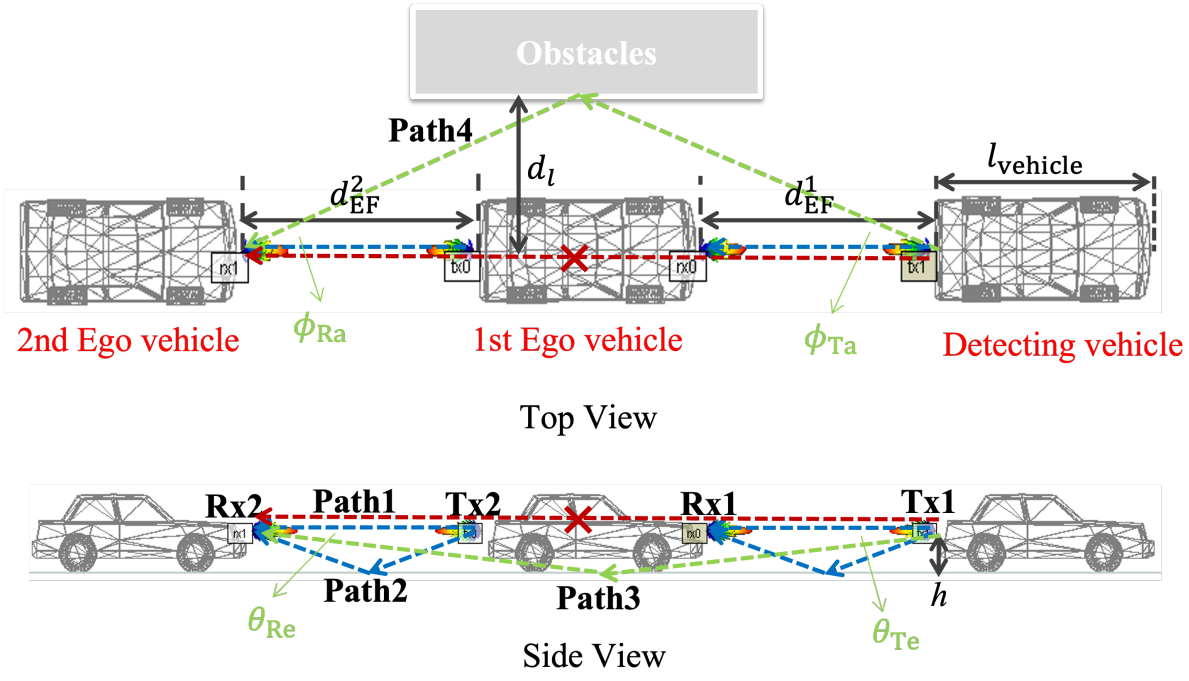

(a) Single straight road

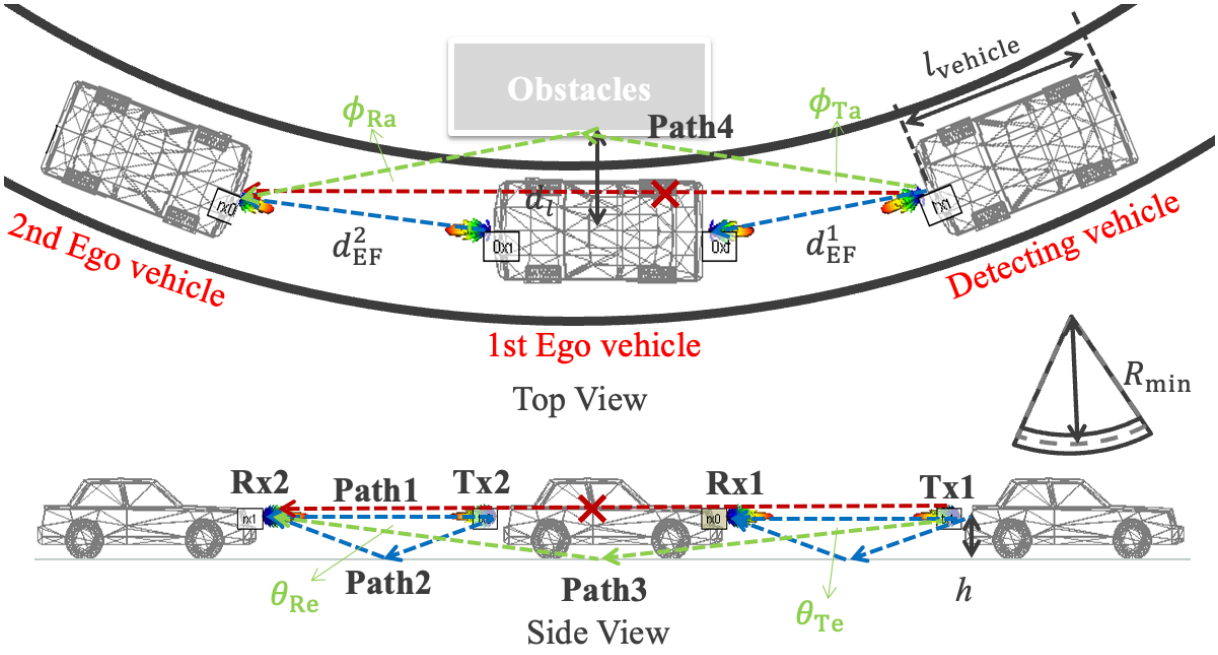

(b) Horizontal curve

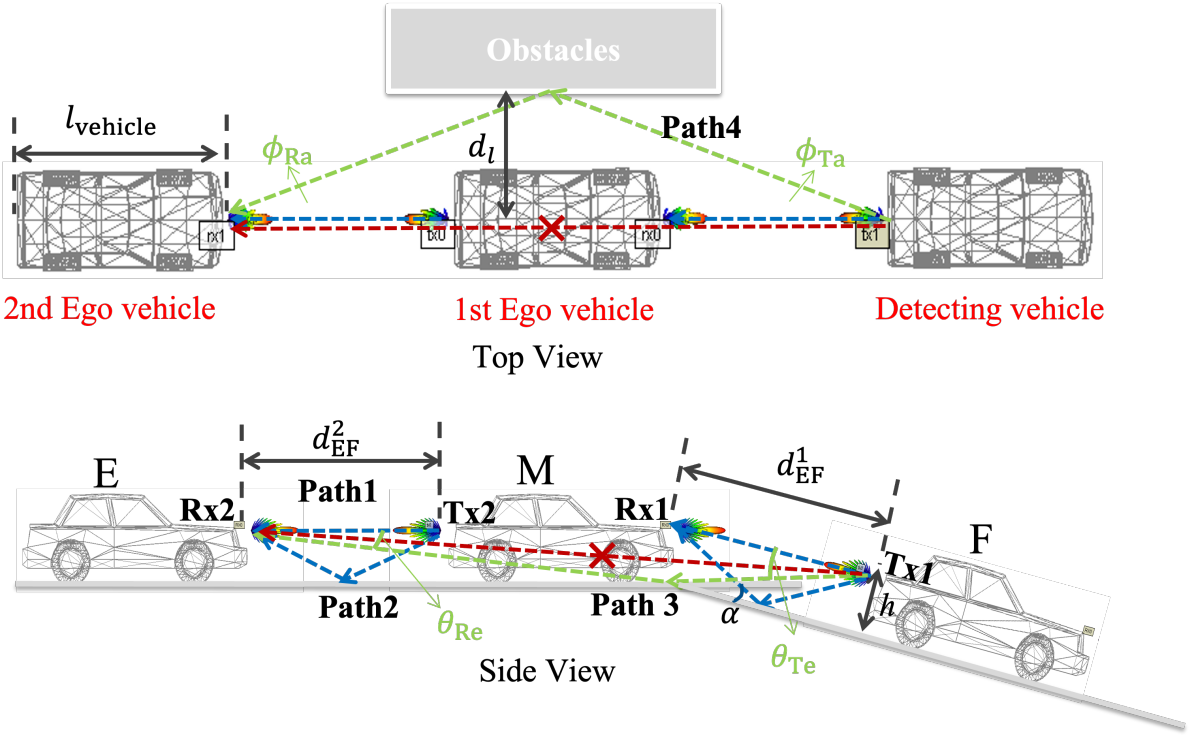

(c) Slope

Figure 2.3: Channel model of mmWave V2V communications with relay in typical road scenarios

the horizontal center-line of the first Ego vehicle. In Fig. 2.3 (b), $R_{\min}$ is minimum horizontal curve radius which is the function of the road speed limit, superelevation, and side-friction factor based on Eq. (2.1). In Fig. 2.3 (c), α is the maximum grade of slope road scenario which is a function of vehicle speed and terrain types. Antennas are located at the center of front and rear of the vehicles, and this antenna configuration is regarded as the conventional antenna configuration in this study. Path 1 and Path 2 (blue lines) are the desired signal paths, Path 3 and Path 4 (green lines) are the paths of the ground and surrounding reflections. Red lines are the direct interference link. Under the conventional antenna configuration, the first Ego vehicle blocked the direct interference links due to the first Fresnel zone in each road scenario.

Before describing the multipath propagation channel model of mmWave V2V communications, some assumptions need to be explained. Firstly, the first-order ground reflection and first-order surrounding reflection are included in calculating the co-channel interference for

mmWave V2V communications because the second-and higher-order reflections do not provide any noticeable impact on the received power [42]. Secondly, all antennas are assumed to be arranged at the same height (h) with the same specs. Thirdly, vertical polarization antennas are adopted in the vertical plane because the vertical polarization is more suitable than horizontal polarization to avoid the interference caused by ground reflection [37].

Therefore, the received desired signal of the second link in Fig. 2.3 based on this ray-tracing model is

$$s(t) = \mathrm{Re}\left\{ \frac{c}{4\pi f} \sqrt{\frac{P_{\mathrm{Tx2}} G_{\mathrm{t}} G_{\mathrm{r}}}{L(d_{\mathrm{path1}})}} \left[\frac{D_1 u(t) e^{\frac{-j2\pi d_{\mathrm{path1}}}{\lambda}}}{d_{\mathrm{path1}}} + \frac{D_2 u(t-\tau) e^{\frac{-j2\pi d_{\mathrm{path2}}}{\lambda}}}{d_{\mathrm{path2}}} \right] e^{j2\pi f t} \right\}, \tag{2.2}$$

where P_{Tx2} is the transmit power of Tx2, G_{t} and G_{r} are the peak antenna gains of transmitter and receiver, $d_{\mathrm{path}k}$ is the length of path k. $L(d_{\mathrm{path}k})$ is the absorption loss and it depends on the length of path and frequency (e.g. 15 dB/km loss by oxygen at 60 GHz [43]). Since $10\log 10(|L\left(d_{\mathrm{path2}}\right) - L\left(d_{\mathrm{path1}}\right)|) < 0.002$ dB, we assume $L\left(d_{\mathrm{path2}}\right) \approx L\left(d_{\mathrm{path1}}\right)$. $\tau = (d_{\mathrm{path2-d_{path1}}})/\mathrm{c}$ is the time delay of ground reflection relative to the LOS path. Ψ_{g} is the reflection coefficient of ground. D_k denotes the coefficients of antenna directivity. The delay spread of the two-ray model equals the delay between the LoS path and the ground reflected path. If the transmitted signal is narrowband relative to the delay spread ($\tau \ll B^{-1}$) then $u(t) \approx u(t-\tau)$. With this approximation, the received power of the desired signal is given by

$$P_{\mathrm{r}} = \frac{P_{\mathrm{Tx2}} G_{\mathrm{t}} G_{\mathrm{r}}}{L(d_{\mathrm{path1}})} \left| D_1(\frac{c}{4\pi f d_{\mathrm{path1}}}) + D_2(\frac{c}{4\pi f d_{\mathrm{path2}}}) \Psi_{\mathrm{g}} e^{-j\frac{2\pi f}{c}(d_{\mathrm{path2}} - d_{\mathrm{path1}}) + \Phi} \right|^2, \tag{2.3}$$

where Φ is the phase rotation angle of ground reflection assumed as π.

Ψ_{g} is the reflection coefficient of ground which depends on the incident angle, polarization and dielectric constant of the ground. The reflected coefficient is expressed as

$$\Psi_{\mathrm{V}} = \frac{\psi^2 \cos\theta_{\mathrm{in}} - \sqrt{\psi^2 - \sin^2\theta_{\mathrm{in}}}}{\psi^2 \cos\theta_{\mathrm{in}} + \sqrt{\psi^2 - \sin^2\theta_{\mathrm{in}}}}, \quad \text{(Vertical polarization)} \tag{2.4}$$

or

$$\Psi_{\mathrm{H}} = \frac{\cos\theta_{\mathrm{in}} - \sqrt{\psi^2 - \sin^2\theta_{\mathrm{in}}}}{\cos\theta_{\mathrm{in}} + \sqrt{\psi^2 - \sin^2\theta_{\mathrm{in}}}}, \quad \text{(Horizontal polarization)} \tag{2.5}$$

where ψ is the dielectric constant of materials and θ_{in} is the incident angle of the reflected path. If the vertical polarization of an antenna is adopted in the vertical plane, Ψ_{g} is derived by Eq. (2.4). For the general case of a wave with arbitrary polarization, it is common

practice to decompose the incident wave into a horizontally polarized component and a vertically polarized component. After determining the reflected waves corresponding to the two incident components, the reflected waves are summed up to represent the total reflected wave that the original incident wave bears on. We consider reflection at the boundary of air and grounds/walls for oblique incidence. The discussion will lead to three well-known optical laws: Snell's law, the law of reflection, and Brewster's law governing polarization by reflection. Therefore, the reflection coefficient is given by

$$\Psi = a_{\mathrm{V}}\Psi_{\mathrm{V}} + a_{\mathrm{H}}\Psi_{\mathrm{H}}, \tag{2.6}$$

where a_{V} and a_{H} are the coefficients of horizontal and vertical components generated through wave decomposition.

D_k that denotes the coefficients of antenna directivity for path k is written by

$$D_k = D_{\mathrm{R}}^k(\theta_{3\mathrm{dB}}, \theta_{\mathrm{e}}, \theta_0, \phi_{3\mathrm{dB}}, \phi_{\mathrm{a}}, \phi_0) \cdot D_{\mathrm{T}}^k(\theta_{3\mathrm{dB}}, \theta_{\mathrm{e}}, \theta_0, \phi_{3\mathrm{dB}}, \phi_{\mathrm{a}}, \phi_0), \tag{2.7}$$

where $D_{\mathrm{R}}^k(\theta_{3\mathrm{dB}}, \theta_{\mathrm{e}}, \theta_0, \phi_{3\mathrm{dB}}, \phi_{\mathrm{a}}, \phi_0)$ and $D_{\mathrm{T}}^k(\theta_{3\mathrm{dB}}, \theta_{\mathrm{e}}, \theta_0, \phi_{3\mathrm{dB}}, \phi_{\mathrm{a}}, \phi_0)$ represent the antenna directivity of path k at the receiver and transmitter side respectively and are modeled in this study as

$$D(\theta_{3\mathrm{dB}}, \theta_{\mathrm{e}}, \theta_0, \phi_{3\mathrm{dB}}, \phi_{\mathrm{a}}, \phi_0) = \left| \frac{\sin(\frac{50.6\pi}{\theta_{3\mathrm{dB}}} \sin(\theta_{\mathrm{e}} - \theta_0))}{\frac{50.6\pi}{\theta_{3\mathrm{dB}}} \sin(\theta_{\mathrm{e}} - \theta_0)} \right| \cdot \left| \frac{\sin(\frac{50.6\pi}{\phi_{3\mathrm{dB}}} \sin(\phi_{\mathrm{a}} - \phi_0)}{\frac{50.6\pi}{\phi_{3\mathrm{dB}}} \sin(\phi_{\mathrm{a}} - \phi_0)} \right|, \tag{2.8}$$

where $\theta_{3\mathrm{dB}}$ and $\phi_{3\mathrm{dB}}$ are the half power beam angle in the elevation and azimuth direction respectively, θ_0 and ϕ_0 are the elevation and azimuth angle of main beam, θ_{e} and ϕ_{a} are the elevation and azimuth angle of propagation path.

Based on the model above, the received power of co-channel interference caused by ground and surrounding reflections can also be expressed as

$$\begin{aligned} I = & \frac{P_{\mathrm{Tx1}} G_{\mathrm{t}} G_{\mathrm{r}}}{L(d_{\mathrm{path3}})} \Bigg| D_3(\frac{c}{4\pi f d_{\mathrm{path3}}}) \Psi_g e^{-j\frac{2\pi f}{c}(d_{\mathrm{path3}} - d_{\mathrm{path1}}) + \Phi} \\ & + D_4(\frac{c}{4\pi f d_{\mathrm{path4}}}) \Psi_s e^{-j\frac{2\pi f}{c}(d_{\mathrm{path4}} - d_{\mathrm{path1}}) + \Phi} \Bigg|^2, \end{aligned} \tag{2.9}$$

where P_{Tx1} is the transmit power of Tx1 and Ψ_s is the reflection coefficient of surrounding reflected paths. $L\left(d_{\mathrm{path3}}\right) \approx L\left(d_{\mathrm{path4}}\right)$.

When antennas are located at the roof of the vehicle, the direct interference link cannot be blocked by the first Ego vehicle in Fig. 2.3. However, the interference links caused by

ground reflection are almost blocked by the first Ego vehicle. Therefore, the received power of co-channel interference is expressed as

$$\begin{aligned} I =& \frac{P_{\mathrm{Tx1}} G_{\mathrm{t}} G_{\mathrm{r}}}{L(d_{\mathrm{path3}})} \Bigg| D_3 \left(\frac{c}{4\pi f d_{\mathrm{path3}}}\right) e^{-j\frac{2\pi f}{c}(d_{\mathrm{path3}} - d_{\mathrm{path1}}) + \Phi} \\ & + D_4 \left(\frac{c}{4\pi f d_{\mathrm{path4}}}\right) \Psi_s e^{-j\frac{2\pi f}{c}(d_{\mathrm{path4}} - d_{\mathrm{path1}}) + \Phi} \Bigg|^2, \end{aligned} \tag{2.10}$$

where d_{path3} is LOS from Tx1 to Rx2.

Until now, co-channel interference can be deduced in the basic scenario. Based on such derivation of co-channel interference in the basic scenario, the co-channel interference suffered by each V2V link can be analyzed in the general scenario. Firstly, the received power of nth V2V link P_{r}^n is given by

$$P_{\mathrm{r}}^n = \frac{P_{\mathrm{Tx}n} G_{\mathrm{t}} G_{\mathrm{r}}}{L(d_{\mathrm{path1}}^n)} \left| D_1^n \left(\frac{c}{4\pi f d_{\mathrm{path1}}^n}\right) + D_2^n \left(\frac{c}{4\pi f d_{\mathrm{path2}}^n}\right) \Psi_{\mathrm{g}}^n e^{-j\frac{2\pi f}{c}(d_{\mathrm{path2}}^n - d_{\mathrm{path1}}^n) + \Phi} \right|^2, \tag{2.11}$$

where $P_{\mathrm{Tx}n}$ is the transmit power of Tx n, $d_{\mathrm{path}k}^n$ is the length of path k for the n-th V2V link, D_k^n is the coefficients of antenna directivity of path k for the n-th V2V link, Ψ_{g}^n is the reflection coefficient of ground for the n-th V2V link.

It is assumed that all mmWave V2V links reuse the same channel. The co-channel interference of the n-th V2V link is calculated by

$$\begin{aligned} I_n =& \sum_{l=1}^{n-1} \frac{P_{\mathrm{Tx}l} G_{\mathrm{t}} G_{\mathrm{r}}}{L(d_{\mathrm{path3}}^l)} \Bigg| D_3^l \left(\frac{c}{4\pi f d_{\mathrm{path3}}^l}\right) \Psi_g^l e^{-j\frac{2\pi f}{c}(d_{\mathrm{path3}}^l - d_{\mathrm{path1}}^n) + \Phi} \\ & + D_4^l \left(\frac{c}{4\pi f d_{\mathrm{path4}}^l}\right) \Psi_s^l e^{-j\frac{2\pi f}{c}(d_{\mathrm{path4}}^l - d_{\mathrm{path1}}^n) + \Phi} \Bigg|^2. \end{aligned} \tag{2.12}$$

If antennas are located at roof of the vehicle, the co-channel interference of nth V2V link is given by

$$\begin{aligned} I_n =& \sum_{l=1}^{n-1} \frac{P_{\mathrm{Tx}l} G_{\mathrm{t}} G_{\mathrm{r}}}{L(d_{\mathrm{path3}}^l)} \Bigg| D_3^l \left(\frac{c}{4\pi f d_{\mathrm{path3}}^l}\right) e^{-j\frac{2\pi f}{c}(d_{\mathrm{path3}}^l - d_{\mathrm{path1}}^n) + \Phi} \\ & + D_4^l \left(\frac{c}{4\pi f d_{\mathrm{path4}}^l}\right) \Psi_s^l e^{-j\frac{2\pi f}{c}(d_{\mathrm{path4}}^l - d_{\mathrm{path1}}^n) + \Phi} \Bigg|^2. \end{aligned} \tag{2.13}$$

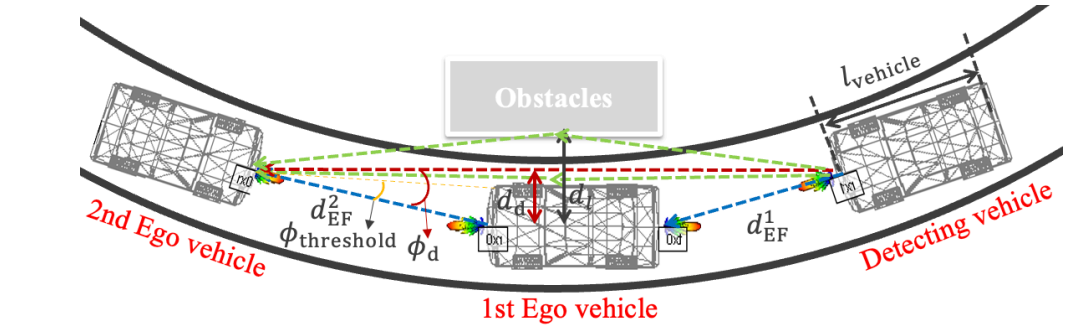

(a) $d_d < d_l$, $\phi_d <= \phi_{\text{threshold}}$

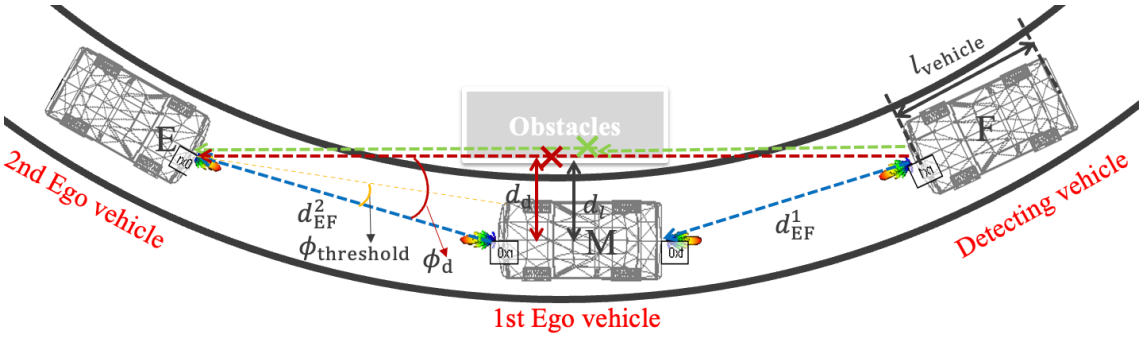

(b) $d_d >= d_l$, $\phi_d > \phi_{\text{threshold}}$

Figure 2.4: Two situations of V2V communications with relay in horizontal curve scenario

2.3 Evaluation of Interference

2.3.1 Interference Difference in Typical Road Scenarios

Before comparing the co-channel interference differences in three typical road scenarios, the two situations of V2V communications with relay in horizontal curve should be analyzed first. V2V communications with relay have two situations in the horizontal curve scenario when the d^1_{EF} and d^2_{EF} change as shown in Fig. 2.4. In Fig. 2.4, d_{d} is the distance of direct interference link (red line) to the horizontal center-line of the first Ego vehicle. ϕ_{d} is the angle between the direct interference link (red line) and desired signal (blue line) at transmitter and receiver sides. $\phi_{\text{threshold}}$ is the angle between the yellow line and desired signal (blue line) at the transmitter and receiver sides. When $d_{\text{d}} < d_{\text{l}}$ and $\phi_{\text{d}} \leq \phi_{\text{threshold}}$, the direct interference link is blocked by the first Ego vehicle so that ground and surrounding reflections are considered. When $d_{\text{d}} \geq d_{\text{l}}$ and $\phi_{\text{d}} > \phi_{\text{threshold}}$, all interference links are blocked by obstacles so that there is no interference in this situation as shown in Fig. 2.4(b). The analysis of interference in the

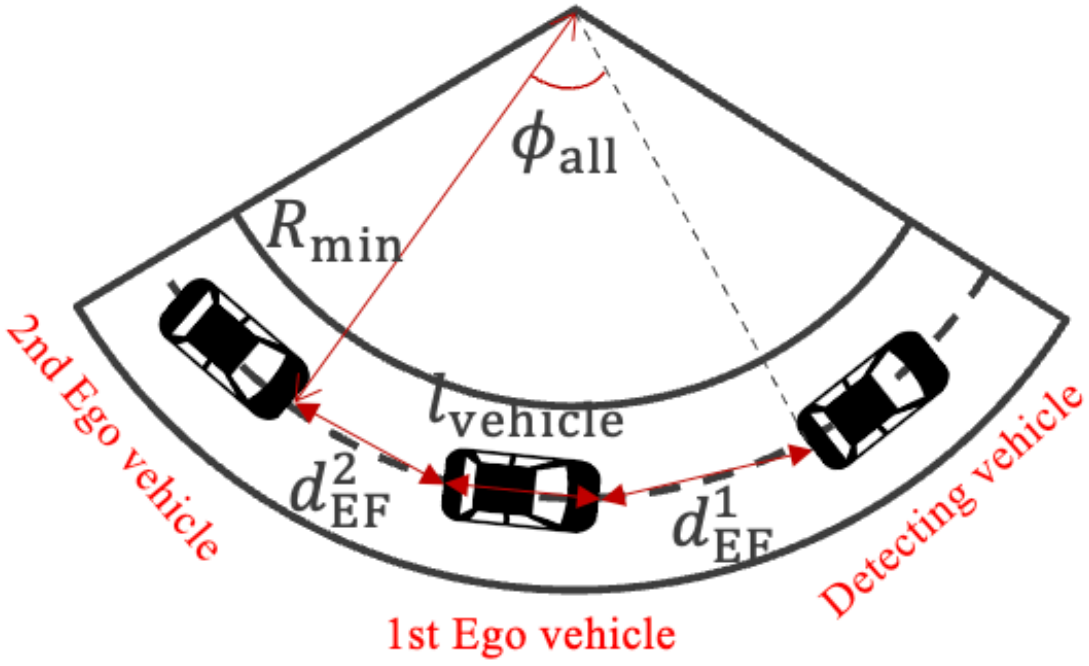

Figure 2.5: Illustration of parameter ϕ_{all}

horizontal curve is implemented in the first situation as shown in Fig. 2.4(a) since there is no interference in the second situation.

The main differences of interference between single straight road, horizontal curve and slope road scenarios depend on length ($d_{\text{path}k}$) and coefficients of antenna directivity (D_k) of path 3 and path 4. Therefore, the length and propagation angle of path 3 and path 4 in three typical scenarios are compared in Table 2.2. In this table, θ_{Te} and θ_{Re} are θ_e in Eq. (2.7) at the transmitter and receiver side respectively and ϕ_{Ta} and ϕ_{Ra} are ϕ_a in Eq. (2.7) at the transmitter and receiver side respectively. In addition,

$$d_{\text{all1}} = d^1_{\text{EF}} + d^2_{\text{EF}} + l_{\text{vehicle}}, \tag{2.14}$$

$$d_{\text{all2}} = 2R_{\text{min}} \sin\left(\frac{\phi_{\text{all}}}{2}\right), \tag{2.15}$$

$$\phi_{\text{all}} = 2\left(\arcsin\left(\frac{d^1_{\text{EF}}}{2R_{\text{min}}}\right) + \arcsin\left(\frac{l_{\text{vehicle}}}{2R_{\text{min}}}\right) + \arcsin\left(\frac{d^2_{\text{EF}}}{2R_{\text{min}}}\right)\right), \tag{2.16}$$

$$d_{\text{all3}} = d_{\text{EF}}^{2} + d_{\text{EF}}^{1} \cos\alpha + l_{\text{vehicle}}, \tag{2.17}$$

where d_{all1}, d_{all2}, d_{all3} represent the horizontal distance between Tx1 on the Detecting vehicle and Rx2 on the second Ego vehicle in the single straight road, horizontal curve and slope road scenarios respectively. In Eq. (2.15), ϕ_{all} is the angle as shown in Fig. 2.5 and is described as Eq. (2.16).

Therefore, based on Table 2.2 and Eq. (2.7) to Eq. (2.9), the received power of co-channel interference caused by ground and surrounding reflections in all road scenarios can be compared via simulation.

Single straight road		
Path3 (Ground reflection)	d_{path3}	$\sqrt{d_{\text{all1}}^2 + (2h)^2}$
	$\theta_{\text{Te}} = \theta_{\text{Re}}$	$\arctan\left(\frac{2h}{d_{\text{all1}}}\right)$
	ϕ_a	$\phi_{\text{T}a} = \phi_{\text{R}a} = 0$
Path 4 (Surrounding reflection)	d_{path4}	$\sqrt{{d_{\text{all1}}}^2 + (2d_l)^2}$
	$\theta_{\text{Te}} = \theta_{\text{Re}}$	0
	$\phi_{\text{Ta}} = \phi_{\text{Ra}}$	$\arctan\left(\frac{2d_l}{d_{\text{all1}}}\right)$
Horizontal curve		
Path3 (Ground reflection)	d_{path3}	$\sqrt{{d_{\text{all2}}}^2 + (2h)^2}$
	$\theta_{\text{Te}} = \theta_{\text{Re}}$	$\arctan\left(\frac{2h}{d_{\text{all2}}}\right)$
	ϕ_a	$\phi_{\text{Ta}} = \frac{\phi_{\text{all}}}{2} - \arcsin\left(\frac{d_{\text{EF}}^1}{2R_{\min}}\right)$ $\phi_{\text{Ra}} = \frac{\phi_{\text{all}}}{2} - \arcsin\left(\frac{d_{\text{ED}}^2}{2R_{\min}}\right)$
Path 4 (Surrounding reflection)	d_{path4}	$\sqrt{d_{\text{all2}}^2 + (2R_{\min}\cos\left(\frac{\phi_{\text{all}}}{2}\right) - 2R_{\min} + 2d_l)^2}$
	$\theta_{\text{Te}} = \theta_{\text{Re}}$	0
	$\phi_{\text{Ta}} = \phi_{\text{Ra}}$	$\arctan\left(\frac{2R_{\min}\cos\left(\frac{\phi_{\text{all}}}{2}\right) - 2R_{\min} + 2d_l}{d_{\text{all2}}}\right)$
Slope		
Path3 (Ground reflection)	d_{path3}	$\sqrt{{d_{\text{all3}}}^2 + (2h - d_{\text{EF}}^1 \sin\alpha)^2}$
	$\theta_{\text{Te}} = \theta_{\text{Re}}$	$\arctan\left(\frac{2h - d_{\text{EF}}^1 \sin\alpha}{d_{\text{all3}}}\right)$
	ϕ_a	$\phi_{\text{T}a} = \phi_{\text{R}a} = 0$
Path 4 (Surrounding reflection)	d_{path4}	$\sqrt{{d_{\text{all3}}}^2 + (d_{\text{EF}}^1 \sin\alpha)^2 + (2d_l)^2}$
	$\theta_{\text{Te}} = \theta_{\text{Re}}$	0
	$\phi_{\text{Ta}} = \phi_{\text{Ra}}$	$\arctan\left(\frac{2d_l}{\sqrt{{d_{\text{all3}}}^2 + (d_{\text{EF}}^1 \sin\alpha)^2}}\right)$

Table 2.2: Difference of interference between three typical road scenarios

Parameters	**Value**
Carrier frequency (f)	60 GHz
Bandwidth (B)	2.16 GHz
Transmitted power (P_{Tx1}, P_{Tx2})	10 dBm
Antenna gain (G_{t}, G_{r})	26 dBi
Azimuth half power beam angle (ϕ_{3dB})	10 degrees
Elevation half power beam angle (θ_{3dB})	6 degrees
Height of antenna (h)	0.95 m
Length of vehicle (l_{vehicle})	4.35 m
Width of vehicle (w_{vehicle})	1.69 m
Height of vehicle (h_{vehicle})	1.48 m
Width of lane (w_{lane})	3.2 m
Height of metal body of vehicle (h_{mb})	1.1 m
Chassis clearance	0.14 m
Dielectric constant of asphalt (ψ_{asphalt})	3.9975-j0.2
Dielectric constant of concrete (ψ_{concrete})	4.94-j0.69
Noise factor (NF)	10 dB
Noise power density (N_0)	-174 dBm/Hz
Distance to the surrounding obstacles (d_l)	3.5 m
Radius of horizontal curve (r_{min})	240 m
Grade of slope (α)	4%
Speed of the Ego vehicle (v_e)	80 km/h

Table 2.3: Simulation parameters for received power of interference in typical road scenarios

2.3.2 Received Power of Interference in Typical Road Scenarios

This subsection compares the received power of co-channel interference in three typical road scenarios. The operating frequency is 60 GHz. Although 60 GHz is the unlicensed frequency band, it is used in this study based on the following reasons. Now IEEE 802.11bd, as a successor of IEEE 802.11p, is being specified for next generation V2X (NGV) communications. Besides the 5.9 GHz, IEEE 802.11bd also targets the mmWave frequency band at 57-71 GHz. In this target frequency band, 63-64 GHz is allocated to ITS in the Europe, and there is an ongoing work in ITU-R to allocate 60GHz band for ITS. In the PHY layer, IEEE 802.11bd is assumed to utilize IEEE 802.11ad. Therefore, here we verify the effectiveness of the proposed scheme at 60 GHz (IEEE 802.11ad) in the PHY layer for mmWave V2V relay communications. In the MAC layer, IEEE 802.11bd borrows the rules of IEEE 802.11p to reduce the association overhead. For example, the Outside of the Context of BSS (OCB) rules allow vehicles to transmit signals without prior association. Thus the simulation is implemented at 60 GHz frequency band in MATLAB. Table 2.3 shows parameters in this simulation.

Before comparing the interference difference between these road scenarios via simulation, the road parameters of the horizontal curve and slope scenarios should be discussed. The road parameter of the horizontal curve is based on the relationship between vehicle speed and radius and their collaborative relationships with superelevation and side friction. In this study, it is assumed that the speed limit of the horizontal curve is 80 km/h; thus, the radius ($R_{\min}$) can be set to 240 m based on Sect. 2.1.2. As for the slope scenario, the maximum grade (α) for freeways are presented as a function of vehicle speed and terrain types to be arranged to 4% with the assumption of 80 km/h vehicle speed.

Figure 2.6 compares the simulated received power of co-channel interference caused by ground and surrounding reflections in each road scenario. In this figure, the received power of ground reflection is at least 10 dB higher than that of surrounding reflection in all road scenarios. Of course, the received power of surrounding reflection shown in this figure only includes the interference caused by one side reflection. The worst case is that there are obstacles on both sides, which will make the received power of surrounding reflection become twice than before if the environment on both sides of the vehicles is assumed to be the same. Therefore, the received power of surrounding reflection will increase by approximately 3 dB, which is still far less than the interference caused by ground reflection. Thus, under conventional antenna configuration, ground reflection is the main interference compared with direct interference and the interference caused by surrounding reflection in all scenarios.

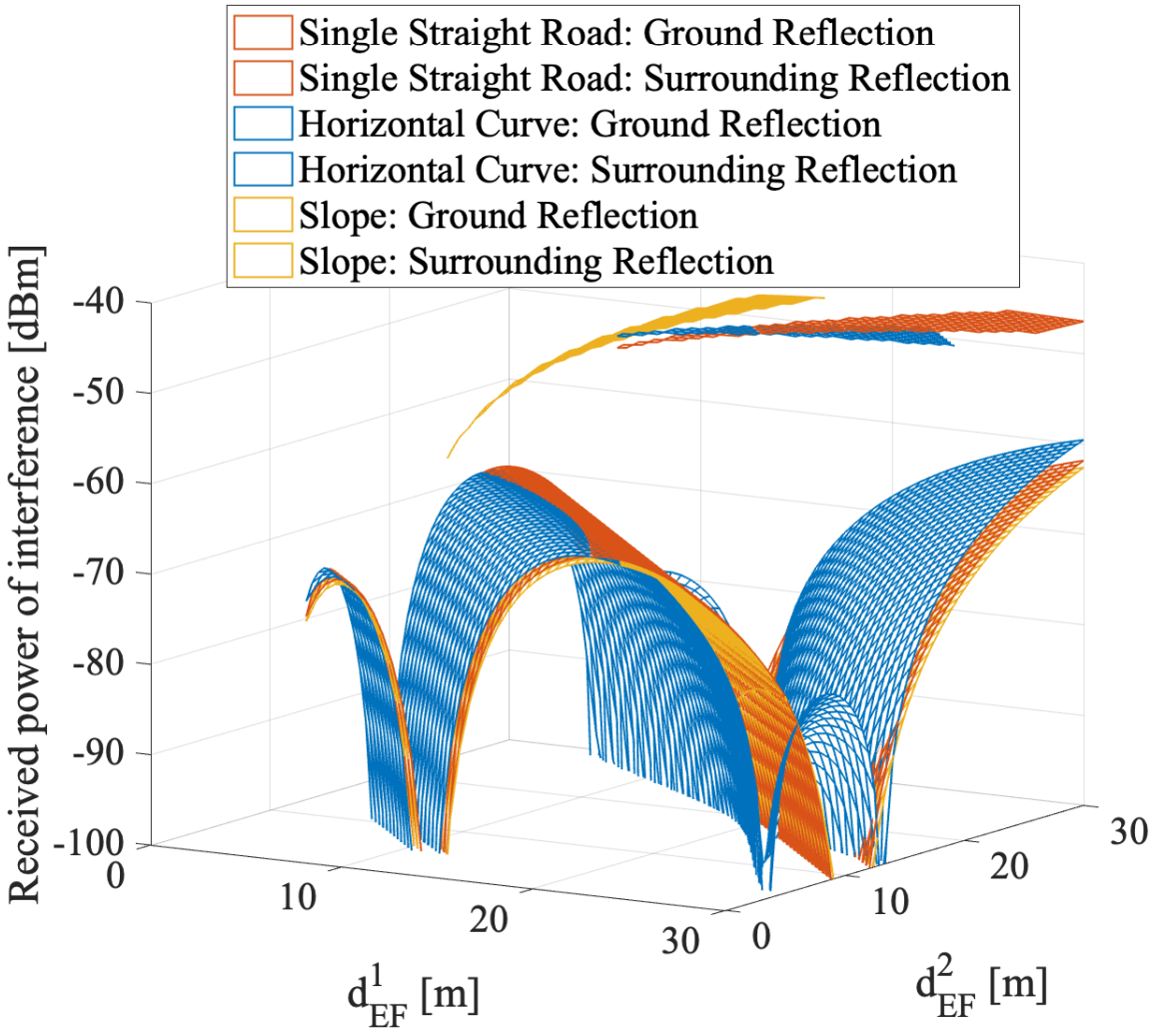

Figure 2.6: Received power of co-channel interference in typical road scenarios

Besides, the received powers of ground reflection in all road scenarios are strongest when d^1_{EF} is equal to d^2_{EF}. Therefore, the main purpose of this research is to weaken the co-channel interference caused by ground reflections, especially in the case of $d^1_{\mathrm{EF}} = d^2_{\mathrm{EF}}$.

MCS	Modulation	Coding rate	EVM value [dB]	Data rate [Mbps]
1	$\pi/2$-BPSK	1/2 with repetition	-6	385.00
2	$\pi/2$-BPSK	1/2	-7	770.00
3	$\pi/2$-BPSK	5/8	-9	962.50
4	$\pi/2$-BPSK	3/4	-10	1155.00
5	$\pi/2$-BPSK	13/16	-12	1251.25
6	$\pi/2$-QPSK	1/2	-11	1540.00
7	$\pi/2$-QPSK	5/8	-12	1925.00
8	$\pi/2$-QPSK	3/4	-13	2310.00
9	$\pi/2$-QPSK	13/16	-15	2502.50
10	$\pi/2$-16QAM	1/2	-19	3080.00
11	$\pi/2$-16QAM	5/8	-20	3850.00
12	$\pi/2$-16QAM	3/4	-21	4620.00
13	SQPSK	1/2	-7	693.00
14	SQPSK	5/8	-9	866.25
15	QPSK	1/2	-10	1386.00
16	QPSK	5/8	-11	1732.50
17	QPSK	3/4	-13	2079.00
18	16QAM	1/2	-15	2772.00
19	16QAM	5/8	-17	3465.00
20	16QAM	3/4	-19	4158.00
21	16QAM	13/16	-20	4504.50
22	64QAM	5/8	-22	5197.50
23	64QAM	3/4	-24	6237.00
24	64QAM	13/16	-26	6756.75

Table 2.4: IEEE 802.11ad standard MCS table

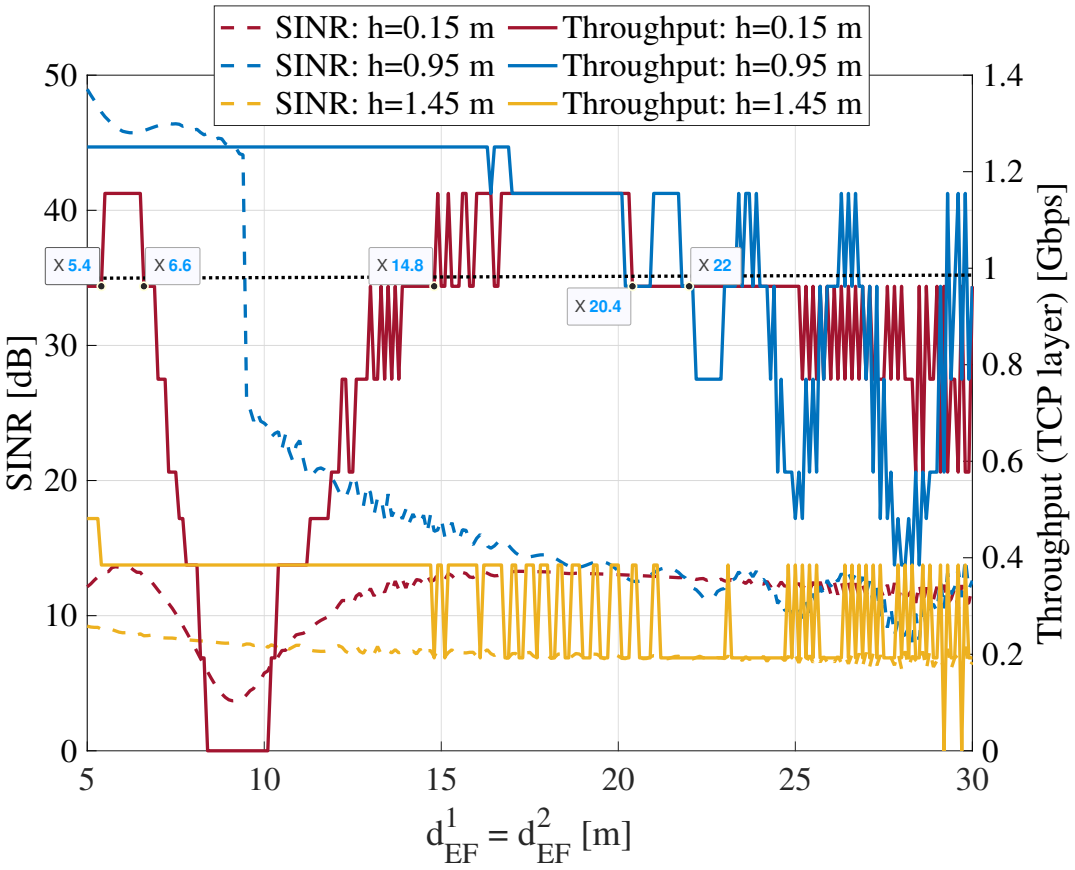

Figure 2.7: SINR and theoretical throughput comparison with conventional antenna configuration when h=0.15 m, 0.95 m and 1.45 m

2.3.3 Effect of Antenna Height on Interference

This subsection compares the signal-to-interference-plus-noise ratio (SINR) and theoretical E2E throughput with different antenna heights under conventional antenna configuration and then explores antenna height's effect on co-channel interference.

It is known that the throughput in TCP (Transmission Control Protocol) layer is about a half of the data rate in PHY (Physical) layer [44]. Then, the data rate in the PHY layer depends on the EVM (Error Vector Magnitude) which is the inverse of SINR. In this simulation, the throughput depends on SINR and is determined by referring to the IEEE 802.11ad MCS (Modulation and Coding Scheme) table as shown in Table 2.4 since most commercially available devices at mmWave band are based on IEEE 802.11ad standard. 802.11ad provides two multiplexing technologies with 32 standard modulation and coding scheme levels. The Single Carrier (SC) MCS levels are MCS 1-12 and use $\pi/2$ BPSK, QPSK, and 16QAM modulations

to achieve PHY data rates from 385 Mbps (MCS1) to 4620 Mbps (MCS 12). MCS levels 13-24 are based on Orthogonal Frequency Division Multiplexing (OFDM), using SQPSK, QPSK, 16QAM and 64 QAM modulations. 802.11ad provides additional error-correction through the use of coding, convolutional or Low Density Parity Check (LDPC). The combination of OFDM modulation and convolutional coding rates result in PHY rates of 693 Mbps (MCS 13) to 6756.75 Mbps (MCS 24). Our lab's devices of IEEE 802.11ad only support MCS index 1-9 so that the maximum throughput is approximately 1.25 Gbps in TCP layer. To facilitate the comparison with the experimental results later, this simulation also supports the MCS index 1-9.

This simulation selects 0.15 m, 0.95 m, and 1.45 m to represent three typical antenna heights. $h = 0.15$ m means that the antenna is close to the chassis of the vehicle. $h = 0.95$ m represents the maximum height at which the vehicle's metal body completely blocks the direct interference signal (more precisely, first-order Fresnel zone). $h = 1.45$ m means the antenna approaches the vehicle's roof where direct interference will have an impact.

The variation of SINR and theoretical maximum throughput in TCP layer at three typical antenna heights with conventional antenna configuration is shown in Fig. 2.7 when $d^1_{\mathrm{EF}} = d^2_{\mathrm{EF}}$ ranges from 5 m to 30 m. With the antenna height $h = 0.15$ m (red lines), as $d^1_{\mathrm{EF}} = d^2_{\mathrm{EF}}$ varies in $[5.4\text{ m}, 6.6\text{ m}]$ and $[14.8\text{ m}, 20.4\text{ m}]$, the throughput is higher than 1 Gbps. With the antenna height $h = 0.95$ m (blue lines), an improvement in the throughput is seen as it remains above 1 Gbps when $d^1_{\mathrm{EF}} = d^2_{\mathrm{EF}}$ changes from 5 m to 22 m. Whereas, with the antenna height $h = 1.45$ m (yellow lines), the SINR and throughput are always lower than 10 dB and 0.4 Gbps respectively due to the serious impact of direct interference on the desired signal. Therefore, $h = 0.95$ m shall be considered as the optimal antenna height under the conventional antenna configuration.

2.3.4 Effect of Antenna Polarization on Interference

Suppose all antennas in V2V communications systems adopt the same configuration. In that case, vertical polarization wave is best to mitigate the interference caused by ground reflection since the ground reflection coefficient of vertical polarization is the lowest among that of other polarizations, as shown in Fig. 2.8. On the other hand, the main interference in mmWave V2V communications is the interference caused by ground reflection. Both of them produce the reason that vertical polarization should be adopted in the vertical plane of the simulation and outdoor experiment.

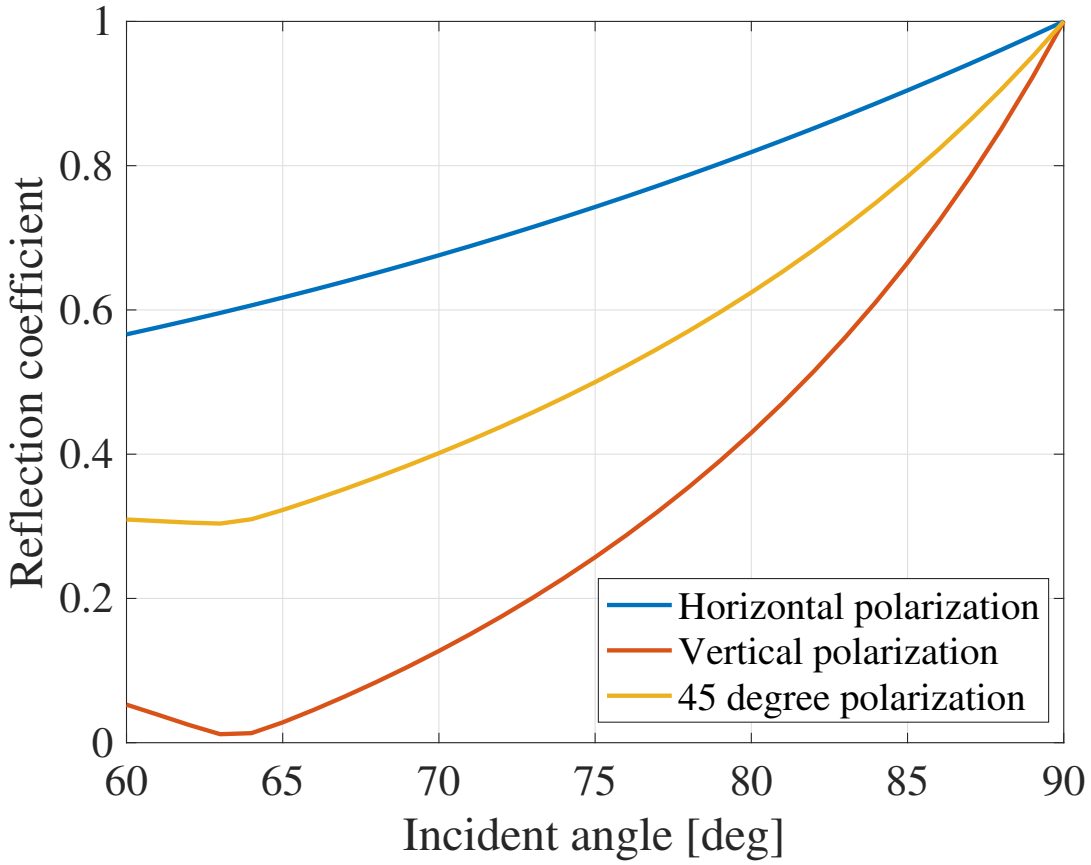

Figure 2.8: Ground reflection coefficient with different polarizations when h= 0.95 m

Besides, with the increase of the incident angle, the ground reflection coefficient increases. In other words, interference caused by reflection becomes strong.

2.4 Conclusion

This chapter introduced the basic and general mmWave V2V relays communications scenarios and three typical road scenarios. Then we derived the co-channel interference strength by ray-tracing based channel models in basic and general scenarios. The co-channel interference differences in three typical road scenarios are analyzed theoretically based on the described channel model. The received power of co-channel interference in these road scenarios is compared by the simulation. Our simulation results show that ground reflection is the main co-channel interference compared with direct co-channel interference and the co-channel

interference caused by surrounding reflection under the conventional antenna configuration. Besides, when the inter-vehicle distances are equal, the co-channel interference is strongest, which is the worst case for mmWave V2V communications with relay. Finally, we investigated the impact of antenna heights on co-channel interference. The simulation revealed that the co-channel interference is strongest when the antennas are placed on the roof of vehicles. The co-channel interference drops off when the antennas are located near the ground at the front and rear of vehicles. The antennas close to the top of the vehicle's metal body at the front and rear show with the weakest co-channel interference.

Chapter3

ZigZag Antenna Configuration for mmWave V2V with Relay

Co-channel interference control is crucial in mmWave V2V relays communications, especially when the channel is reused. This chapter proposes a novel and efficient co-channel interference control method using radio resource management in the spatial domain. This new approach is referred to as the ZigZag antenna configuration. In geometry, the ZigZag pattern is described as a skew apeirogon. From the point of view of symmetry, a regular zigzag can be generated from a simple motif like a line segment by repeated application of a glide reflection. We apply this geometric pattern to the connection pattern of mmWave V2V relays communications. Let the continuous V2V links form a regular ZigZag shape. To facilitate the formation of the ZigZag pattern, antennas must be installed on the four corners of the vehicle. This kind of antenna configuration that supports the ZigZag pattern link connection is called the ZigZag antenna configuration. This chapter firstly describes the feature of the ZigZag antenna configuration in mmWave V2V communications with relay and then explains the principle of co-channel interference mitigation with this novel antenna configuration. Next, we compare the performance of the proposed method with that of conventional antenna configuration by the simulation based on standard IEEE 802.11ad and show the superiority of the proposed method on co-channel interference mitigation and E2E throughput improvement. Finally, an outdoor experiment is designed and implemented to verify the effectiveness of the ZigZag antenna configuration.

3.1 Motivation

V2V communications have been identified as an essential technology to improve driving behaviors and increase safety levels of autonomous vehicles since it can unleash the restriction of onboard sensors, break the line-of-sight constraints, and enhance the overall contextual awareness by acquiring more data from surroundings. A vehicular sensor system for V2V communications is composed of high spatial resolution LiDAR, high-definition cameras, radar, GPS (Global Positioning System), odometry, etc. It perceives dynamic environments, which helps autonomous vehicles to determine their real-time moving strategies. Sharing sensor information like a precise three-dimensional map of vehicle surroundings requires ultra-high data rate and ultra-low latency on V2V communications. For example, one of the enhanced V2V use cases specified by 3GPP release 14/15, extended sensors, requires over 1 Gbps data rate and less than 10 ms end-to-end latency per link [45]. MmWave with ultra-wide continuous bandwidth has the potential to support ultra-high data rate V2V communications. Now IEEE is specifying IEEE 802.11bd to adapt to advanced V2X applications, assuring backward compatibility with IEEE 802.11p (5.9 GHz) [7] and IEEE 802.11ad (60 GHz) [14]. Its peak data rate will be higher than 6.75 Gbps. 3GPP is also specifying New Radio (NR)-V2X (FR2: 24.25 GHz - 52.6 GHz) [12, 15] with the peak data rate of 20 Gbps. However, because of the strong co-channel interference of mmWave V2V relays communications under conventional antenna configurations, the performance such as throughput is degraded.

Regarding antenna configurations for V2V communications, there are two conventional methods. One is placing antennas on the roof of vehicles [26, 25]. However, under this antenna configuration, direct interference links cannot be blocked by nearby vehicles, which degrades the throughput and increases the latency of desired V2V links. The other antenna configuration is locating antennas at the vehicle's front and rear center. The elevation and azimuth angles of antenna main beam are set to 0 degree [46, 24, 37]. Although vehicle bodies can completely block direct interference links, the reflected interference links still exist. It is almost unavoidable that the practical throughput of V2V communications becomes lower than the required data rate with the antenna configurations mentioned above. Therefore, an open challenge is left for pioneering researchers to investigate more reliable antenna configuration paradigms for mmWave V2V communications.

This chapter describes a new method of ZigZag antenna configuration, which aims to control the co-channel interference and improve the performance of mmWave V2V with relay

communications. Its outstanding performance is demonstrated by comparing the throughputs of mmWave V2V communications with/without ZigZag antenna configuration in three typical scenarios at the 60 GHz frequency band. Moreover, an outdoor experiment is carried out to verify the effectiveness of the proposed ZigZag antenna configuration in the worst interference scenario.

3.2 Feature of ZigZag Antenna Configuration

The typical features of ZigZag antenna configuration are presented in Fig. 3.1. In each road scenario, the antenna configuration follows the ZigZag paradigm, and the antenna's main beam is aligned as the variation of inter-vehicle distance. The ZigZag antenna configuration introduces a new parameter d_{tr} which represents the distance between the transmitter and receiver along the y-axis as in Fig. 3.1(a). The rotation angle of the antenna main beam in the horizontal plane depends on the value of d_{tr} and inter-vehicle distance. When the inter-vehicle distance is fixed, larger d_{tr} can lead to the larger rotation angle of antenna main beam as shown in Eqs. (3.1) and (3.2).

$$\phi_{\mathrm{T0}} = \pm \arctan\left(\frac{d_{\mathrm{tr}}}{d^{1}_{\mathrm{EF}}}\right), \tag{3.1}$$

$$\phi_{\mathrm{R0}} = \pm \arctan\left(\frac{d_{\mathrm{tr}}}{d^{2}_{\mathrm{EF}}}\right), \tag{3.2}$$

where ϕ_{T0} and ϕ_{R0} are the ϕ_0 in Eq. (2.7) at transmitter and receiver sides.

3.3 Principle of Interference Mitigation with ZigZag Antenna Configuration

As explained in Sect. 2.2, the interference comes from the reflection path (path3 and path4) of the signal transmitted by Tx1. Fig. 3.2 shows an example to explain the principle of mitigating the interference of ground reflection (path3) with ZigZag antenna configuration. In this figure, ϕ_{3dB} is half power beam angle in the horizontal plane, ϕ_{a} is the azimuth angle of path3 which is equal to 0 degree with conventional and ZigZag antenna configurations and ϕ_0 is the azimuth angle of the main beam. With conventional antenna configuration, ϕ_0 is always equal to 0 degree, whereas ϕ_0 is a function of d_{tr} and inter-vehicle distance in

the case of ZigZag antenna configuration. Therefore, compared with conventional antenna configuration ($|\phi_a - \phi_0| = 0$), the angle between the antenna main beam and the propagation

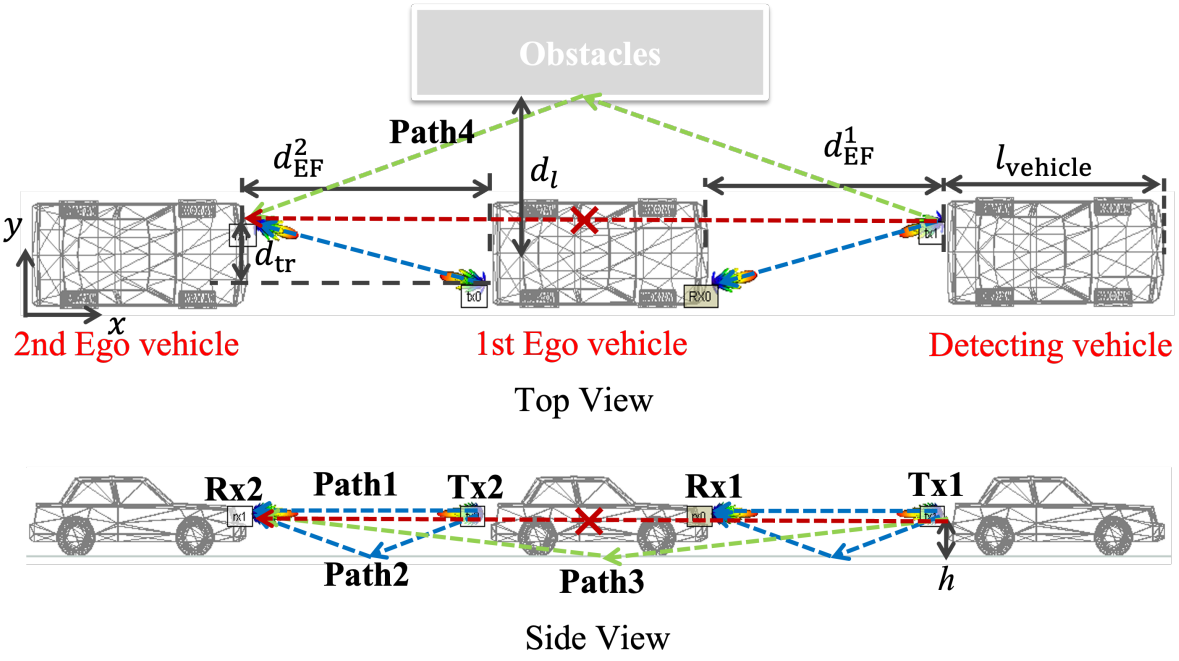

(a) Single straight road

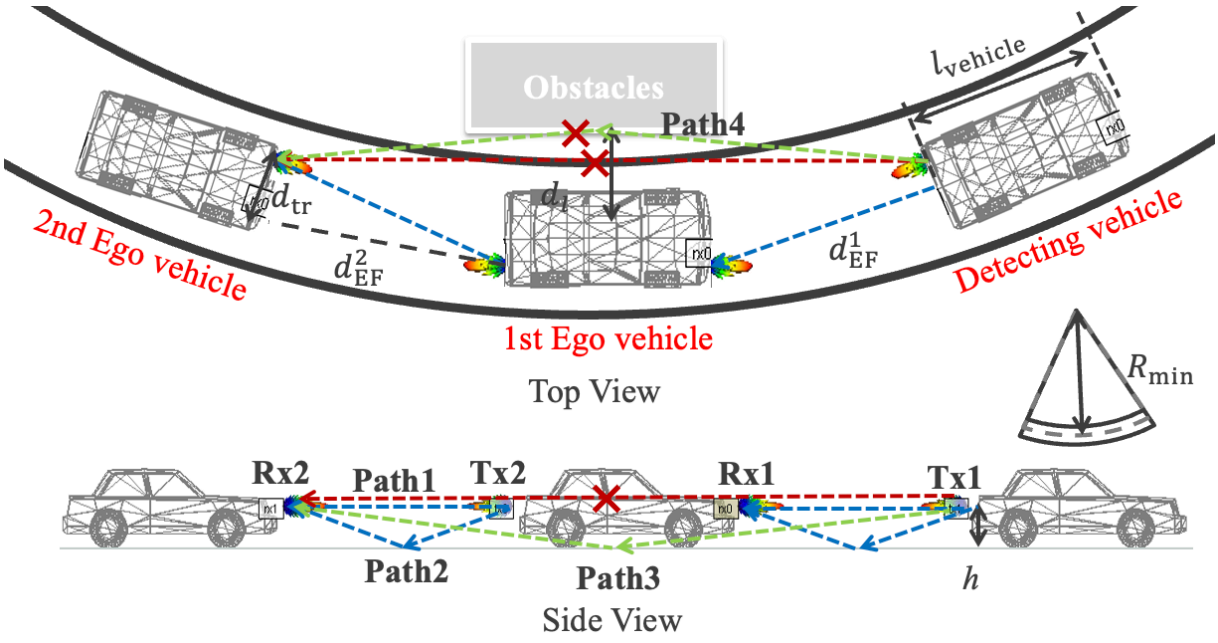

(b) Horizontal curve

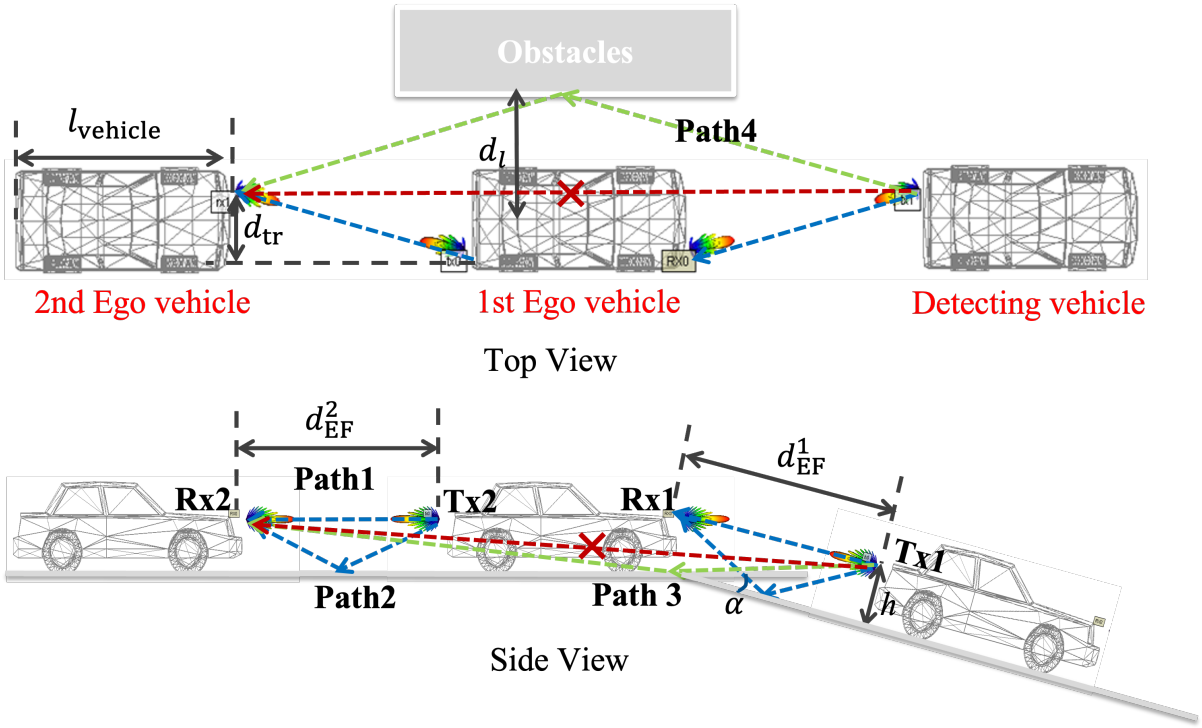

(c) Slope

Figure 3.1: ZigZag antenna configuration in typical road scenarios

path which is equal to $|\phi_{\text{a}} - \phi_0|$ increases under the ZigZag antenna configuration as shown in Fig. 3.2, thereby the antenna directivity of path3 on Rx2 side decreases. For instance, the antenna directivity of path3 on Rx2 side decreases from 0 dB to -10 dB if ϕ_{3dB} is equal to 10 degrees when $|\phi_{\text{a}} - \phi_0|$ changes from 0 to 10 degrees. Eventually, the received power of path3 will be reduced, which means that the interference caused by ground reflection can be mitigated.

The principle of influence of the ZigZag antenna configuration on the interference caused by surrounding reflections is the same. The interference caused by the surrounding reflection (path4) shown in Fig. 3.1 is suppressed because the angle between path4 and the antenna main beam with ZigZag antenna configuration increases. In practice, there are cases that reflectors such as obstacles and vehicles in the oncoming lane exist on both sides, as shown in Fig. 3.3. The probability of occurrence of reflection from the oncoming vehicle is much smaller than that from obstacles. If the traffic pattern in Fig. 3.3 appears, the surrounding reflection path on one side (path5) will be enhanced, and the other surrounding reflection path (path4) will be suppressed when the ZigZag antenna configuration is deployed. On the whole,

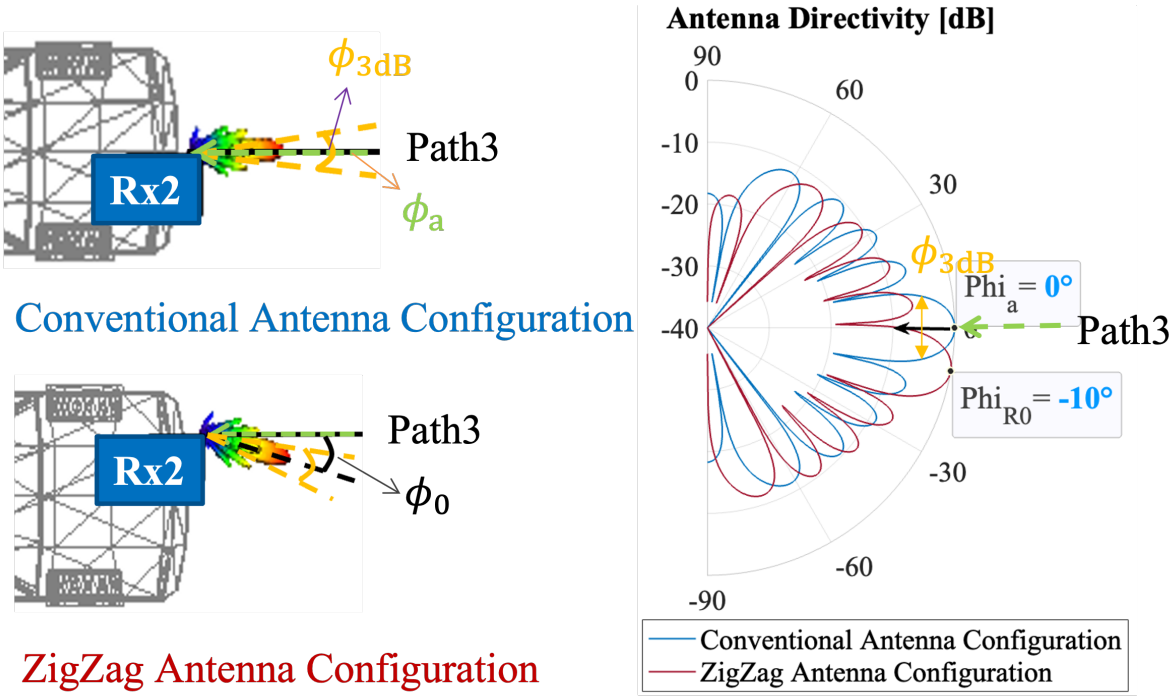

Figure 3.2: Antenna directivity with conventional and ZigZag antenna configurations

compared with the conventional antenna configuration, the received power of surrounding reflections from two sides with ZigZag antenna configuration increase a little, as shown in Fig. 3.4. On the other hand, the interference caused by ground reflections is far greater than the interference caused by surrounding reflections, as shown in Fig. 2.6. Therefore, even though the received power of surrounding reflection on both sides slightly increases, the overall interference reduction performance of ZigZag doesn't degrade since ZigZag has significantly suppressed the significant interference source ground reflection.

3.4 Performance Evaluation: Conventional V.S. ZigZag Antenna Configuration

This section provides numerical evaluations of the proposed ZigZag antenna configuration. Simulation evaluation assumes a ray-tracing-based propagation channel model, and all antennas have the exact specifications located at the same height. It is noted that this simulation is based on commercially available devices of IEEE 802.11ad, and the supported MCS index is 1-9. To visually express the suppression effect of the ZigZag antenna configuration on the co-

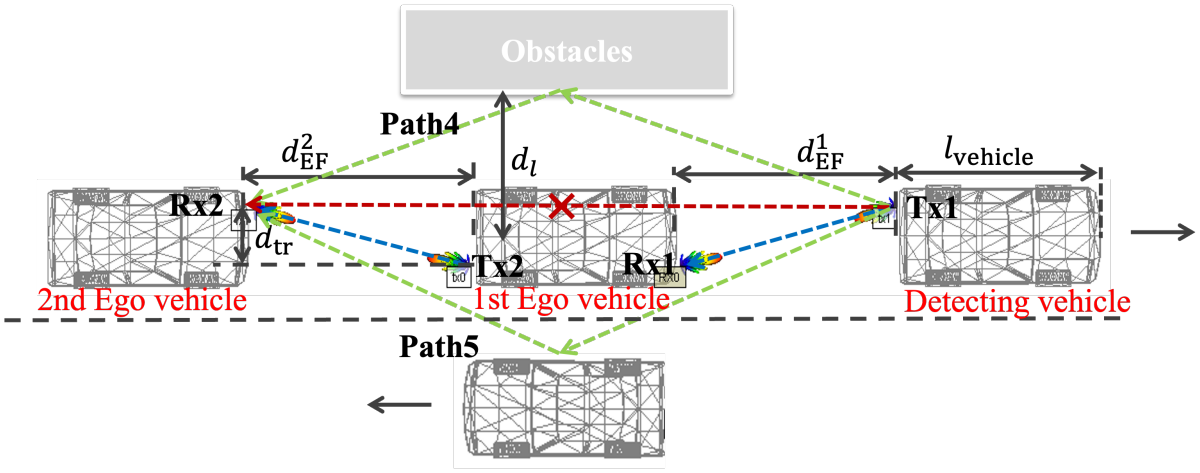

Figure 3.3: Channel model of ZigZag antenna configuration with two sides surrounding reflections

channel interference, firstly, the received power of co-channel interference at optimal antenna height (0.95 m) with conventional and ZigZag antenna configuration are compared in the single straight road, horizontal curve, slope road scenarios. Then, the theoretical throughput performance with and without ZigZag antenna configuration is evaluated in three typical road scenarios. d_{tr} is set to 1.6 m since the larger d_{tr} is better to mitigate the impact of interference caused by ground reflections. The simulation parameters for the performance evaluation of ZigZag antenna configuration are summarized in Table 3.1.

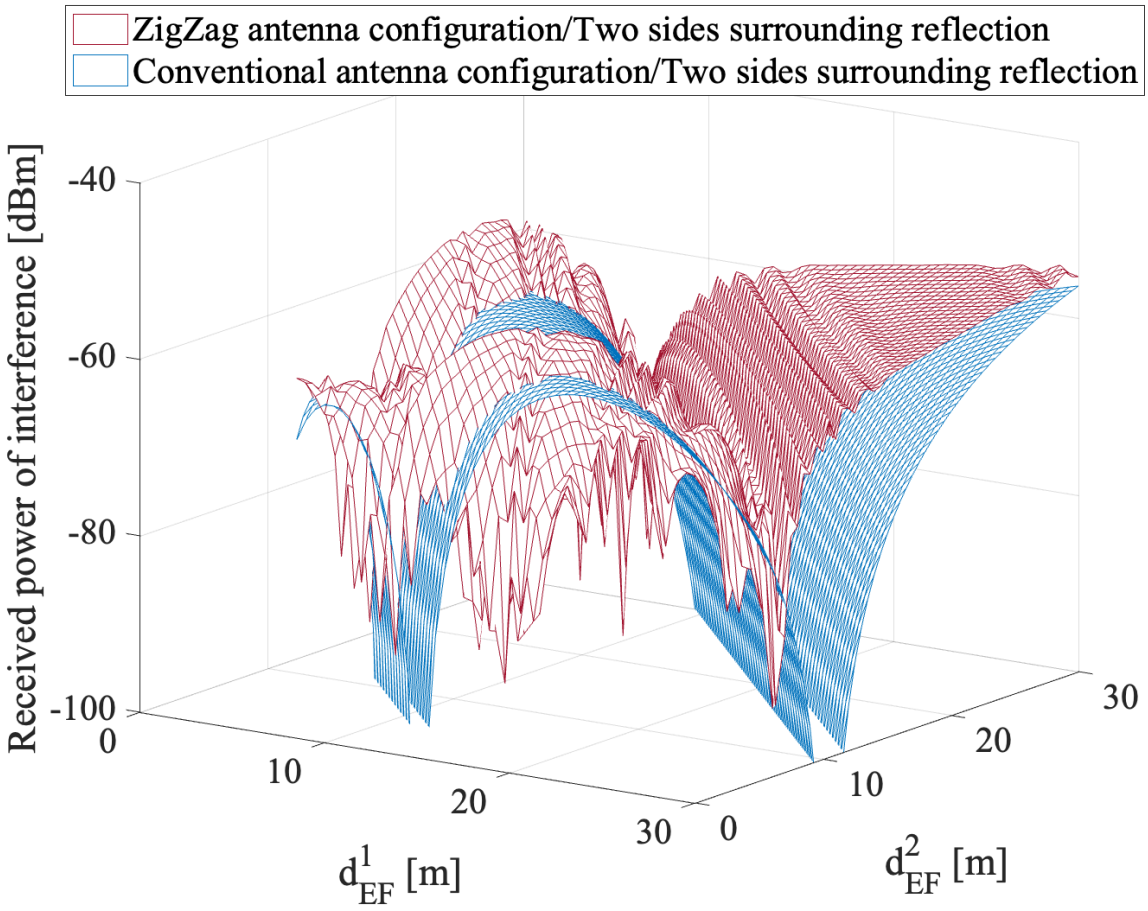

Figure 3.4: Received power of co-channel interference with two sides surrounding reflections

Parameters	**Value**
Carrier frequency (f)	60 GHz
Bandwidth (B)	2.16 GHz
Transmitted power (P_{Tx1}, P_{Tx2})	10 dBm
Antenna gain (G_{t}, G_{r})	26 dBi
Azimuth half power beam angle (ϕ)	10 degrees
Elevation half power beam angle (θ)	6 degrees
Height of antenna (h)	0.95 m
MCS index	1-9
Length of vehicle (l_{vehicle})	4.35 m
Width of vehicle (w_{vehicle})	1.69 m
Height of vehicle (h_{vehicle})	1.48 m
Width of lane (w_{lane})	3.2 m
Height of metal body of vehicle (h_{mb})	1.1 m
Chassis clearance	0.14 m
Dielectric constant of asphalt (ψ_{asphalt})	3.9975-j0.2
Dielectric constant of concrete (ψ_{concrete})	4.94-j0.69
Noise factor (NF)	10 dB
Noise power density (N_0)	-174 dBm/Hz
Distance to the surrounding obstacles (d_l)	3.5 m
Radius of horizontal curve (R_{min})	240 m
Grade of slope (α)	4%
Speed of the Ego vehicle (v_e)	80 km/h

Table 3.1: Simulation parameters for performance evaluation of ZigZag antenna configuration

Figure 3.5 compares the received power of total co-channel interference with conventional and ZigZag antenna configurations in three typical road scenarios. In Fig. 3.5(a), at the point of ($d^1_{\mathrm{EF}} = 15$ m, $d^2_{\mathrm{EF}} = 15$ m), the difference in received power of co-channel interference with conventional and ZigZag antenna configuration reach the maximum value of 10.47 dB. Although at the point of ($d^1_{\mathrm{EF}} = 30$ m, $d^2_{\mathrm{EF}} = 30$ m), the difference in received power of co-channel interference with two kinds of antenna configuration is minimum, the co-channel interference power of ground reflection with ZigZag antenna configuration is also about 2 dB lower than that with conventional antenna configuration. In the horizontal curve scenario, although the direct interference appears under ZigZag antenna configuration, compared with the total co-channel interference with conventional antenna configuration, the received power of co-channel interference with ZigZag antenna configuration still decreases as shown in Fig. 3.5(b). For example, at the point of ($d^1_{\mathrm{EF}} = 15$ m, $d^2_{\mathrm{EF}} = 15$ m), the difference in received power of co-channel interference with conventional and ZigZag antenna configuration is about 15 dB. Besides, the ZigZag antenna configuration easily blocks the direct link by the obstacles around the curve when the inter-vehicle distance is larger. Therefore, in Fig. 3.5(b), when the d^1_{EF} and d^2_{EF} are larger, the received power of co-channel interference is small enough.

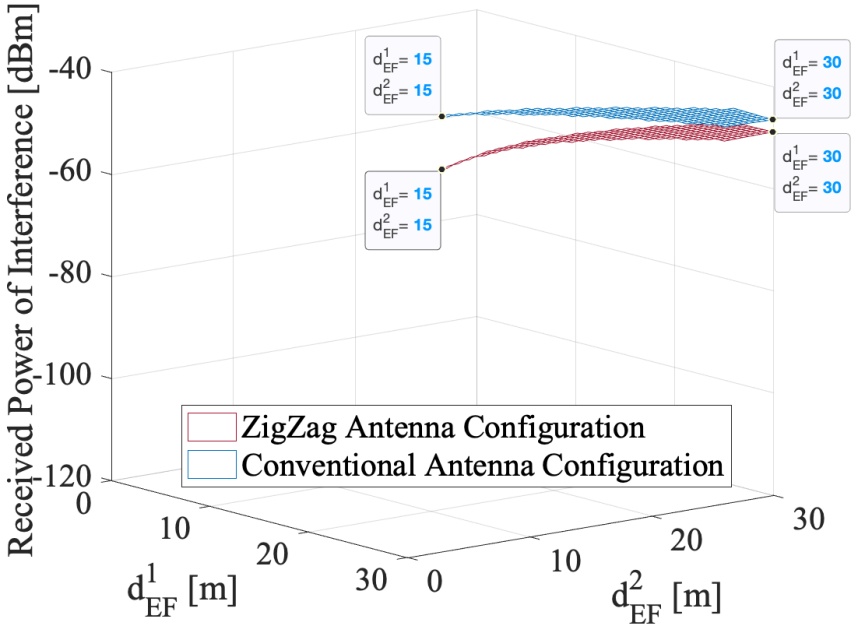

(a) Single straight road

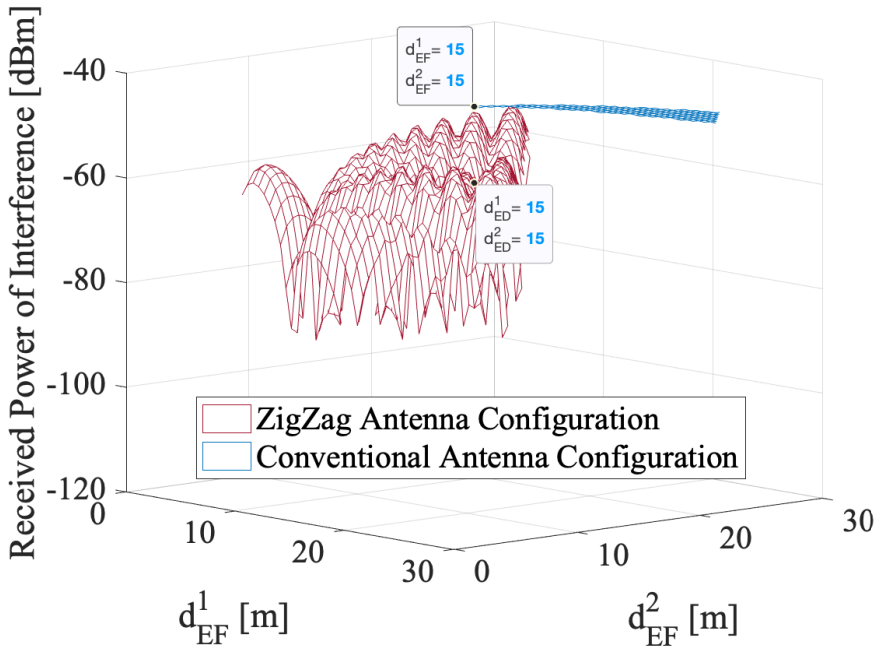

(b) Horizontal curve

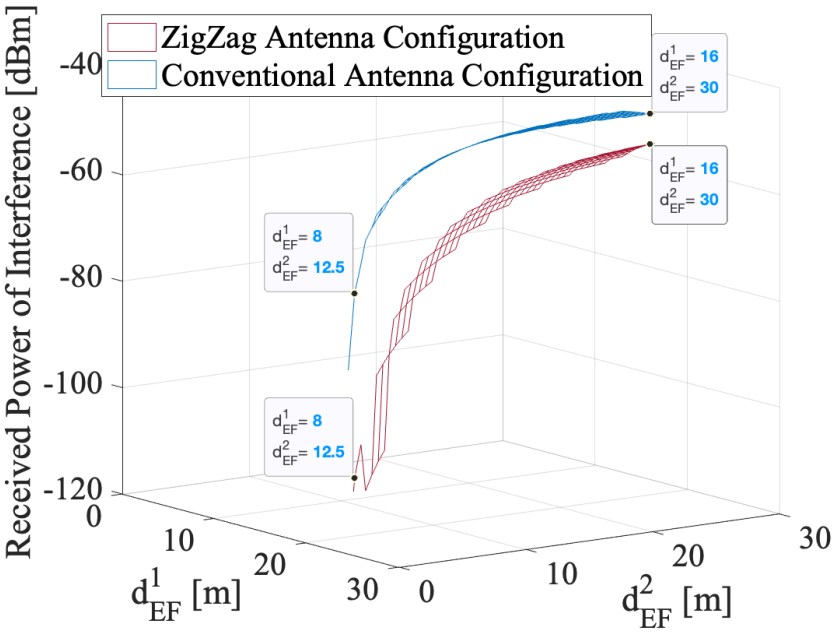

(c) Slope

Figure 3.5: Comparison of received power of co-channel interference with conventional and ZigZag antenna configuration in single straight/curve/slope road scenarios

In the slope scenario, the minimum and maximum differences in co-channel interference power of ground reflection with conventional and ZigZag antenna configuration are 4.72 dB and 34.72 dB at the point of (d^1_{EF} = 16 m, d^2_{EF} = 30 m) and (d^1_{EF} = 8 m, d^2_{EF} = 12.5 m) respectively. It is concluded that ZigZag antenna configuration can decrease the co-channel interference power of ground reflection.

Figure 3.6 compares the throughput of second link in basic scenario in TCP layer with conventional and ZigZag antenna configuration under three typical road scenarios when d^1_{EF} and d^2_{EF} change from 5 m to 30 m. Fig. 3.6(a), (c) and (e) show the theoretical throughput with conventional antenna configuration. In these figures, red points represent the value of throughput lower than 1 Gbps, which means that conventional antenna configuration cannot support the over 1 Gbps required data rate in all scenarios. Instead, Fig. 3.6 (b),(d) and (f) show the throughput of link2 in TCP layer with ZigZag antenna configuration. In the

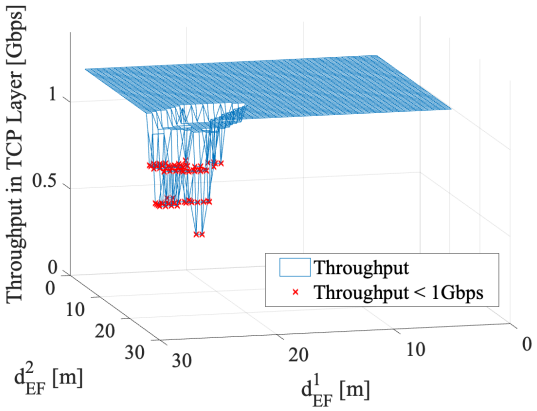

(a) Single straight road / conventional

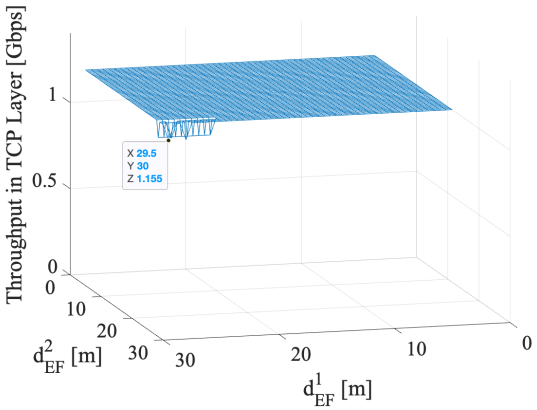

(b) Single straight road / ZigZag

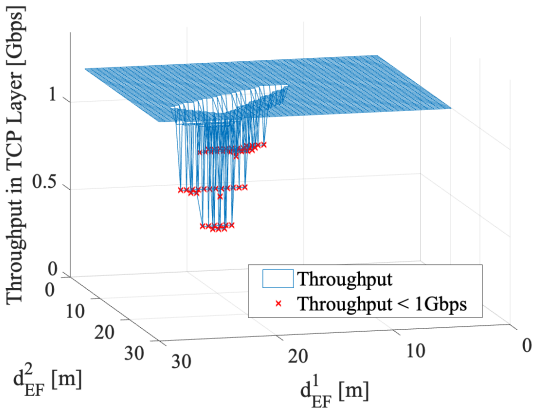

(c) Horizontal curve / conventional

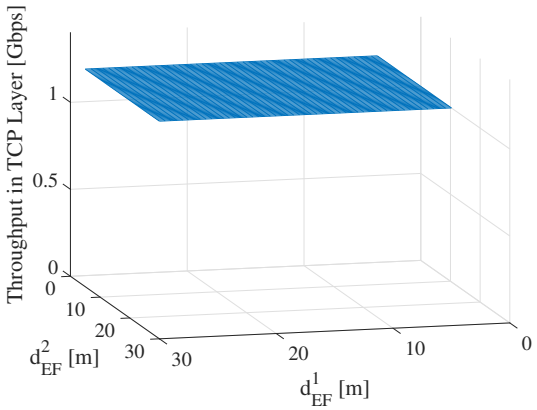

(d) Horizontal curve / ZigZag

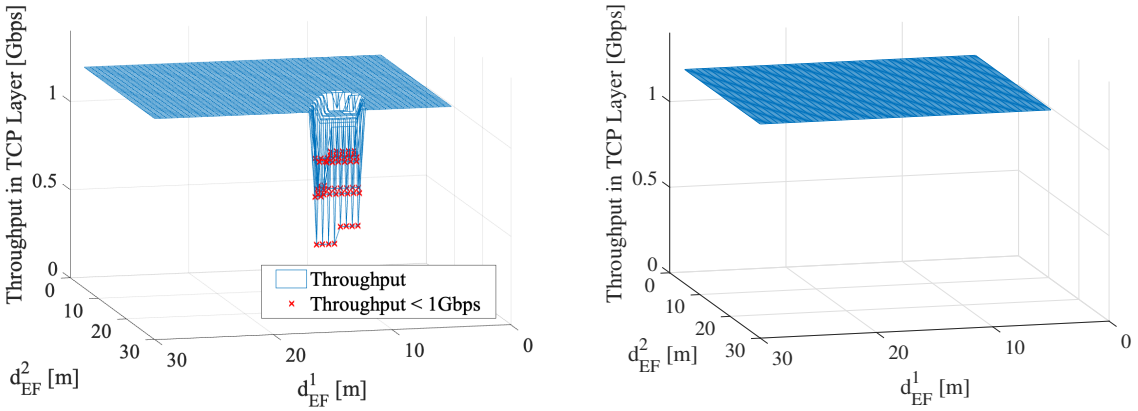

(e) Slope / conventional

(f) Slope / ZigZag

Figure 3.6: Comparison of theoretical throughput in TCP layer with conventional and ZigZag antenna configuration in single straight/curve/slope road scenarios

single straight road scenario, the minimum throughput with ZigZag antenna configuration is 1.155 Gbps when $d^2_{\mathrm{EF}} = 30$ m and $d^1_{\mathrm{EF}} = 29.5$ m at $h = 0.95$ m. The throughputs in the horizontal curve and slope scenarios always maintain 1.25 Gbps. These simulation results mean that the throughput with ZigZag antenna configuration can mitigate the effect of co-channel interference and support more than 1 Gbps required data rate.

Therefore, it is concluded that using ZigZag antenna configuration can significantly mitigate the impact of co-channel interference caused by ground reflections and improve the throughput, which keeps higher than the required data rate regardless of the arbitrary inter-vehicle distance and different road scenarios.

3.5 Outdoor Experiment

To demonstrate the performance of the proposed ZigZag antenna configuration, an outdoor experiment is carried out. The experiment is conducted in a single straight road because it suffers from the strongest co-channel interference caused by the ground reflection based on the analysis in Fig. 3.5. In the single straight road, when d^1_{EF} is equal to d^2_{EF}, the value of throughput decreases most drastically. Therefore, the scenario of three vehicles driving in a single straight road with equal inter-vehicle distance is considered in this experiment as shown in Fig. 3.7. Note that $d_{\mathrm{tr}} = 1.6$ m represents ZigZag antenna configuration while $d_{\mathrm{tr}} = 0$ represents conventional antenna configuration.

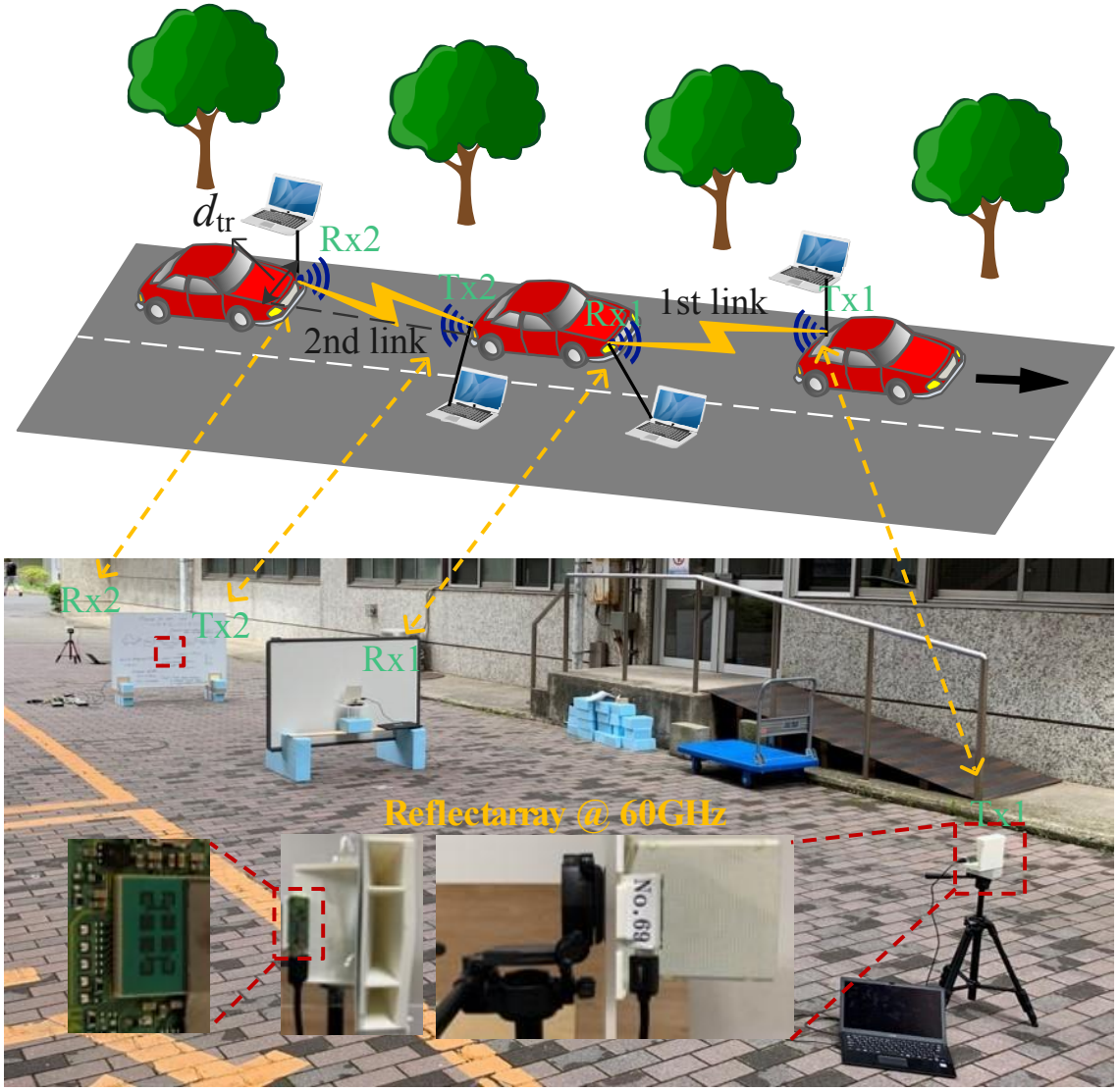

Figure 3.7: Experiment scenario of mmWave V2V communications with relay

Two spaced whiteboards, of which the setting parameters are almost the same as the spec of Toyota Yaris [47]. The width and length of the whiteboards are 1.1 m and 1.64 m, respectively. The distance between two whiteboards is set to 4.35 m, equal to the length of a Toyota Yaris. Two whiteboards were erected perpendicular to the ground at a distance of 0.14 m from the ground. This imitates the height of the actual vehicle's chassis from the ground. Besides, two whiteboards are used to mimic the front and back of a vehicle because signals cannot penetrate them.

The 60 GHz reflectarray antenna is used in this measurement that is composed of a 2×4 antenna array and a reflective surface as shown in Fig. 3.8. The 2×4 antenna array is a feeding antenna that generates the 60 GHz mmWave. The reflection surface consists of multiple unit cells. These unit cells are usually backed by a ground plane, and the incident wave reflects off them towards the direction of the beam. Fig. 3.9. The half power beam widths in horizontal and vertical planes are 6 and 10 degrees. Besides, the other parameters of this 60 GHz reflectarray antenna are summarized in the Table 3.2. According to the previous chapter's analysis of the influence of antenna height on co-channel interference, four 60 GHz reflectarray antennas are set to the same height of 0.95 m by tripods.

About the polarization of the reflectarray, the direction of electrical field ($\overrightarrow{E}$) is always along to X axis. When the antenna is placed as shown in Fig. 3.10 (a), the ground incident wave is horizontal polarization wave and wall incident wave is vertical polarization wave. If the antenna is rotated 90 degrees clockwise as shown in Fig. 3.10 (b), the ground incident wave is vertical polarization wave and wall incident wave is horizontal polarization wave.

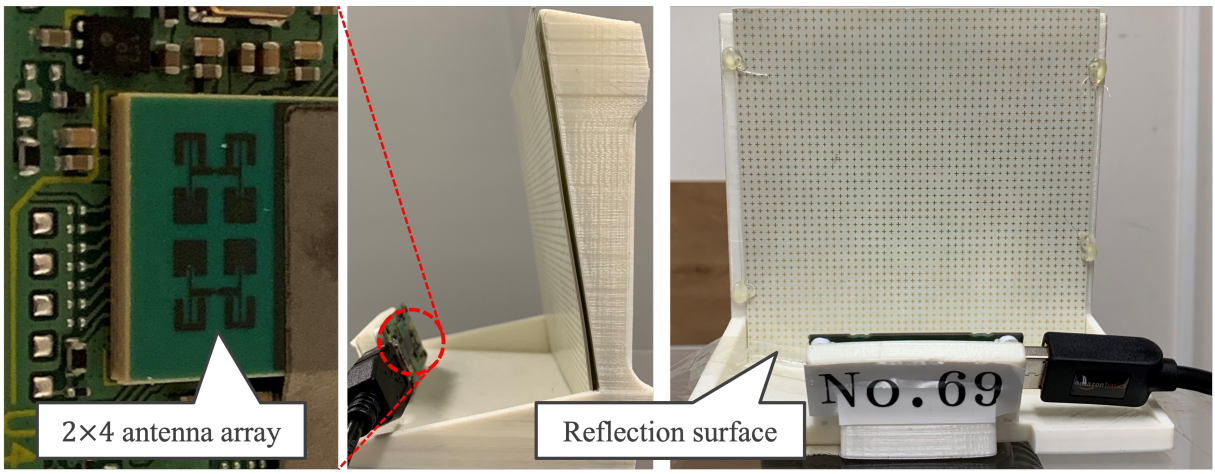

Figure 3.8: Experiment device of 60 GHz reflectarray

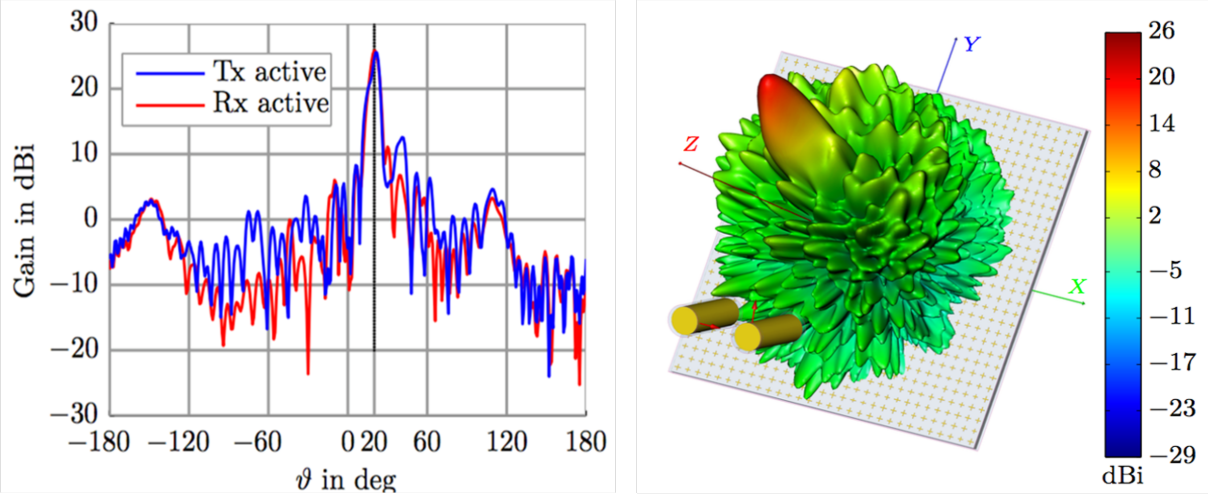

Figure 3.9: Radiation pattern of 60 GHz reflectarray

To reduce the co-channel interference caused by ground reflection [37], the vertical polarization of the antenna is set in the vertical plane because the reflection coefficient of using a vertical polarization antenna is lower than that of using a horizontal polarization antenna. This requires the reflectarray antenna to be rotated 90 degrees in the placement state shown in Fig. 3.8.

Parameters	**Value**
Frequency	60 GHz
Support channel	2, 3
Transmit power	10 dBm
Half power beam width in vertical plane	10 degrees
Half power beam width in horizontal plane	6 degrees
Antenna gain	26 dBi
Support MCS Index	1-9
Beam control	Mechanical control

Table 3.2: Parameters of 60 GHz reflectarray

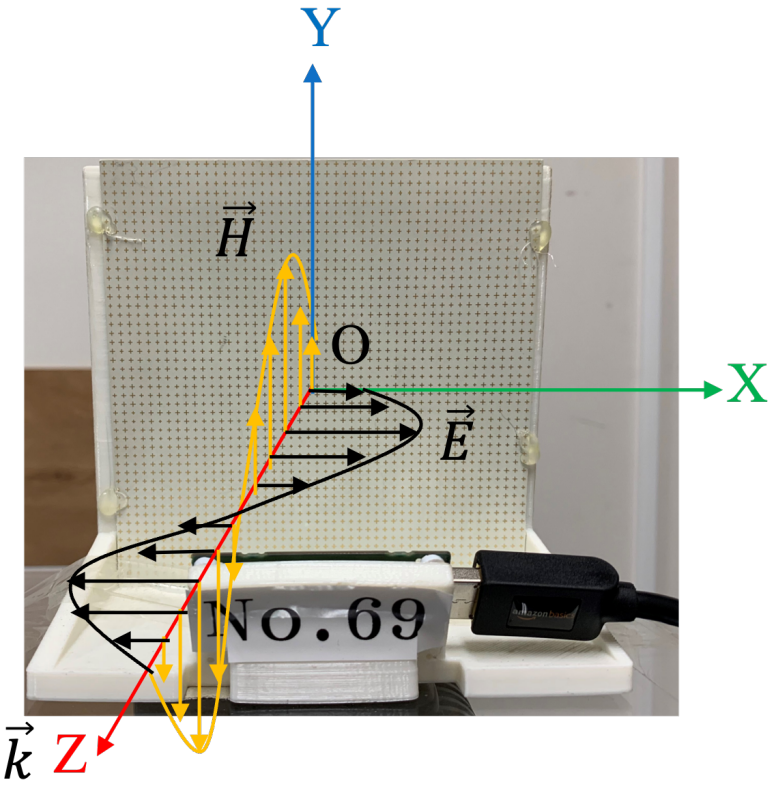

(a) horizontal placement

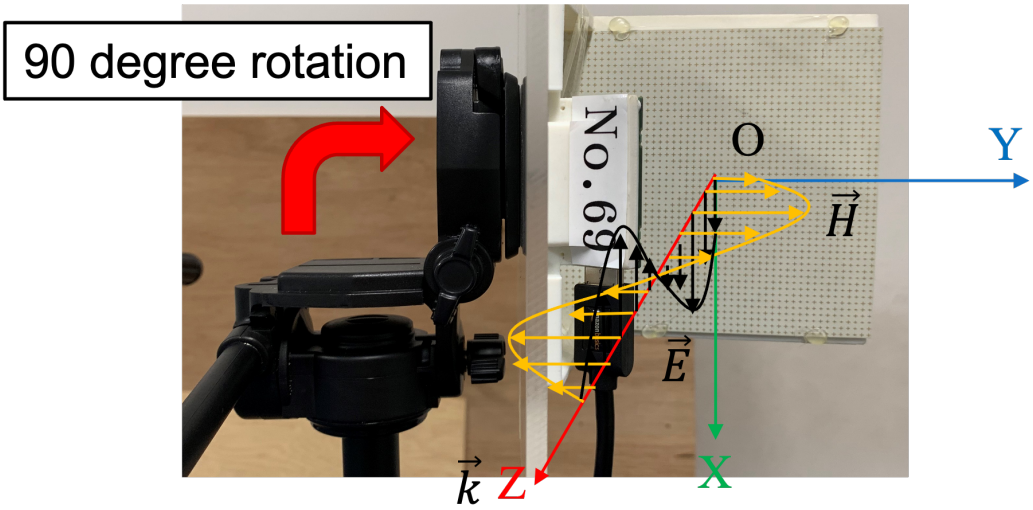

(b) 90 degrees rotation

Figure 3.10: Antenna polarization

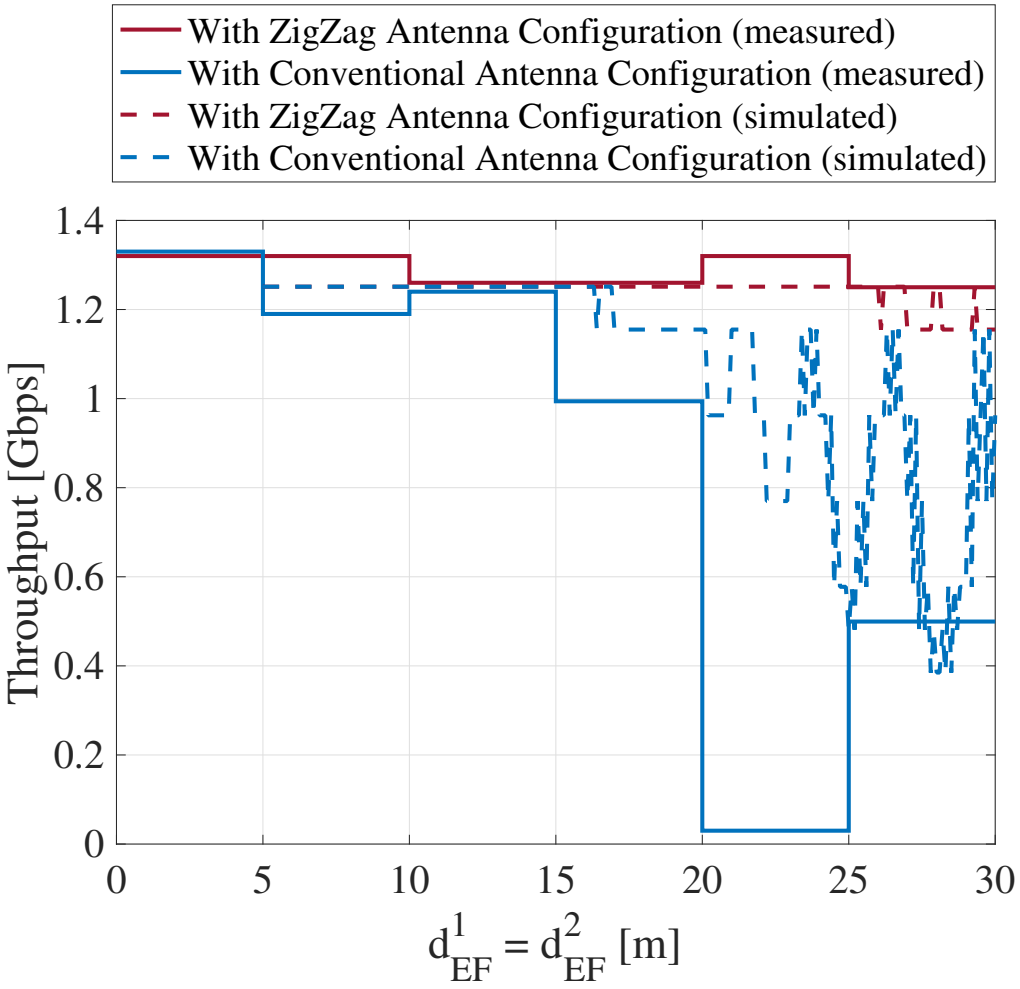

Figure 3.11: Comparison between measured and simulated throughputs with ZigZag and conventional antenna configurations

In the experiment, V2V throughputs of the first link and the second link are measured by two pairs of iperf3 Client/Server [48]. TCP messages are transmitted simultaneously in the same channel. Fig. 3.11 compares the simulated and measured throughputs of the second mmWave V2V link in TCP layer with conventional and ZigZag antenna configurations. It can be seen that after the inter-vehicle distance exceeds 20 m, the measured throughput is lower than 1 Gbps with conventional antenna configuration. That means that conventional antenna configuration cannot support the requirement when the inter-vehicle distance is larger than 20 m. Instead, with ZigZag antenna configuration, the measured throughput shows significant improvement. It remains above 1.2 Gbps at all inter-vehicle distances, which indicates that ZigZag antenna configuration can achieve over 1 Gbps sensor data sharing via mmWave V2V communications. Since the results from the measurement match with those from the simulations to a large extent, the effectiveness of ZigZag antenna configuration to mitigate the co-channel interference in mmWave V2V communications is demonstrated in natural environments.

In reality, to deploy the ZigZag antenna configuration, each vehicle should be equipped with two pairs of antennas on the left and right sides. This proposed ZigZag antenna configuration focuses on the basic multi-hop relay system, where only two links are connected simultaneously. When more than two links need to be connected simultaneously, the link with ZigZag antenna configuration is established sequentially. It means that if the first V2V link is established, the following antenna side is automatically selected by the first Ego vehicle in Fig. 2.3. Chapter 4 conducts more in-depth research and formulates detailed protocols to establish ZigZag antenna configuration with an arbitrary number of mmWave V2V links.

3.6 Conclusion

This chapter firstly described the features of the ZigZag antenna configuration in mmWave V2V communications with relay. It then explained the principle of co-channel interference mitigation with this novel antenna configuration. Next, we compared the performance of the proposed method with that of conventional antenna configuration by the simulation based on standard IEEE 802.11ad and showed the superiority of the proposed method on co-channel interference mitigation and E2E throughput improvement. The simulation results revealed that the ZigZag antenna configuration significantly suppresses the co-channel interference. Therefore, it is capable of supporting more than 1 Gbps required data rate regardless of the

arbitrary inter-vehicle distance and different road scenarios over mmWave V2V communications. Finally, we demonstrated the effectiveness of ZigZag antenna configuration by outdoor experiments.

Chapter4

Distributed and Scalable Radio Resource Management for mmWave V2V with Relays

As explained in Chapter 1, most road scenarios contain multiple vehicles. It means that multiple mmWave V2V links are connected at the same time to service multiple vehicles. Therefore, an efficient radio resource management scheme is essential to ensure the scalability of mmWave V2V relays communications. However, mmWave V2V communications confront intractable scalability challenges due to the co-channel inter-link interference. To overcome such limitations, this chapter firstly analyzes the required data rate ensuring maneuver safety via mmWave V2V relays in an overtaking traffic scenario. Based on these preparations, we propose a distributed radio resource management scheme that integrates spatial, frequency, and power domains for two transmission ranges (short/long). In the spatial domain, ZigZag antenna configuration is utilized to mitigate the co-channel interference, which plays a decisive role in the short inter-vehicle distance. In frequency and power domains, two resource blocks are allocated alternately, and transmit power is controlled to suppress the co-channel interference, which has a decisive impact on co-channel interference mitigation in the long inter-vehicle distance. Finally, we compare the achievable E2E throughput with the required data rate for all vehicles and show the superiority of this proposed radio resource management scheme.

4.1 Motivation

To support advanced V2V use cases [1, 3], exchanging raw sensor data is necessary, which poses demanding requirements on V2V [49]. As mentioned before, a data rate over 1 Gbps and end-to-end latency of less than 10 ms per link is the typical requirement for extended sensors [50]. However, these requirements do not have an explicit description of considering safety of automated driving. To meet the same high-level safe driving requirements in different road scenarios, the amount of transmitted data required is different. If the radio resource can be allocated based on the required data rate in different situations, the high-level safe driving requirements not only are satisfied, but also the radio resource can be saved. For this purpose, we firstly analyze the required data rate considering driving safety in mmWave V2V communications with relays at different inter-vehicle distances and vehicle speeds in an overtaking traffic situation, which is the basis for radio resource management.

To satisfy the required data rate at Gbps level, having large continuous spectrum resources, mmWave becomes a promising frequency band to support such high data rate V2V communications. For example, the IEEE 802.11bd [51] is being specified to adapt to advanced V2X applications, assuring backward compatibility with IEEE 802.11p [7] and IEEE 802.11ad [14]. Its peak data rate will be higher than 6.75 Gbps. NR-V2X [12,15] is also being specified by 3GPP with the peak data rate of 20 Gbps.

Wireless communications in the mmWave band experience a higher signal attenuation and blockage than conventional frequency bands such as 760 MHz and 5.9 GHz. Although high-gain directional antennas and multi-hop relaying are employed to cope with the blockage, many other challenges remain such as the scalability of V2V topology and co-channel interference management. To the best of our knowledge, most related works about mmWave radio resource management are so far limited to beam allocation and alignment [25, 52, 53]. All of them study single-hop mmWave V2V link scenarios. Chapter 3 proposed a ZigZag antenna configuration to mitigate the co-channel interference among mmWave V2V relay links [54]. Although it can maintain the throughput over 1 Gbps by reusing a single channel, this spatial resource control was only suitable for two mmWave V2V links and short inter-vehicle distance. It becomes one of the critical issues to design scalable radio resource management for mmWave V2V relays.

In addition, a dynamic V2V topology formed by high mobility vehicles requires a fast resource management mechanism. It can be divided into two types: centralized and distributed

radio resource controls. The centralized one is more reliable. For instance, Mei *et al.* and Ashraf *et al.* proposed the centralized resource allocation schemes for Long Term Evolution V2V communications systems to guarantee reliability requirement [32,33]. Gao *et al.* targeted the energy efficiency and proposed a centralized power control and resource allocation for V2V communications [34]. These centralized radio resource management schemes have high control latency, high uplink transmission cost and cannot work out of coverage of the central node. By contrast, distributed radio resource control can reduce the control latency and work even out of coverage. However, existing distributed schemes mainly adopt IEEE 802.11p as an access layer, which cannot support services that require data rate over 1 Gbps [35, 36]. Crucially, the collision of resource utilization becomes inevitable as the traditional carrier sense multiple access with collision avoidance strategy suffers from its low efficiency. Therefore, the design of distributed radio resource mechanisms in dynamic vehicular scenarios to reduce the control latency and avoid the collision of resource utilization is another essential issue.

To cope with the above two issues, this chapter proposes a distributed radio resource management scheme for a scalable mmWave V2V relay topology. Our proposal aims to ensure that the achievable end-to-end (E2E) throughput satisfies the required data rate for all vehicles in overtaking scenario. It is noteworthy that, in this proposal, individual nodes have autonomy in resource management rather than relying on the global knowledge from a centralized control node, rapidly adapting to the dynamics of mmWave V2V communications.

The main contributions of this work are outlined as follows:

1) The required data rate considering driving safety is analyzed in mmWave V2V communications with relays at different inter-vehicle distances and vehicle speeds in an overtaking traffic situation, which is the basis for radio resource management.

2) A distributed radio resource management scheme is proposed to ensure mmWave V2V relaying topology scalability. First, ZigZag antenna configuration is employed in the spatial domain to mitigate the inter-link co-channel interference impact caused by the reuse of RBs. Further, in frequency and power domains, two transmission modes (Mode 1 and Mode 2) are defined according to the inter-vehicle distance and are switched based on the required data rate for each V2V link. The full available bandwidth is divided into two RBs, called $\{RB_1, RB_2\}$ respectively. In mode 1, all bandwidth is used for the current V2V link. In mode 2, one of RB_1 and RB_2 is selected for the current V2V link. If continuous V2V links are in the same mode, RB_1 and RB_2 are alternately allocated

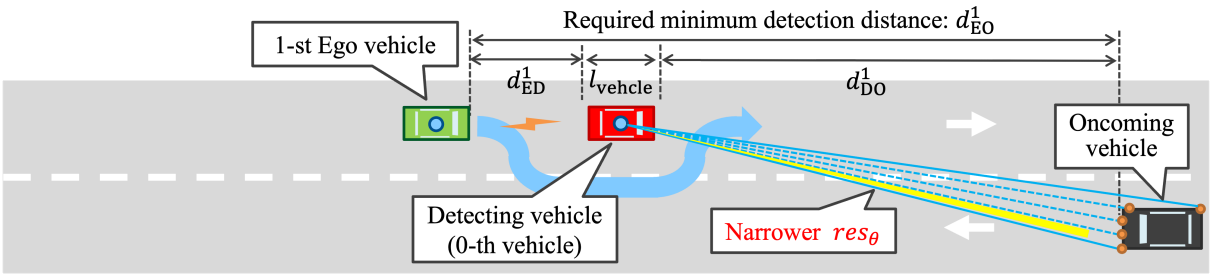

(a) Single-hop case: Oncoming vehicle is far from Detecting vehicle that requires higher data rate for LiDAR with narrower (original) resolution

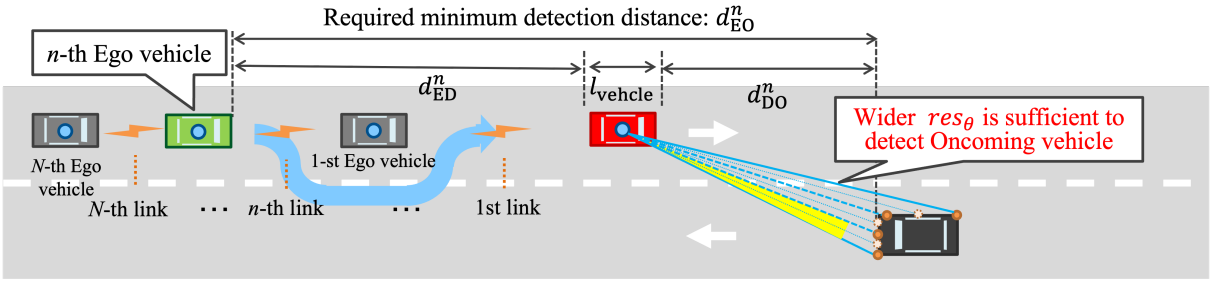

(b) Multi-hop case: Oncoming vehicle is closer to Detecting vehicle where lower data rate is sufficient for LiDAR with wider (down sampled) resolution

Figure 4.1: MmWave V2V relays with extended sensors in overtaking traffic situation

for each V2V link in a ZigZag manner.

Theoretical analysis and simulation verify the effectiveness of the proposed scheme that can guarantee the achievable E2E throughput higher than the required data rate for all vehicles in overtaking scenario.

4.2 Required Data Rate of Extended Sensors

This section defines the overtaking scenario with multiple Ego vehicles and theoretically analyzes the required data rate for safe automated driving. Then, the supposed V2V relay scheme is described where rate control (down sampling) is introduced as a mechanism to match the data rate with corresponding requirements during multi-hop relay. Finally, some numerical examples reveal the required data rate with different speeds of the Ego vehicle and inter-vehicle distances.

4.2.1 Overtaking Scenarios

Although the original study of safe overtaking by cooperative perception was introduced in [49], it only analyzed a fundamental setup of cooperative perception in the case with a single Ego vehicle and a single V2V link as shown in Fig. 4.1 (a). In practical traffic scenarios, there are usually more than two vehicles. This paper bridges this gap by extending the situation to multiple Ego vehicles and multiple mmWave V2V links as shown in Fig. 4.1 (b). This study considers the overtaking traffic situation in a straight two-lane road with width w_{lane}. $N+1$ vehicles, equipped with a LiDAR, are running in the middle of their lanes. Let the 0-th vehicle be the Detecting vehicle and following n-th ($n \in \{1, \ldots, N\}$) Ego vehicles are trying to achieve safe overtaking by avoiding collision with the Oncoming vehicle. Since the perception of each Ego vehicle is blocked by its front vehicles, the Ego vehicle requests the LiDAR data on the Detecting vehicle to perform cooperative perception. The rate of exchanging raw sensor data for safe overtaking is defined as the required data rate.

To achieve safe overtaking, the n-th Ego vehicle must detect the Oncoming vehicle at the minimum distance from itself. Otherwise, the Ego vehicle will collide with the Oncoming vehicle during overtaking. Here this minimum distance is called required minimum detection distance d^n_{EO} as shown in Fig. 4.1. This required minimum detection distance is defined as the sum of the individual required braking distances of Ego vehicle (n-th vehicle) and Oncoming vehicle for collision avoidance in the overtaking scenario like $d^n_{\text{EO}} = 0.039 \times \frac{{v^n_e}^2 + {v_o}^2}{3.4}$ [49], where v^n_e and v_o are speeds of n-th Ego vehicle and Oncoming vehicle respectively. It shows that v^n_e and v_o are the hidden parameters that determine the required d^n_{EO}. This study assumes all Ego vehicles and the Oncoming vehicle are traveling at the same speed ($v_o = v^n_e = v_e, n \in \{1, \ldots, N\}$), so the required minimum detection distances of all Ego vehicles are same $d^n_{\text{EO}} = d_{\text{EO}}, n \in \{1, \ldots, N\}$.

Note that the required data rate is derived under the extreme condition of safe stop to avoid collision between the Ego vehicle and the Detecting vehicle. This extreme condition is: the n-th Ego vehicle can brake safely to avoid collision with the Oncoming vehicle when it manages to overtake the Detecting vehicle. In reality, it has difficulty overtaking the Detecting vehicle at once. However, if the derived required data rate in this extreme condition ensures a safe stop, that means the n-th Ego vehicle can also safely stop when it wants to overtake any intermediate vehicle between itself and the Detecting vehicle.

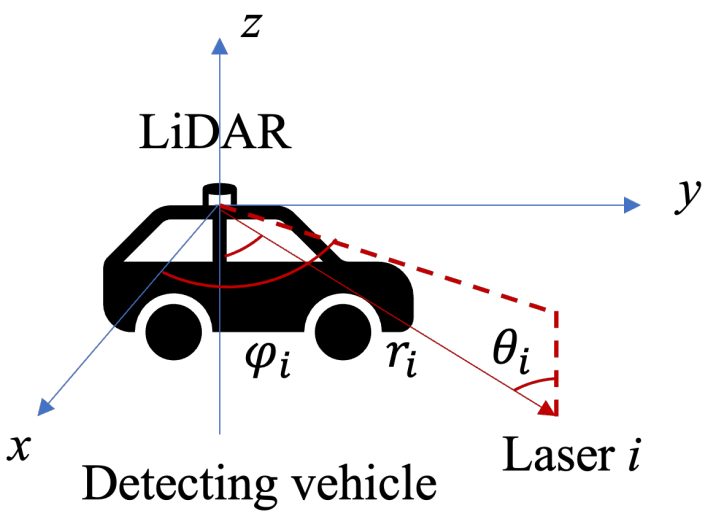

Figure 4.2: The coordinate of LiDAR on the Detecting vehicle

4.2.2 Required Data Rate for Extended Sensors

Figure 4.1 presents simplified examples of V2V relay-based Oncoming vehicle detection to provide an intuitive understanding of required data rates. In the single-hop case of Fig. 4.1 (a), i.e., $n = 1$, the 1st Ego vehicle can detect the Oncoming vehicle with the assistance of the front Detecting vehicle. Multi-hop case is shown in Fig. 4.1 (b). In front of the n-th Ego vehicle, several relay vehicles follow the Detecting vehicle. Each Ego vehicle attempts overtaking the front vehicle. Under the premise of equal required minimum detection distance d^n_{EO}, the Detecting vehicle is relatively close to the Oncoming vehicle compared with the single-hop case. Hence, LiDAR can recognize it even with wider angular resolution; point cloud data can be down sampled, reducing the required data rate. To rephrase, the required data rate is inversely proportional to the Ego-Detecting vehicle distance, d^n_{ED}. Its detailed definition is described below.

A coordinate system is established with the position of LiDAR on the Detecting vehicle as to the origin as shown in Fig. 4.2. The position of each laser point (i.e. laser i) can be expressed as $r_i \times [\sin\theta_i \cos\phi_i, \sin\theta_i \sin\phi_i, \cos\theta_i]$, where i is the index of laser beam, r_i is the distance between origin and laser point on the obstacles, θ_i is the angle between the laser beam and the negative z-axis, ϕ_i is the angle between the laser beam and the positive x-axis. Therefore, the geometric model of LiDAR can be created as shown in Fig. 4.3. The point cloud model of the vehicle surface is then imported into the coordinate system. In

this figure, $(0, 0, 0)$ is the position of LiDAR on the Detecting vehicle. Blue points represent the vehicle model of the Oncoming vehicle, and red points represent the laser points from LiDAR detecting the Oncoming vehicle. In the scenario of this paper, only the side surface near the LiDAR, the roof, and the front surface of the Oncoming vehicle can be detected by the Detecting vehicle; only these three surfaces are taken into consideration. Let the number of detected points by the LiDAR denote N_{detected}, and the total number of points of vehicle model is N_{vehicle}. Their relationship S_n, is expressed as

$$S_n = \frac{N_{\text{detected}}(d^n_{\text{DO}}, res_\theta, res_\phi)}{N_{\text{vehicle}}}, \tag{4.1}$$

where $d^n_{\text{DO}} = d^n_{\text{EO}} - d^n_{\text{ED}} - l_{\text{vehicle}}$ in Fig. 4.1. Based on the assumptions in Sect. 4.2.1, v^n_e is the hidden parameter that determines the required d^n_{EO}. d^n_{DO} can be substituted with d^n_{ED} and v^n_e in Eq. (4.1), which is rewritten as

$$S_n = \frac{N_{\text{detected}}(d^n_{\text{ED}}, v^n_e, res_\theta, res_\phi)}{N_{\text{vehicle}}}, \tag{4.2}$$

where res_θ and res_ϕ are the angular resolution in vertical and horizontal planes respectively. When v^n_e and d^n_{ED} are given, N_{detected} can be changed by adjusting the angular resolution res_θ and res_ϕ. Since N_{vehicle} is fixed, P_n can be changed by adjusting the angular resolution res_θ and res_ϕ. This paper assumes that LiDAR on the Detecting vehicle can detect and identify the Oncoming vehicle when $S_n \geq 90\%$. Meanwhile, res^n_θ and res^n_ϕ are recorded and used to calculate the required data rate of n-th vehicle according to Eqs. (4.3) and (4.4).

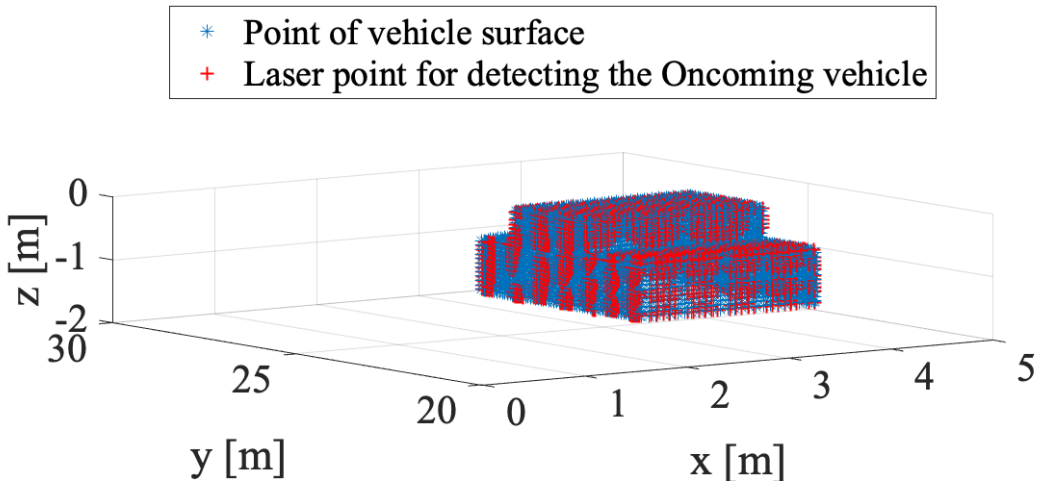

(a) $S_n(d^n_{\text{DO}} = 20m) \geq 90\%$

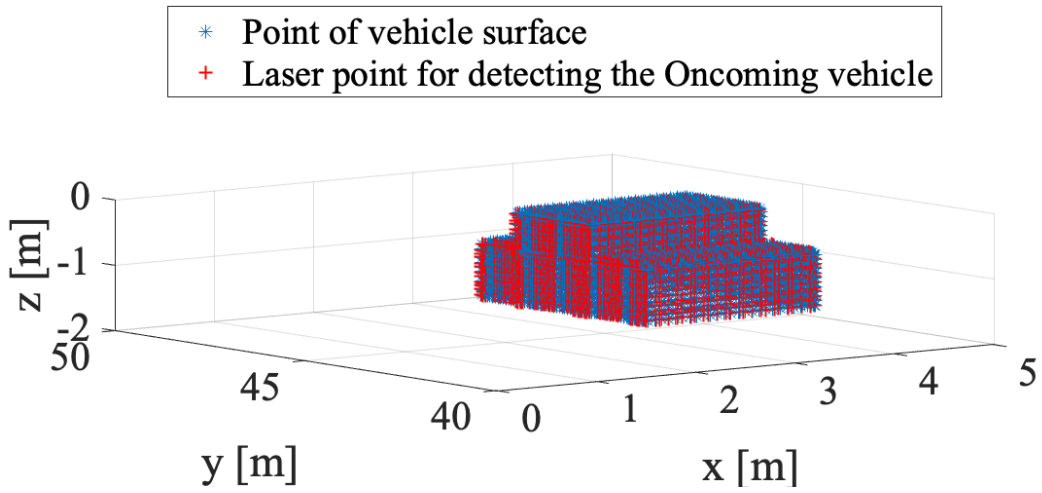

(b) $S_n(d^n_{\mathrm{DO}} = 40m) \geq 90\%$

Figure 4.3: Model for detecting Oncoming vehicle by LiDAR on the Detecting vehicle

$$\{res^n_\theta, res^n_\phi\} = \arg\min S_n(res_\theta, res_\phi | v^n_e, d^n_{\mathrm{ED}}) \geq 0.9 \tag{4.3}$$

$$R^n_{\mathrm{req}} = f_{\mathrm{scan}} B_{\mathrm{laser}} \left(\left\lfloor \frac{\Theta}{res^n_\theta} \right\rfloor + 1 \right) \left(\left\lfloor \frac{\Phi}{res^n_\phi} \right\rfloor + 1 \right) \tag{4.4}$$

where f_{scan} is scan frequency of LiDAR, B_{laser} is the number of bits per laser, Θ and Φ are the angular scan range in horizontal and vertical planes respectively.

4.2.3 V2V Relay Communications

In the topology of V2V communications with relays, vehicles are important nodes to forward required data with a receiver and a transmitter at the front and rear respectively. Each node has two roles in the network: one is an Ego vehicle performing cooperative perception with the received information from the previous node, and the other is a relay node simply forwarding the information to the next node. Such receiving and relaying actions are the basic mechanism in V2V communications with relays. In relay networks, the E2E throughput is the minimum cut of link throughputs as $\Gamma_n = \min\{\gamma_j\}, j \in \{1, \ldots, n\}$, where Γ_n represents the E2E throughput between the n-th vehicle and the Detecting vehicle, and γ_j is the throughput of the j-th V2V link. In addition, the throughput of a single V2V link depends on the inter-vehicle distance in the assumed scenarios.

Parameters	**Value**
Width of lane (w_{lane})	3.2 m
Length of vehicle (l_{vehicle})	4.35 m
Width of vehicle (w_{vehicle})	1.69 m
Height of vehicle (h_{vehicle})	1.48 m
Height of metal body of vehicle (h_{mb})	1.1 m
Chassis clearance	0.14 m
Height of LiDAR (h_{l})	1.6 m
FOV (vertical)	30 degree ($\pm$15 degree)
FOV (horizontal)	180 degree
Scan frequency (f)	20 Hz
Number of bits per laser (B_{laser})	28 bits
Number of points of vehicle surface (N_{vehicle})	2615

Table 4.1: Simulation parameters for LiDAR detection

It is necessary to apply the rate control (down sampling) to each node based on the required data rate. As stated in Sect. 4.2.2, the required data rate is proportional to the Detecting-Oncoming vehicle distance while inversely proportional to the Ego-Detecting vehicle distance. This strategy can save the spectrum usage and is quite reasonable for the relay-based V2V cooperative perception where transmission capacity diminishes with hop counts.

4.2.4 Numerical Examples

Simulation analysis is implemented with the parameters listed in Table 4.1. The FOV in vertical and horizontal plane are $\pm$15 degrees and 360 degrees based on the spec of Velodyne LiDAR VLP-16 [55]. In this simulation, the FOV in horizontal plane is assumed to be 180 degrees since the LiDAR only needs to detect the obstacle ahead in overtaking traffic scenarios.

Figure 4.4 shows the required data rate of V2V relay communications with various v_e and d_{ED}. For each vehicle speed v_e, the required data rate will decrease as the Ego-Detecting vehicle distance d_{ED} increases. For instance, when v_e is 80 km/h (blue line in Fig. 4.4), the required data rate decreases from 5.403 Gbps to 0.049 Gbps as d_{ED} increases from 1 m to 130

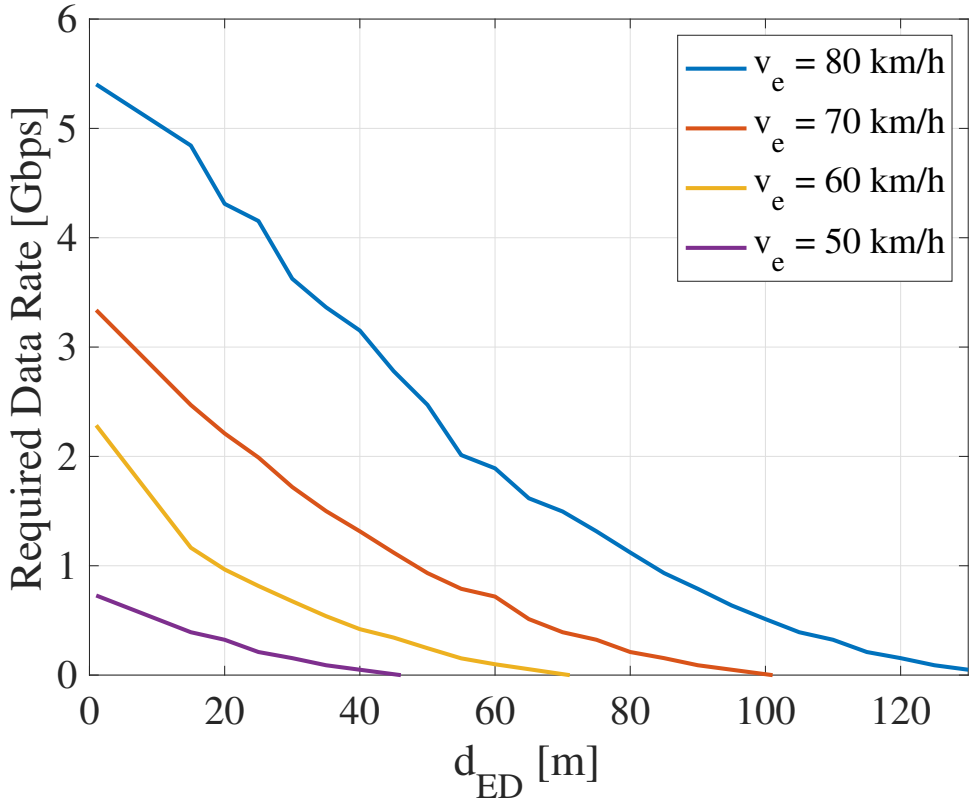

Figure 4.4: Required data rate of mmWave V2V relays ($d_{\mathrm{ED}} \in (0, 130]$ m, $v_e \in [50, 80]$ km/h)

m. For each d_{ED}, with increasing the vehicle speed, the required data rate also grows. When d_{ED} is equal to 20 m, the required data rate is increased from 0.323 Gbps to 4.31 Gbps as the vehicle speed rises from 50 km/h to 80 km/h. These tendencies of the required data rate are referred to as the basis of resource management.

4.3 Basic Concept of Distributed Radio Resource Management Scheme

MmWave communications have weak penetration, they are easily blocked by surrounding obstacles. It is a well-known drawback and barrier to the development of mmWave communications. Meanwhile, this feature can be leveraged for co-channel interference mitigation and spectrum reuse. A single mmWave channel can potentially be used by all V2V links in V2V communications with relays. Chapter 3 has conceived ZigZag antenna configuration to

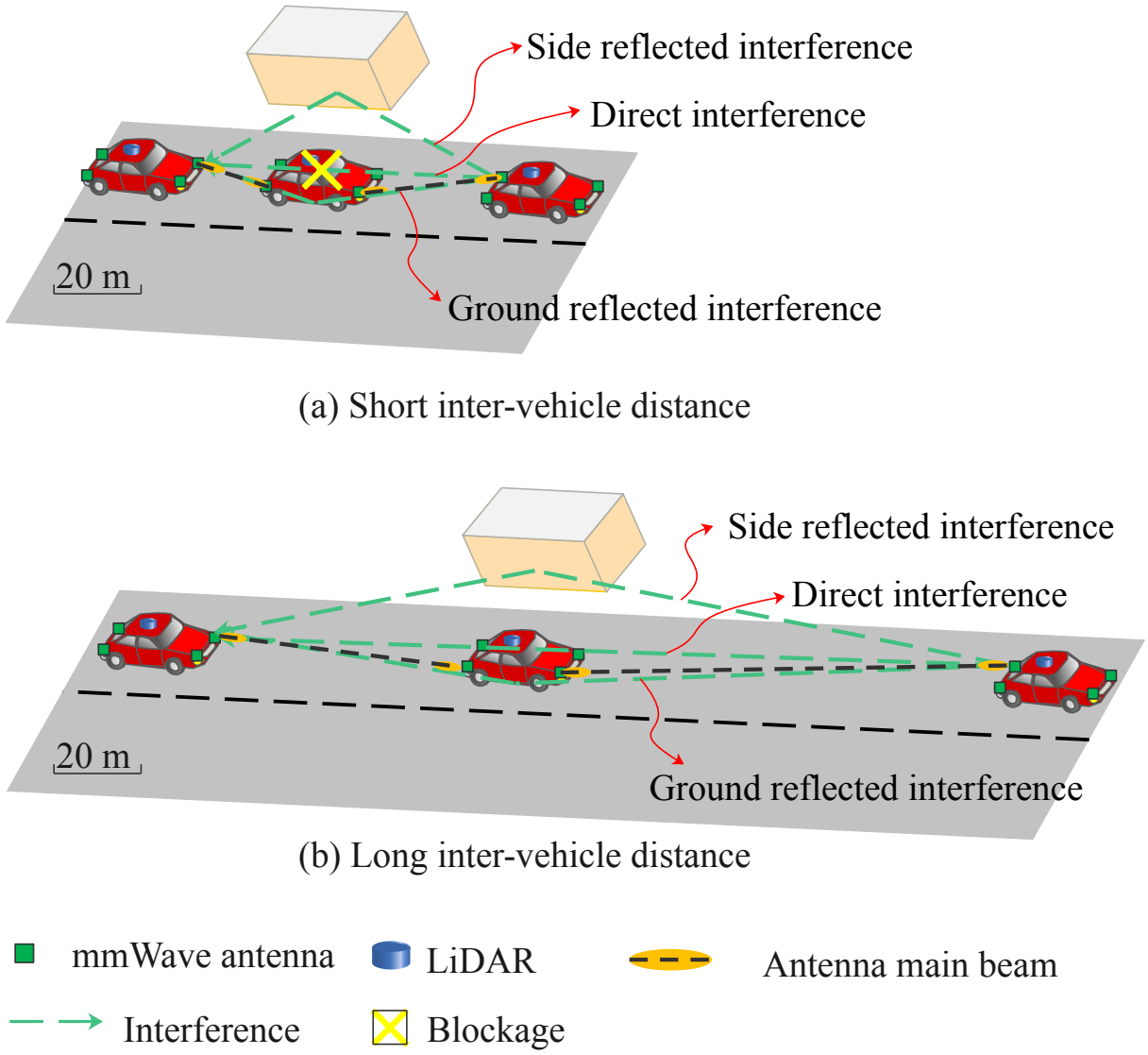

Figure 4.5: Diagram of ZigZag antenna configuration in short and long inter-vehicle distance scenarios

mitigate the co-channel interference. The scenario in Chapter 3 has two features as drawn in Fig. 4.5 (a): (1) two mmWave V2V links are connected at the same time by reusing a single mmWave channel, (2) it merely evaluates mmWave V2V performance with short inter-vehicle distance from 10 m to 30 m. In this context, the direct interference can be completely blocked by the front vehicle from the field of view of the third vehicle. Besides, the reflected interference paths from the ground and side objects are effectively suppressed thanks to the ZigZag antenna configuration. The intrinsic principle is to increase the angle between each

reflected interference path and the antenna main beam. This increased angle can reduce the antenna directivity of each reflected interference path. Eventually, the total received power of co-channel interference can be reduced.

However, in the case of long inter-vehicle distance as depicted in Fig. 4.5 (b), the direct interference may not be entirely blocked by the front vehicle. Moreover, it is difficult to avoid the reflected interference even by the ZigZag antenna configuration. The angle between each reflected interference path and the antenna main beam becomes extremely small at a long inter-vehicle distance. Therefore, the reflected interference is received with almost the same power as the desired signal. To satisfy the required data rate in the case of long inter-vehicle distance, co-channel interference mitigation again becomes a critical challenge.

To cope with this problem, we propose a distributed resource management scheme. The whole bandwidth is divided into two RBs and allocated to each link based on the inter-vehicle distance. The required data rate decreases with the increase of inter-vehicle distance under the same vehicle speed. It is because the Ego-Detecting vehicle distance, d_{ED}, is also lengthened. In the case of short inter-vehicle distance, all RBs are allocated to support the high required data rate for each V2V link. ZigZag antenna configuration is deployed to mitigate the co-channel interference when all RBs are reused. On the other hand, in the case of long inter-vehicle distance, divided RBs are alternately allocated to each V2V link in a ZigZag manner which can avoid inter-link co-channel interference. If inter-vehicle distances are equal, RB allocation in a ZigZag manner can avoid co-channel interference; especially, the interference caused by ground reflection can be completely eliminated. Otherwise, parameters such as the transmit power of each RB should be controlled to mitigate the co-channel interference at an arbitrary inter-vehicle distance.

Combining resource management in spatial (ZigZag antenna configuration), frequency (resource block allocation), and power (transmit power control) domains can reduce the overall co-channel interference independent of the inter-vehicle distance. It can enhance the achievable E2E throughput in mmWave V2V relay link that can always satisfy the required data rate.

4.4 Definition of Two Transmission Modes

Based on the basic concept, two transmission modes are defined to support all V2V links. Figure 4.6 shows the definition of two transmission modes determined by the inter-vehicle

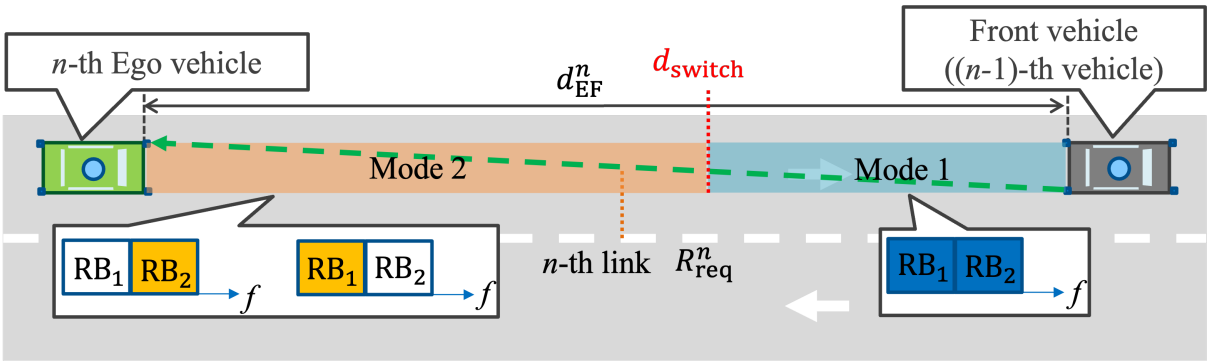

Figure 4.6: Regions and RBs allocation corresponding to two transmission modes

distance. In this figure, the n-th Ego vehicle requests the raw data from the $(n-1)$-th Front vehicle. d^n_{EF} is the straight-line distance between the front of the Ego vehicle and the rear of the Front vehicle, and their communication link is represented as the n-th link. R^n_{req} is the required data rate of the n-th Ego vehicle. The proposed scheme aims to ensure that the achievable E2E throughput of the n-th vehicle (Γ_n) is always higher than R^n_{req}. Antennas are installed on the four corners of each vehicle, as drawn in the figure. Front Antennas are receivers, and rear antennas are transmitters. This antenna installation is used to deploy ZigZag antenna configuration to mitigate co-channel interference, especially in the case of short inter-vehicle distance. Then, the inter-vehicle distance can be divided into two regions (colored blue and orange). The transmission mode is designed for each region called Mode 1 and Mode 2. Let d_{switch} denote the threshold of switching between Mode 1 and Mode 2, which will be optimized based on the required data rate. As a prerequisite, the maximum supported throughput with a full-bandwidth allocation should be higher than the maximum required data rate. For example, 5.403 Gbps is the maximum required data rate at 80 km/h in the overtaking traffic scenarios according to Fig. 4.4. It can be satisfied by full-bandwidth allocation as it is under the upper-bound data rate, i.e., 6.75 Gbps. The whole bandwidth is divided into two RBs in the frequency domain, $\{\text{RB}_1$ and $\text{RB}_2\}$ respectively.

When $d^n_{\text{EF}} < d_{\text{switch}}$, the transmission mode of the n-th link adopts Mode 1. Full bandwidth must be allocated to the current V2V link to meet that high required data rate. When $d^n_{\text{EF}} \geq d_{\text{switch}}$, the transmission mode of the n-th link adopts Mode 2. A half of full bandwidth is sufficient because its achievable throughput is already higher than the required data rate in this region. When multiple continuous V2V links are in Mode 2, the allocation of RB_1 and RB_2 is alternant to avoid the co-channel interference.

The transmit powers in Mode 1 and Mode 2 are denoted as p_{Mode1} and p_{Mode2} respectively. They will be optimized to guarantee the E2E throughput to satisfy the required data rate when Mode 1 and Mode 2 are alternating in continuous V2V links.

4.5 Parameters Optimization

With the randomness of inter-vehicle distance, the continuous two V2V links have four combinations of transmission modes: Mode1-Mode1, Mode1-Mode2, Mode2-Mode1, and Mode 2-Mode2. In the case of Mode1-Mode1, ZigZag antenna configuration can mitigate the co-channel interference. In the case of Mode2-Mode2, resource block allocation in the ZigZag manner can be used to avoid co-channel interference. In the case of Mode1-Mode2 and Mode2-Mode1, ZigZag in spatial and frequency domains cannot reduce the impact of co-channel interference effectively, so power control is required to handle such a problem. The objective is to find the minimum required transmit power of two transmission modes. In the case of Mode1-Mode2 and Mode2-Mode1, the minimum required transmit power can ensure that the E2E throughput is always higher than the required data rate. On the other hand, the minimum required transmit power can minimize the co-channel interference to other mmWave V2V links. The problem is formulated as

$$\begin{aligned} \mathbf{\Omega}^* = & \arg\min(p_{\text{Mode1}} + p_{\text{Mode2}}), \\ & \text{s.t. } \Gamma_n \geq R^n_{\text{req}}, 1 \leq n \leq N, \\ & G_{\text{t}}, G_{\text{r}} \leq G_{\max}, \\ & p_{\text{Mode1}}, p_{\text{Mode2}} \leq p_{\max}, \end{aligned} \tag{4.5}$$

where $\mathbf{\Omega}$ is a finite set including combinations of parameters. $\mathbf{\Omega}^* = \{p^*_{\text{Mode1}}, p^*_{\text{Mode2}}, G^*_{\text{t}}, G^*_{\text{r}}, d^*_{\text{switch}}, B^*\}$ represents the optimized parameter values vector. G_{t} and G_{r} are the antenna gains on the transmitter and receiver, respectively. B is the full bandwidth. $p_{\text{Mode1}}, p_{\text{Mode2}}, G_{\text{t}}, G_{\text{r}}, d_{\text{switch}}, B$ are the parameters to be optimized. $G_{\max}, p_{\max}$ represent the constraints, e.g. antenna gain of 47 dBi and transmit power of 10 dBm in the case of 60 GHz band [56].

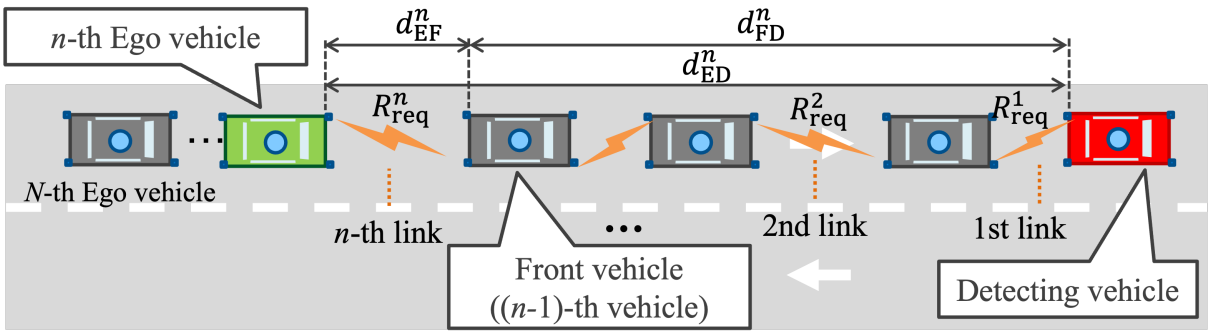

Figure 4.7: The mmWave V2V topology

4.6 Scalability Issue of Distributed Radio Resource Management

Figure 4.7 illustrates the mmWave V2V topology. The n-th Ego vehicle requests resource management for the n-th link to the $(n-1)$-th Front vehicle. The Front vehicle only needs to know the following local information to complete the resource management for the $(n-1)$-th link: (1) d^n_{EF}, (2) the resource block allocation of the $(n-1)$-th link, and (3) the working antenna of the $(n-1)$-th link.

If $d^n_{\mathrm{EF}} < d_{\mathrm{switch}}$, all bandwidth is allocated to the n-th link by the Front vehicle since the Ego vehicle is driving in the region of Mode 1. The transmit power of the n-th link is p_{Mode1}. If $d^n_{\mathrm{EF}} \geq d_{\mathrm{switch}}$, RB_1 or RB_2 is assigned to the n-th link, according to the following condition. If the n-th link is the first V2V link ($n = 1$), RB_1 is allocated to the n-th link. When $n > 1$, if the $(n-1)$-th link uses all bandwidth or RB_2, RB_1 is allocated to the n-th link. If the $(n-1)$-th link uses RB_1, RB_2 is allocated to the n-th link. The detailed workflow is summarized in Algorithm 1. Based on this algorithm, the RB allocation of the n-th V2V link, and the transmit power of the n-th V2V link, P_n, can be derived and allocated to the n-th link by the $(n-1)$-th Front vehicle.

As for the ZigZag antenna allocation of the n-th link, if the left receiver on the Front vehicle is working for the previous $(n-1)$-th link, the left transmitter on the Front vehicle is employed for the n-th link, and vice versa.

Algorithm 1 Distributed Resource Block Allocation Scheme for V2V with relays

Require: $d_{\text{switch}},\ p_{\text{Mode1}},\ p_{\text{Mode2}},\ d_{\text{EF}}^{n}$

Ensure: Resource block allocation of n-th link

Allocated transmit power of n-th link : P_n

if $d_{\text{EF}}^{n} < d_{\text{switch}}$ **then**

n-th link belongs to Mode 1.

n-th link $\leftarrow$ All bandwidth

$P_n \leftarrow p_{\text{Mode1}}$

else

n-th link belongs to Mode 2.

$P_n \leftarrow p_{\text{Mode2}}$

if $n = 1$ **then**

n-th link $\leftarrow \text{RB}_1$

else

if $(n-1)$-th link $\leftarrow$ Mode 1

or $(n-1)$-th link $\leftarrow$ Mode 2 RB_2 **then**

n-th link $\leftarrow \text{RB}_1$

else

n-th link $\leftarrow \text{RB}_2$

end if

end if

end if

return RB allocation result of n-th link , P_n

4.7 Performance Evaluation

Suppose IEEE 802.11ad standard, and here we verify the effectiveness of the proposed scheme for mmWave V2V relay communications. Simulation evaluation assumes a ray-tracing-based propagation channel model. First, the optimized parameters of the two transmission modes with different antenna specs are analyzed. Then, the achievable E2E throughputs under four situations are compared with the required data rate, which demonstrates the effectiveness of our proposed resource control scheme.

4.7.1 Simulation Assumptions

Before showing the simulation result, the following assumptions are emphasized. Detailed parameters are listed in Table 4.2.

- Antennas are located at the center of front and rear of the vehicle under the conventional antenna configuration.
- The transmit power is uniformly distributed to each RB.
- Both ground reflection and surrounding reflection are considered as the main co-channel interference.
- The standard deviation of vertical fluctuation caused by the motor of vehicles is set to 0.0319 m [37] to evaluate the beam alignment error due to the narrow beamwidth.
- The antenna gains on the transmitter and receiver sides are assumed to be same and a general radiation pattern of rectangular aperture antenna is used in this simulation as $G_{\mathrm{t}} = G_{\mathrm{r}} = \frac{4\pi}{\frac{\pi\theta^{\circ}_{\mathrm{HP}}}{180}\frac{\pi\phi^{\circ}_{\mathrm{HP}}}{180}}$, where $\theta^{\circ}_{\mathrm{HP}}$ and $\phi^{\circ}_{\mathrm{HP}}$ are the beamwidth of antennas in the vertical and horizontal planes respectively [57].
- To support the RB allocation, the simulation is analysed based on Orthogonal Frequency Division Multiplex PHY (OFDMPHY). The supported MCS index is 13–24.
- Channel gain of each RB is determined based on the ray-tracing model assuming urban street canyon scenario, which considers ground and wall reflections.
- The throughput of the n-th link depends on β_{nm} and is determined by referring to MCS table.
- The E2E throughput between the n-th Ego vehicle and the Detecting vehicle is the minimum cut of link throughputs as $\Gamma_n = \min\{\gamma_j\}, j \in \{1, \ldots, n\}$.

4.7.2 Co-channel Interference Derivation

For n-th link, $n \in [1, N]$, the received power is given by

$$\mathbf{P}^n_{\mathbf{r}} = [P^{n1}_{\mathrm{r}} \quad P^{n2}_{\mathrm{r}}], \tag{4.6}$$

where p_{r}^{nm} represents the received power of m-th RB for n-th link, which can be calculated based on Eq. (2.11). m is the RB index ($m = 1, 2$).

The resource block allocation matrix of mmWave V2V links (1st link to $(n-1)$-th link) in front of n-th link is defined as

$$\mathbf{X}_{\mathbf{p}}^{n} = \begin{bmatrix} x_{11} & x_{12} \\ x_{21} & x_{22} \\ \vdots & \vdots \\ x_{n-1\ 1} & x_{n-1\ 2} \end{bmatrix}, \tag{4.7}$$

where binary variable x takes 1 or 0 based on the distributed resource block allocation scheme. For example, if RB_1 is allocated to link_1, x_{11} is set to 1 whereas x_{12} is set to 0.

$\mathbf{I}_{\mathbf{p}}^{n}$ is defined as the co-channel interference matrix of n-th link, which is caused by previous mmWave V2V links (1st link to $(n-1)$-th link) when all RBs are assumed to be reused by 1st link to n-th link. $\mathbf{I}_{\mathbf{p}}^{n}$ is given by

$$\mathbf{I}_{\mathbf{p}}^{n} = \begin{bmatrix} I_{11}^{n} & I_{12}^{n} \\ I_{21}^{n} & I_{22}^{n} \\ \vdots & \vdots \\ I_{n-1\ 1}^{n} & I_{n-1\ 2}^{n} \end{bmatrix}, \tag{4.8}$$

where I^n represents the interference of n-th link from each of previous V2V link when each RB is assumed to be reused by this previous V2V link and n-th link. For instance, I_{11}^{n} is the interference of n-th link, which comes from 1st link when RB_1 is used for 1st link and n-th link. Each I^n is calculated according to Eq. (2.9). Therefore, the all co-channel interference of n-th link from 1st link to $(n-1)$-th link can be expressed as

$$\mathbf{I}_n = [I_{n\ 1} \quad I_{n\ 2}] = \|\mathbf{X}_{\mathbf{p}}^{n} \odot \mathbf{I}_{\mathbf{p}}^{n}\|_1, \tag{4.9}$$

where I_{nm} donates the all interference of each RB for n-th link, $\|\cdot\|_1$ stands for the 1-norm of matrix, $\odot$ marks the Hadamard product. Then the SINR of each RB for n-th link can be calculated by

$$\beta_{nm} = \frac{p_{\mathrm{r}}^{nm}}{I_{nm} + \frac{p_{\mathrm{noise}}}{n_{\mathrm{RB}}}}, \tag{4.10}$$

where p_{noise} is the power of additive white Gaussian noise (AWGN) for all RBs that is assumed to be uniform distribution, n_{RB} is the number of RBs. The supported throughput of each RB for n-th link is given by $\mathbf{Y}_n = [y_{n\ 1} \quad y_{n\ 2}]$ that depends on β_{nm} and is determined

Parameters	Value
Number of RBs (n_{RB})	2
Carrier frequency (f)	60 GHz
Height of antenna (h)	1 m
MCS index	13-24
Dielectric constant of asphalt (ψ_{asphalt})	3.9975-j0.2
Dielectric constant of concrete (ψ_{concrete})	4.94-j0.69
Noise figure (NF)	10 dB
Noise power density (N_0)	-174 dBm/Hz
Speed of Ego vehicle (v_e)	80 km/h
Distance between right and left antennas (d_{tr})	1.69 m
Variation of inter-vehicle distance	(0,100] m

Table 4.2: Simulation parameters for V2V relay communications

by referring to MCS table. The resource block allocation matrix of n-th link is defined as $\mathbf{X}_n = [x_{n\ 1} \quad x_{n\ 2}]$. The total throughput of n-th link is written as

$$\Gamma_n = \|\mathbf{Y}_n^T \odot \mathbf{X}_n^T\|_1, \tag{4.11}$$

where $[\cdot]^T$ donates matrix transpose.

4.7.3 Results: Parameters Optimization

First, parameters are optimized based on Eq. (4.5). Here, the required data rate at 80 km/h is selected as a basis of radio resource management. The proposed scheme is still applicable for other vehicle speeds.

According to the analysis in Chapter 2, the worst interference case is in a single straight road with equal inter-vehicle distance. Therefore, this study compares the achievable E2E throughput of Mode 1 and Mode 2 with the required data rate in the worst case to determine the value of d_{switch}. If the optimized d_{switch} can support E2E throughput larger than the required data rate in the worst case, the optimized d_{switch} can also help other situations. It should be noted that the throughput of each mmWave V2V link is maintained or reduced due to the effect of co-channel interference as the hop count increases under the equal inter-vehicle

$G_{\mathrm{t}} = G_{\mathrm{r}}$ (dBi)	p_{Mode1} (dBm)	p_{Mode2} (dBm)
36	-25	-15
34	-20	-7
32	-15	-1
30	-11	4

Table 4.3: Minimum required transmit power of two modes

distance. This means that the E2E throughput from each Ego vehicle to the Detecting vehicle is equal to the throughput between the Ego vehicle and its Front vehicle as $\Gamma_n = \min\{\gamma_j\} = \gamma_n, j \in \{1, \ldots, n\}$ in the situation of equal inter-vehicle distance.

In IEEE 802.11ad, the maximum achievable throughput of a single channel with 2.16 GHz bandwidth at 60 GHz carrier frequency is 6.757 Gbps. To support the maximum required data rate of 5.403 Gbps at 80 km/h, the minimum required full bandwidth can actually be lower than 2.16 GHz. Considering the practical use of this resource management scheme in 60 GHz and facilitating the deployment by fitting the commercialized IEEE 802.11ad standard, the value of 2.16 GHz is kept as the minimum required full bandwidth in this simulation.

Table 4.3 shows the minimum required transmit power of two modes under the different antenna specifications. The range of antenna gain is set to [30, 36] dBi. If the antenna gain is less than 30 dBi, antenna wider beamwidth hinders the effectiveness of co-channel interference suppression using the ZigZag antenna configuration. If the antenna gain is more significant than 36 dBi, too narrow beamwidth reduces the tolerance to vehicle vibration, which causes severe beam alignment errors. Only the antenna gain in this range can ensure the E2E throughput satisfies the required data rate. Therefore, under different antenna specifications within the range of antenna gain, the corresponding minimum required transmit power of two modes can be found by the optimization.

To determine the optimized d_{switch}, the E2E throughputs of Mode 1 and Mode 2 are compared with the required data rate as shown in Fig. 4.8. Because the first V2V link cannot suffer from strong co-channel interference from the front, it is regarded as a particular case. In the distributed resource allocation mechanism, it is easy to identify the first V2V link. Therefore, the parameters such as d_{switch} of the first V2V link are different from other V2V links based on practical applications. Fig. 4.8 (a) shows the comparison between E2E throughput (Mode 1 and Mode 2) and required data rate in the particular case. In this figure,

when $d^1_{\mathrm{EF}} > 39$ m, Γ_1 in Mode 1 is lower than the required data rate of 1st vehicle because of the severe path loss and multipath fading. However, when $d^1_{\mathrm{EF}} > 36$ m, Γ_1 in Mode 2 is higher than the required data rate since the higher transmit power of Mode 2 can compensate for the increased path loss in long inter-vehicle distance. Therefore, for 1st link, possible range

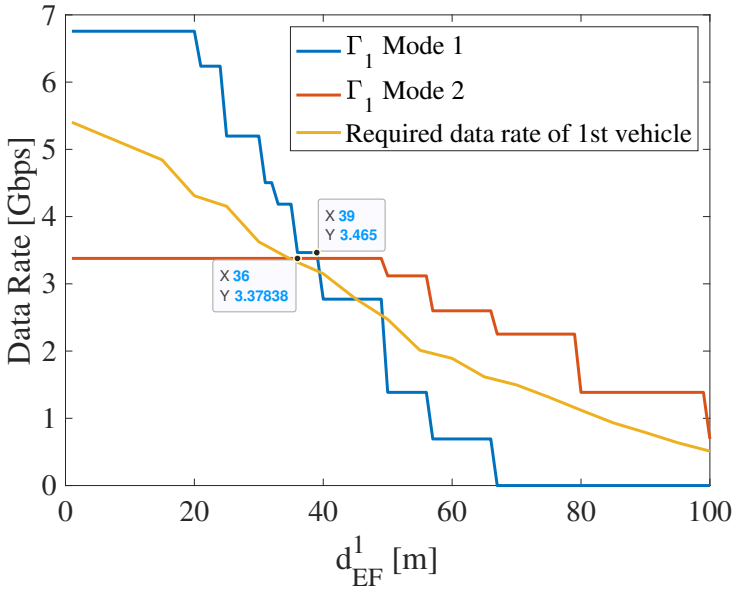

(a) 1st vehicle

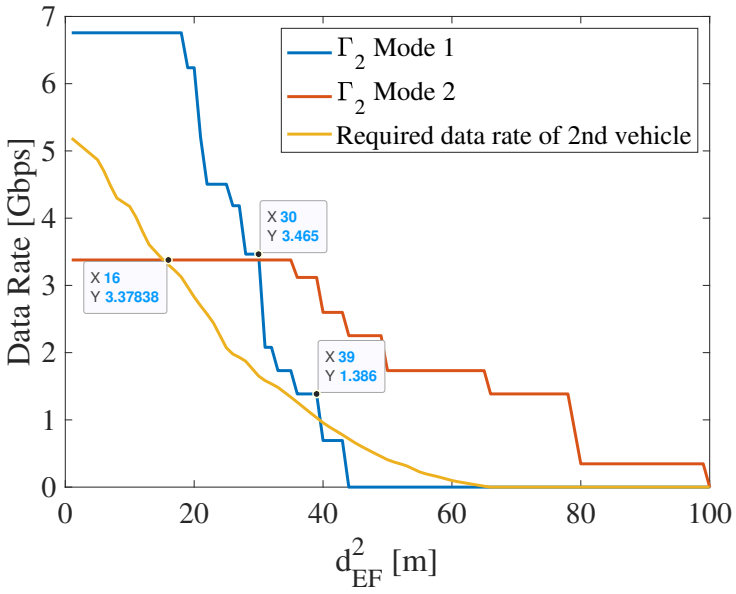

(b) 2nd vehicle

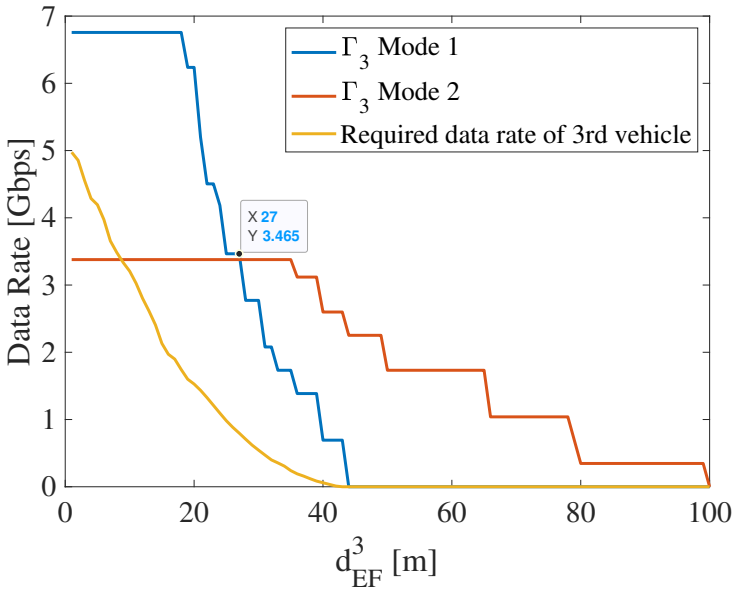

(c) 3rd vehicle

Figure 4.8: Comparison between achievable E2E throughput (Mode 1 and Mode 2) and required data rate ($G_{\mathrm{t}} = G_{\mathrm{r}} = 30$ dBi, $p_{\mathrm{Mode1}} = -11$ dBm, $p_{\mathrm{Mode2}} = 4$ dBm, $B = 2.16$ GHz, $d^n_{\mathrm{EF}} \in (0, 100]$)

of d_{switch} is $[36, 39]$ m. There should be a reserved margin between E2E throughput and the required data rate, especially for the 1st link. This margin is critical since the practical E2E throughput may not reach the theoretical value due to the hardware limitations and other impact factors such as congestion control and packet loss. To this end, p_{Mode1} and p_{Mode2} are set to be higher than the minimum required transmit power for algorithm robustness.

In Figs. 4.8 (b) and (c), the distance values corresponding to the intersections are 30 m and 27 m, which are smaller than that in Fig. 4.8 (a) (39 m). It is because that the 2nd link to the N-th link suffers from the co-channel interference caused by its previous links. This co-channel interference makes the Γ_2 Mode 1 and Γ_3 Mode 1 reduce rapidly than Γ_1 Mode 1. In Fig. 4.8 (b), since the required data rate of the 2nd vehicle decreases, the range of d_{switch} for the 2nd link is expanded as $[16, 39]$ m. As for the 3rd link, both Mode 1 and Mode 2 can support Γ_3 always to keep higher than the required data rate of the 3rd vehicle. There is no limitation on the value of d_{switch}. Although the range of d_{switch} becomes wider, the optimized d_{switch} had better be 30 m or 27 m to reserve the margin for possible E2E throughput degradation in the actual deployment. To ensure the scalability of this radio

resource management scheme, the value of d_{switch} should be independent of the V2V link index. Therefore, the optimized range of d_{switch} applicable for the 1st link can be determined as $[36, 39]$ m and the optimized d_{switch} for the 2nd link to the N-th link is about 30 m.

4.7.4 Results: Achievable E2E Throughput

Figure 4.9 presents the comparison between achievable E2E throughputs in the worst case under four situations and the required data rate. The four situations include: (1) w/o resource block allocation (RA), w/o ZigZag antenna configuration; (2) w/o RA, w/ ZigZag antenna configuration; (3) w/ RA, w/o ZigZag antenna configuration; (4) w/ RA, w/ ZigZag antenna configuration. The situation of w/o RA means that the V2V link keeps Mode 1. The w/o ZigZag antenna configuration situation means that antennas are located at the center of a vehicle's front and rear.

From Fig. 4.9 (a), when $d^1_{\text{EF}} \geq 36$ m, Γ_1 w/o RA is lower than the required data rate of 1st vehicle because of the strong path loss and multipath fading. Γ_1 w/ RA is always higher than the required data rate since Mode 1 is switched to Mode 2 when $d^1_{\text{EF}} \geq 36$ m. The higher transmit power in Mode 2 can compensate for the high path loss. In addition, ZigZag antenna configuration does not affect Γ_1 because 1st link does not suffer from the co-channel interference.

From Fig. 4.9 (b), when $d^2_{\text{EF}} \in [18, 65]$ m, Γ_2 w/o RA and w/o ZigZag is lower than the required data rate of the 2nd vehicle because 2nd link V2V suffers from the strong co-channel interference. To cope with this problem, when $d^2_{\text{EF}} \in [18, 30)$ m, due to the short inter-vehicle distance, the ZigZag antenna configuration is used to suppress the strong co-channel interference. When $d^2_{\text{EF}} \in [30, 65]$ m, the co-channel interference suppression by only using ZigZag antenna configuration becomes weak because of long inter-vehicle distance, so the resource block allocation is used to avoid the co-channel interference. Since RB_1 and RB_2 are allocated to the 1st and 2nd links respectively, the co-channel interference especially ground reflection can be eliminated. Therefore, Γ_2 w/ RA and ZigZag antenna configuration can always keep higher than the required data rate of the 2nd vehicle.

From Fig. 4.9 (c), the curves of Γ_3 with four situations are almost the same as those of Γ_2, which means that the first link before the current link causes serious co-channel interference, and the co-channel interference caused by other earlier links can be neglected. Here, increasing the index of the V2V link reduces the required data rate at the same d_{EF} because the required data rate is a function of d^n_{ED}. For the 3rd link, only when $d^3_{\text{EF}} \in [30, 42]$ m, Γ_3 w/o RA is

lower than the required data rate of the 3rd vehicle. In Fig. 4.9 (d), when the V2V link index is 4, Γ_4 is always higher than the required data rate of the 4th vehicle regardless of RA and ZigZag antenna configuration. Therefore, when $n > 4$, the achievable E2E throughput also surpasses the required data rate. It can be concluded that the proposed distributed radio

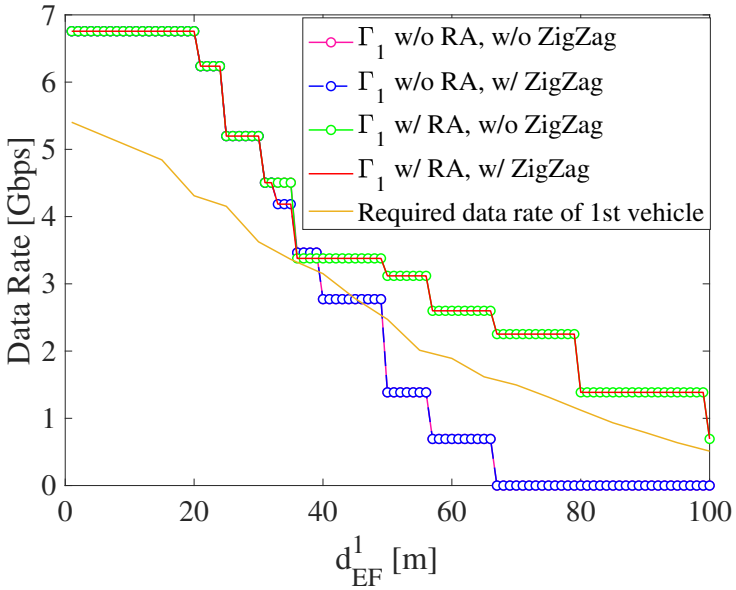

(a) 1st vehicle

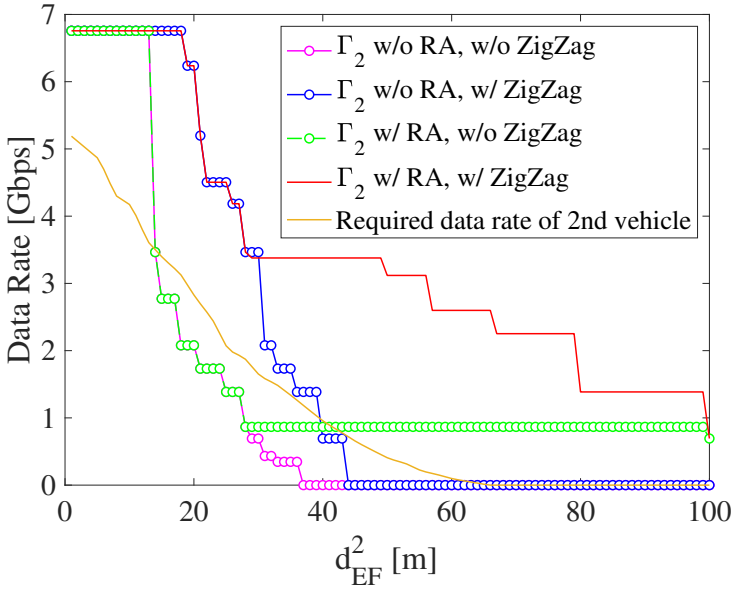

(b) 2nd vehicle

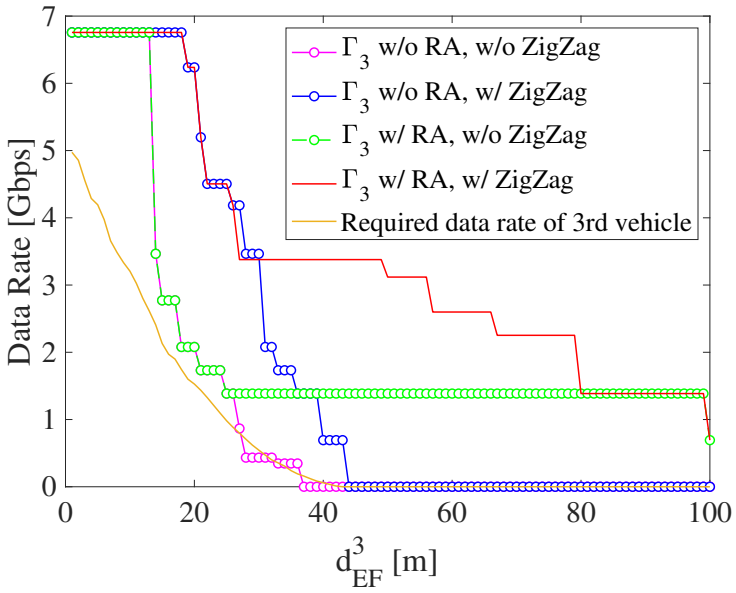

(c) 3rd vehicle

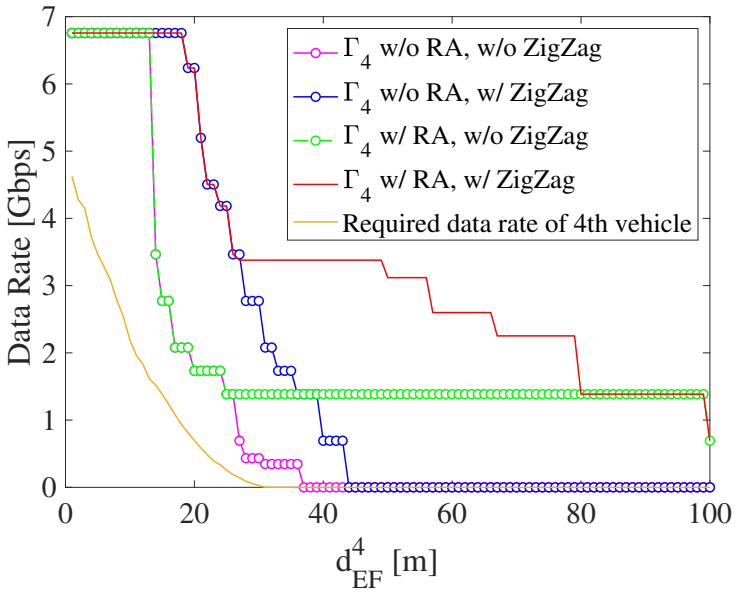

(d) 4th vehicle

Figure 4.9: Comparison between achievable E2E throughput and required data rate with equal inter-vehicle distance ($G_{\mathrm{t}} = G_{\mathrm{r}} = 30$ dBi, $p_{\mathrm{Mode1}} = -11$ dBm, $p_{\mathrm{Mode2}} = 4$ dBm, $d_{\mathrm{switch}} = 36$ m$(n = 1)$ or 30 m$(n > 1)$, $B = 2.16$ GHz, $d^n_{\mathrm{EF}} \in (0, 100]$)

resource management scheme is independent of the V2V link index, which implies that this scheme can support scalable mmWave V2V communications topology.

Figure 4.10 compares the achievable E2E throughput with the required data rate at arbitrary inter-vehicle distances. In the situation of arbitrary inter-vehicle distance, $\Gamma_n = \min\{\gamma_j\}$. In Fig. 4.10 (a), Γ_2 provided by the proposed scheme can ensure the required data rate irrespective of both d^2_{FD} and d^2_{EF} from 1m to 100 m. In Fig. 4.10 (b), Γ_3 can also keep higher than the required data rate of 3rd vehicle regardless of variation of d^3_{FD}. Therefore, the proposed distributed radio resource management scheme is independent with d^n_{FD}.

The above results verify the effectiveness of the proposed scheme that can achieve sufficient E2E throughput performance to ensure safe automated driving.

4.8 Conclusion

In this chapter, the theoretical analysis of the required data rate for safe automated driving was given in an overtaking scenario with multiple Ego vehicles. The simulation results revealed that the increase of Ego vehicles alleviates their required data rate. With these preparations, a novel distributed and scalable radio resource management scheme was proposed for mmWave V2V relay communications. It optimizes the allocation of resource blocks in spatial, frequency, and power domains. The simulation results demonstrated that our proposal ensures the achievable E2E throughput is always higher than the required data rate for each vehicle. It also verifies the scalability of the proposed scheme for dynamics of mmWave V2V communications topology. It can be a fundamental strategy for the realization of the coming automated driving era.

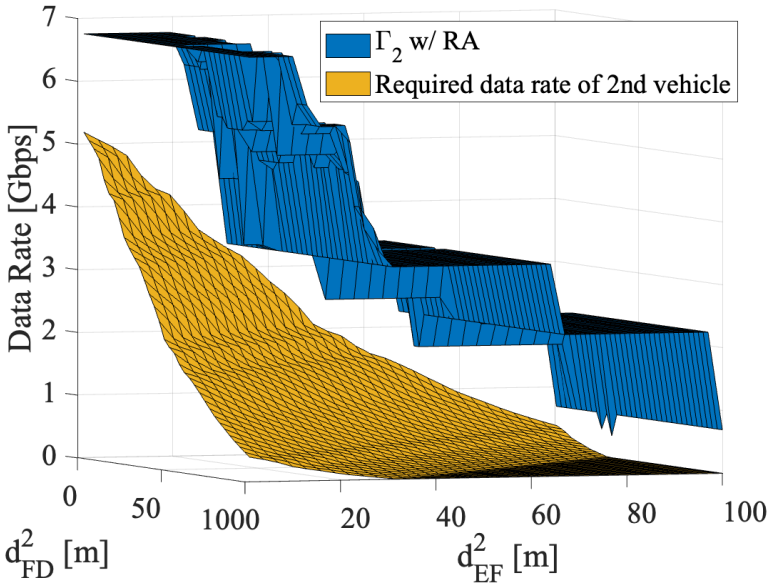

(a) 2nd vehicle

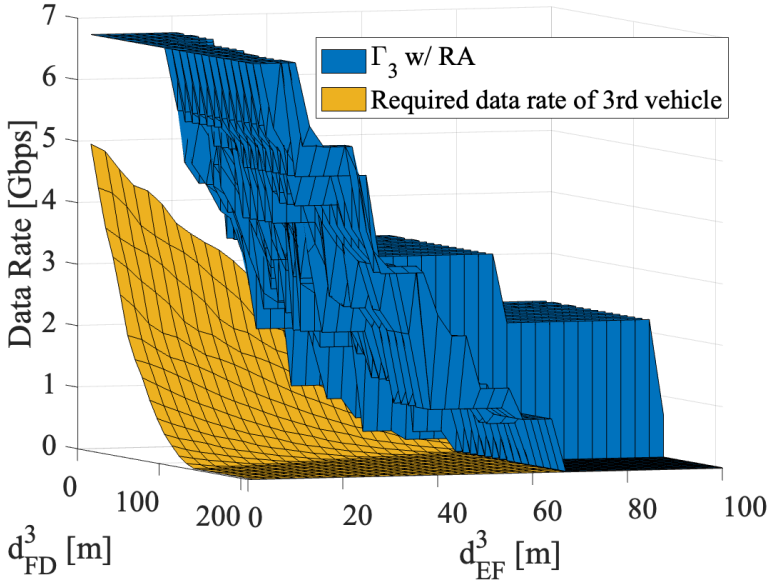

(b) 3rd vehicle

Figure 4.10: Comparison between achievable E2E throughput and required data rate with arbitrary inter-vehicle distance ($G_{\mathrm{t}} = G_{\mathrm{r}} = 30$ dBi, $p_{\mathrm{Mode1}} = -11$ dBm, $p_{\mathrm{Mode2}} = 4$ dBm, $d_{\mathrm{switch}} = 36$ m$(n = 1)$ or 30 m$(n > 1)$, $B = 2.16$ GHz, $d^n_{\mathrm{EF}} \in (0, 100]$)

Chapter5

Conclusion

The high data rate capability of mmWave can enable a whole new range of V2X applications such as specified four advanced V2X use cases. Wireless communication in the mmWave band experiences a higher signal attenuation and blockage than conventional frequency bands such as 760 MHz and 5.9 GHz. Although high gain directional antennas are used to compensate for such large path loss and multi-hop relays is deployed to cope with the problem of blockage, these kinds of solutions also introduce numerous other challenges such as beam alignment, co-channel interference control, antenna placement and scalability. In this dissertation, focusing on mmWave V2V relays communications system, we addressed the challenges of co-channel interference control and scalability by radio resource management in spatial, frequency, and power domain. Most importantly, this proposed radio resource management scheme can be executed at each node in mmWave V2V topology. This kind of distributed resource control mechanism can fast adapt to the rapid variation of dynamic V2V topology and work even out of coverage. Eventually, this distributed radio resource management approach is supposed to improve the performance of mmWave V2V relay communications and ensure a high level of safe automated driving. A summary of the main contributions presented in this dissertation is now follows.

5.1 Summary of the Thesis

- Chapter 2: We introduced basic and general mmWave V2V relays scenarios on the basis of scenario complexity and introduced single straight road, horizontal curve, and slope on the basis of road scenarios. We established ray-tracing channel models of mmWave

V2V communications in three typical road scenarios and summarized the characteristics of these typical road scenarios. The co-channel interference was evaluated in different scenarios. The simulation results show that (1) the ground reflection is the main co-channel interference in all road scenarios; (2) the co-channel interference is strangest in the case of equal inter-vehicle distance for mmWave V2V communications with relay; (3) the maximum height at which the direct co-channel interference signal (more precisely, first-order Fresnel zone) is completely blocked by the metal body of the vehicle is optimal antenna height because it has the strongest suppression of co-channel interference.

- Chapter 3: We proposed a ZigZag antenna configuration to mitigate the co-channel interference for mmWave V2V communications with relay. The intrinsic principle is to increase the angle between each reflected co-channel interference path and the antenna main beam. This increased angle can reduce the antenna directivity of each reflected interference path. Eventually, the total received power of co-channel interference can be reduced. Next, the performance of the proposed method with that of conventional antenna configuration was compared by the simulation based on standard IEEE 802.11ad. Numerical evaluations using realistic channels from ray-tracing simulations show that the ZigZag antenna configuration significantly suppresses the co-channel interference and satisfies the over 1 Gbps required data rate. Finally, we demonstrated the effectiveness of ZigZag antenna configuration by outdoor experiments. The measured E2E throughput with ZigZag antenna configuration is about 1.3 Gbps when the inter-vehicle distance varies from 1 m to 30 m.

- Chapter 4: We theoretically analyzed the required data rate for safe automated driving in an overtaking scenario with multiple Ego vehicles. The simulation results revealed that the increase of Ego vehicles alleviates their required data rate. With these preparations, we developed a distributed radio resource management scheme that integrates spatial, frequency, and power domains for two transmission ranges (short/long). In the spatial domain, ZigZag antenna configuration is utilized to mitigate the co-channel interference, which plays a decisive role in the short inter-vehicle distance. In frequency and power domains, two resource blocks are allocated alternately, and transmit power is controlled to suppress the co-channel interference, which has a decisive impact on co-channel interference mitigation in the long inter-vehicle distance. The simulation results demonstrated that our proposal ensures the achievable E2E throughput is always

higher than the required data rate for each vehicle. It also verified the scalability of the proposed scheme for dynamics of mmWave V2V communications topology.

5.2 Suggestion for Future Works

This section outlines several research directions related to the work presented in this dissertation.

5.2.1 Experimental Verification of Distributed Radio Resource Management Scheme

In Chapter 4, we theoretically investigated the impact of the proposed radio resource management scheme. While the results make theoretical sense, verification in real measurements is lacking in the literature. The main difficulty in verifying the effectiveness of this approach is the need for commercial mmWave band devices to support narrow beam high-precision beamforming. Some mmWave antenna devices can support the narrow beam width. For example, the beamwidth of 60 GHz reflectarray antennas in Fig. 3.8 is 6 and 10 degrees in vertical and horizontal planes respectively. Based on the narrow beamwidth of these devices, simulation results show that the resource management method we proposed can effectively suppress the impact of interference, meet the achievable data rate greater than the required data rate, and support the multi-hop relay. However, these devices have many limitations. First, because the MCS index only supports 1-9, the maximum measured throughput is about 1.3 Gbps. It means that these mmWave antenna devices based on the 802.11ad standard cannot achieve the highest supported data rate (6.75 Gbps). But the required data rate is more significant than 1.3 Gbps, especially at high vehicle speeds. Therefore, these mmWave antenna devices cannot be used to compare the relationship between the achievable E2E throughput and the required data rate. In addition, most mmWave antenna devices do not support beam scanning. Although we can achieve beam alignment by mechanical rotation, when the inter-vehicle distance is long, the error of the beam alignment achieved by an automatic process is substantial, which leads to a very unstable V2V link connection. Besides, transmit power control also cannot be supported by the current mmWave devices.

5.2.2 Learning for mmWave V2V Topology in Multiple Same-direction Lanes Scenarios

In this dissertation, we focus on the single lane scenario and show that the proposed radio resource management involving ZigZag antenna configuration, resource block allocation and transmit power control is helpful in reducing the co-channel interference. We expect this approach to be beneficial for multi-lanes scenarios as well, but there will be different challenges. There are three research questions here. Firstly, co-channel interference is more complicated in multiple lane scenarios than that in single lane scenarios. How to control the radio resource in spatial (e.g. antenna configuration), frequency, and power domains to mitigate such complicated co-channel interference is one of the critical issues. Secondly, finding the optimal V2V relay route, which ensures that adequate information is transmitted to achieve cooperative perception to ensure safe automatic driving, and suppresses interference to ensure the quality of the mmWave V2V links, is another challenge. Thirdly, when there are vehicles driving on multiple lanes, appropriate scheduling and association are also important because relay choices for one of the vehicles may have two or more.

5.2.3 Extension Radio Resource Management to other Traffic Scenarios

This dissertation focuses on the overtaking traffic scenarios. Some ideas are also applicable for other traffic scenarios such as crossroads. In different traffic scenarios, the required data rate is also different and needs to be re-analyzed. According to the required data rate and interference analysis under different traffic scenarios, the same idea can be used to satisfy the requirements of V2V communications even V2I communications to achieve cooperative perception.

AppendixA

List of Publications

A.1 Journal Papers

- Y. Yin, H. Chen, Z. Li, T. Yu and K. Sakaguchi. "ZigZag Antenna Configuration for MmWave V2V with Relay in Typical Road Scenarios: Design, Analysis and Experiment." *IEICE Transactions on Communications*, 2021, Volume E104.B, Issue 10, Pages 1307-1317.

- Y. Yin, T. Yu, K. Maruta, K. Sakaguchi. "Distributed and Scalable Radio Resource Management for mmWave V2V Relays towards Safe Automated Driving," *Sensors* 22.1 (2022): 93.

A.2 International Conferences

- Y. Yin, H. Chen, Z. Li, R. Fukatsu, T. Yu and K. Sakaguchi, "Design of Antenna Configuration for Interference Control in MmWave V2V Communication Systems," *2020 IEEE 92nd Vehicular Technology Conference (VTC2020-Fall)*, 2020, pp. 1-5, doi: 10.1109/VTC2020-Fall49728.2020.9348872.

- Y. Yin, T. Yu and K. Sakaguchi, "Required-Data-Rate-Based Distributed Resource Allocation Scheme for MmWave V2V with Relay," *IEEE CCNC*, Jan, 2022.

A.3 Domestic Conferences

- Y. Yin, T. Yu, K. Sakaguchi, "ZigZag Antenna Configuration for Interference Control in Millimeter-wave V2V Communication Systems," *IEICE Mobile Communication Research Workshop*, Mar. 2020.
- Y. Yin, T. Yu, K. Maruta, K. Sakaguchi, "Distributed and Scalable Radio Resource Management for mmWave V2V Relays towards Safe Automated Driving," *IEICE Mobile Communication Research Workshop*, Mar. 2022.

AppendixB

Abbreviations

mmWave millimater-wave

V2V vehicle-to-vehicle

SINR signal-to-interference-plus-noise

WISE-SSS Tokyo Tech Academy for Super Smart Society

ITS Intelligent Transport System

V2X vehicle-to-everything

V2I vehicle-to-infrastructure

V2N vehicle-to-network

V2P vehicle-to-pedestrian

3GPP 3rd Generation Partnership Project

ETSI European Telecommunications Standards Institute

CAM cooperative awareness message

DENM decentralized environmental notification message

SAE Society of Automotive Engineers

BSM basic safety message

CPM collective perception message

QoS Quality of Service

IEEE Institute of Electrical and Electronics Engineers

DSRC Dedicated Short Range Communications

LTE Long Term Evolution

C-V2X Cellular V2X

LOS line-of-sight

CSMA/CA carrier sense multiple access with collision avoidance

E2E end-to-end

RB resource block

LiDAR light detection and ranging

AASHTO American Association of State Highway and Transportation Officials

TCP Transmission Control Protocol

PHY Physical

NGV next generation V2X

OCB Outside of the Context of BSS

BSS Base Station Subsystem

EVM Error Vector Magnitude

MCS Modulation and Coding Scheme

SC Single Carrier

OFDM Orthogonal Frequency Division Multiplexing

LDPC Low Density Parity Check

GPS Global Positioning System

NR New Radio

FOV field-of-view

AWAG additive white Gaussian noise

AppendixC

Mathematical Notation

- d : Distance between transmitter and receiver
- P_L : Free-space path loss
- P_{t} : Transmit power
- P_{r} : Received power
- G_{t} : Antenna gains in LOS direction at transmitter side
- G_{r} : Antenna gains in LOS direction at receiver side
- λ : Wave length
- f : Carrier frequency
- c : Light speed
- r_1 : Radius of the first Fresnel zone
- d_1 : Current position to the transmitter in first Fresnel zone
- d_2 : Current position to the receiver in first Fresnel zone
- $r_{1\mathrm{max}}$: Maximum radius of the first Fresnel zone
- R_{min} : Minimum horizontal curve radius
- v_{limit} : Road speed limit

- g : Gravitational acceleration
- e : Superelevation in horizontal curve scenario
- f_s : Side-friction factor
- d_{EF}^1 : Straight line distance between the first Ego vehicle and its front vehicle
- d_{EF}^2 : Straight line distance between the second Ego vehicle and its front vehicle
- d_l : Distance to the surrounding obstacles
- α : Maximum grades of slope road scenario
- h : Antenna height
- $s(t)$: Received desired signal
- $P_{\mathrm{Tx1}}/P_{\mathrm{Tx2}}$: Transmit power of Tx1 and Tx2 respectively
- $d_{\mathrm{path}k}$: Length of path k
- k : Index of path
- $L(*)$: Absorption loss
- τ : Time delay of ground reflection relative to the LOS path
- $\Psi_{\mathrm{g}}/\Psi_{\mathrm{s}}$: Reflection coefficient of ground and surrounding obstacles respectively
- $\Psi_{\mathrm{V}}/\Psi_{\mathrm{H}}$: Reflection coefficient of vertical and horizontal polarization respectively
- $a_{\mathrm{V}}/a_{\mathrm{H}}$: Coefficients of horizontal and vertical components generated through wave decomposition
- D_k : Coefficients of antenna directivity
- P_{r} : Received power of the desired signal
- Φ : Phase rotation angle of ground reflection
- ψ : Dielectric constant of materials

- θ_{in} : Incident angle of the reflected path
- $\theta_{\text{3dB}}/\phi_{\text{3dB}}$: Half power beam angle in elevation and azimuth direction respectively
- θ_0/ϕ_0 : Elevation and azimuth angle of main beam
- $\theta_{\text{e}}/\phi_{\text{a}}$: Elevation and azimuth angle of propagation path
- I : Power of co-channel interference
- P_{r}^n : Received power of n-th V2V link
- n : Index of vehicle/V2V link
- I_n : Received power of co-channel interference of n-th V2V link
- d_{d} : Distance of direct interference link to the horizontal center-line of the first Ego vehicle (Fig. 2.4)
- ϕ_{d} : Angle between the direct interference link and desired signal (blue line) at transmitter and receiver sides (Fig. 2.4)
- $\phi_{\text{threshold}}$: Angle between the yellow line and desired signal (blue line) at the transmitter and receiver sides (Fig. 2.4)
- $d_{\text{all1}}/d_{\text{all2}}/d_{\text{all3}}$: Horizontal distance between Tx1 on the Detecting vehicle and Rx2 on the second Ego vehicle in the single straight road, horizontal curve and slope road scenarios respectively
- l_{vehicle} : Length of vehicle
- w_{vehicle} : Width of vehicle
- h_{vehicle} : Height of vehicle
- w_{lane} : Width of lane
- h_{mb} : Height of metal body of vehicle
- NF : Noise factor
- N_0 : Noise power density

- v_e : Speed of Ego vehicle
- d_{tr} : Distance between the transmitter and receiver along the y-axis (Fig. 3.1)
- d_{EO}^n : Required minimum detection distance for n-th Ego vehicle
- v_e^n : Speed of n-th Ego vehicle speed
- v_o : Speed of Oncoming vehicle
- d_{ED}^n : n-th Ego vehicle-Detecting vehicle distance
- i : Index of laser beam of LiDAR
- r_i : Distance between origin and laser point on the obstacles (Fig. 4.2)
- θ_i : Angle between the laser beam and the negative z-axis (Fig. 4.2)
- ϕ_i : Angle between the laser beam and the positive x-axis (Fig. 4.2)
- N_{detected} : Number of detected points by the LiDAR
- N_{vehicle} : Total number of points of vehicle model
- S_n : Ratio of N_{detected} and N_{vehicle}
- res_θ/res_ϕ : Angular resolution in vertical and horizontal planes respectively
- f_{scan} : Scan frequency of LiDAR
- B_{laser} : Number of bits per laser
- Θ/Φ : Angular scan range in horizontal and vertical planes respectively
- Γ_n : E2E throughput between the n-th vehicle and the Detecting vehicle
- γ_j : Throughput of the j-th V2V link
- R_{req}^n : Required data rate of the n-th Ego vehicle
- d_{switch} : Threshold of switching between Mode 1 and Mode 2
- $p_{\text{Mode1}}/p_{\text{Mode2}}$: Transmit powers in Mode 1 and Mode 2

- $\mathbf{\Omega}$: A finite set including combinations of parameters
- $\mathbf{\Omega}^*$: Optimized parameter values vector
- $G_{\max}/p_{\max}$: Constraints of antenna gain and transmit power
- P_n : Transmit power of the n-th V2V link
- $\theta^{\circ}_{\mathrm{HP}}/\phi^{\circ}_{\mathrm{HP}}$: Beamwidth of antennas in the vertical and horizontal planes respectively
- β_{nm} : SINR of m-th RB for n-th link
- m : Index of RB
- $\mathbf{P}^n_{\mathbf{r}}$: Received power of n-th link
- p^{nm}_{r} : Received power of m-th RB for n-th link
- $\mathbf{X}^n_{\mathbf{p}}$: Resource block allocation matrix
- $\mathbf{I}^n_{\mathbf{p}}$: Co-channel interference matrix of n-th link
- I^n : Interference of n-th link from each of previous V2V link when each RB is assumed to be reused by this previous V2V link and n-th link
- $\mathbf{I}_n$: All co-channel interference of n-th link from 1st link to $(n-1)$-th link
- p_{noise} : Power of additive white Gaussian noise (AWGN)
- n_{RB} : Number of RBs
- $\mathbf{Y}_n$: Supported throughput of each RB for n-th link

Reference

[1] 3GPP. Study on enhancement of 3GPP support for 5G V2X services. Technical Specification (TS) 22.886, 3rd Generation Partnership Project (3GPP), Dec 2018. Version 16.2.0.

[2] 3GPP. Study on LTE support for Vehicle to Everthing (V2X) services. Technical Specification (TS) 22.885, 3rd Generation Partnership Project (3GPP), Dec 2015. Version 14.0.0.

[3] Kei Sakaguchi, Ryuichi Fukatsu, Tao Yu, Eisuke Fukuda, Kim Mahler, Robert Heath, Takeo Fujii, Kazuaki Takahashi, Alexey Khoryaev, Satoshi Nagata, and Takayuki Shimizu. Towards mmwave V2X in 5G and beyond to support automated driving. *IEICE Transactions on Communications*, E104.B(6):587–603, 2021.

[4] ETSI EN 302 637-2 (V1.3.1). Intelligent Transport System (ITS); Vehicular Communications; Basic Set of Applications; Part 2: Specification of Cooperative Awareness Basic Service. Technical Report (TR), ETSI, Sep 2014.

[5] ETSI EN 302 637-3 (V1.2.1). Intelligent Transport System (ITS); Vehicular Communications; Basic Set of Applications; Part 3: Specifications of Decentralized Environmental Notification Basic Service. Technical Report (TR), ETSI, Sep 2014.

[6] ETSI TR 103 562 (V2.1.1). Intelligent Transport System (ITS); Vehicular Communications; Basic Set of Applications; Analysis of the Collective Perception Service (CPS); Release 2. Technical Report (TR), ETSI, Dec 2019.

[7] IEEE Standard for Information technology– Local and metropolitan area networks– Specific requirements– Part 11: Wireless LAN Medium Access Control (MAC) and Physical Layer (PHY) Specifications Amendment 6: Wireless Access in Vehicular Environments. pages 1–51, 2010.

[8] 3GPP. Technical Specification Group Radio Access Network; Study on LTE-based V2X Services; (Release 14). Technical Report (TR) 36.885, 3rd Generation Partnership Project (3GPP), Jun 2016. Version 14.0.0.

[9] 3GPP. Technical Specification Group Radio Access Network; Study on evaluation methodology of new Vehicle-to-Everything (V2X) use cases for LTE and NR; (Release 15). Technical Report (TR) 37.885, 3rd Generation Partnership Project (3GPP), Jun 2019. Version 15.3.0.

[10] John B Kenney. Dedicated short-range communications (dsrc) standards in the united states. *Proceedings of the IEEE*, 99(7):1162–1182, 2011.

[11] ETSI ES 202 663 (V1.1.0). Intelligent Transport System (ITS); European profile standard for the physical and medium access control layer of Intelligent Transport Systems operating in the 5 GHz frequency band. Technical Report (TR), ETSI, Jan 2010.

[12] 3GPP. Technical Specification Group Radio Access Network; NR; Study on NR Vehicle-to-Everything (V2X) (Release 16). Technical Report (TR) 38.885, 3rd Generation Partnership Project (3GPP), Mar 2019. Version 16.0.0.

[13] Tsutomu Tsuboi. Study for Traffic Management by WAVE Technology. Technical Report (TR), Feb 2017.

[14] IEEE 802.11ad-2012. IEEE Standard for Information technology-Telecommunications and information exchange between systems-Local and metropolitan area networks-Specific requirements - Part 11: Wireless LAN Medium Access Control (MAC) and Physical Layer (PHY) Specifications Amendment 3: Enhancements for Very High Throughput in the 60GHz Band. Technical report, Dec 2012.

[15] 3GPP TR38.886. V2X Services based on NR. Technical Report (TR) 38.886, 3rd Generation Partnership Project (3GPP), Oct 2019.

[16] M. Marcus and B. Pattan. Millimeter wave propagation: spectrum management implications. *IEEE Microwave Magazine*, 6(2):54–62, 2005.

[17] Theodore S Rappaport, George R MacCartney, Shu Sun, Hangsong Yan, and Sijia Deng. Small-scale, local area, and transitional millimeter wave propagation for 5g communications. *IEEE Transactions on Antennas and Propagation*, 65(12):6474–6490, 2017.

[18] Hang Zhao, Rimma Mayzus, Shu Sun, Mathew Samimi, Jocelyn K. Schulz, Yaniv Azar, Kevin Wang, George N. Wong, Felix Gutierrez, and Theodore S. Rappaport. 28 ghz millimeter wave cellular communication measurements for reflection and penetration loss in and around buildings in new york city. In *2013 IEEE International Conference on Communications (ICC)*, pages 5163–5167, 2013.

[19] George R. MacCartney, Sijia Deng, Shu Sun, and Theodore S. Rappaport. Millimeter-wave human blockage at 73 ghz with a simple double knife-edge diffraction model and extension for directional antennas. In *2016 IEEE 84th Vehicular Technology Conference (VTC-Fall)*, pages 1–6, 2016.

[20] Christoph F. Mecklenbrauker, Andreas F. Molisch, Johan Karedal, Fredrik Tufvesson, Alexander Paier, Laura Bernado, Thomas Zemen, Oliver Klemp, and Nicolai Czink. Vehicular channel characterization and its implications for wireless system design and performance. *Proceedings of the IEEE*, 99(7):1189–1212, 2011.

[21] Wooseong Kim. Experimental demonstration of mmwave vehicle-to-vehicle communications using ieee 802.11ad. *Sensors*, 19(9), 2019.

[22] Yijia Feng, Dazhi He, Yunfeng Guan, Yihang Huang, Yin Xu, and Zhiyong Chen. Beamwidth optimization for millimeter-wave v2v communication between neighbor vehicles in highway scenarios. *IEEE Access*, 9:4335–4350, 2021.

[23] Jaejoon Park, Juyul Lee, KyungWon Kim, Kwang-Chun Lee, and Myung-Don Kim. Vehicle antenna position dependent path loss for millimeter-wave v2v communication. *2018 11th Global Symposium on Millimeter Waves (GSMM)*, pages 1–3, 2018.

[24] Vitaly Petrov, Joonas Kokkoniemi, Dmitri Moltchanov, Janne Lehtomäki, Markku Juntti, and Yevgeni Koucheryavy. The impact of interference from the side lanes on mmwave/thz band v2v communication systems with directional antennas. *IEEE Transactions on Vehicular Technology*, 67(6):5028–5041, 2018.

[25] Cristina Perfecto, Javier Del Ser, and Mehdi Bennis. Millimeter-wave v2v communications: Distributed association and beam alignment. *IEEE Journal on Selected Areas in Communications*, 35(9):2148–2162, 2017.

[26] Cristina Perfecto, Javier Del Ser, Mehdi Bennis, and Miren Nekane Bilbao. Beyond wysiwyg: Sharing contextual sensing data through mmwave v2v communications. In *2017 European Conference on Networks and Communications (EuCNC)*, pages 1–6. IEEE, 2017.

[27] Yijia Feng, Dazhi He, Yunfeng Guan, Yihang Huang, Yin Xu, and Zhiyong Chen. Beamwidth optimization for millimeter-wave v2v communication between neighbor vehicles in highway scenarios. *IEEE Access*, 9:4335–4350, 2020.

[28] Mumin Ozpolat, Osama Alluhaibi, Erik Kampert, and Mattew D Higgins. Connectivity analysis for mmwave v2v networks: Exploring critical distance and beam misalignment. In *2019 IEEE Global Communications Conference (GLOBECOM)*, pages 1–6. IEEE, 2019.

[29] Mattia Brambilla, Monica Nicoli, Sergio Savaresi, and Umberto Spagnolini. Inertial sensor aided mmwave beam tracking to support cooperative autonomous driving. In *2019 IEEE International Conference on Communications Workshops (ICC Workshops)*, pages 1–6. IEEE, 2019.

[30] Xiaosha Chen, Supeng Leng, Zuoyin Tang, Kai Xiong, and Guanhua Qiao. A millimeter wave-based sensor data broadcasting scheme for vehicular communications. *IEEE Access*, 7:149387–149397, 2019.

[31] Mustafa S Aljumaily and Husheng Li. Opportunistic routing protocol for ad-hoc networks using mmwave and random beamforming. In *2019 IEEE 90th Vehicular Technology Conference (VTC2019-Fall)*, pages 1–6. IEEE, 2019.

[32] Jie Mei, Kan Zheng, Long Zhao, Yong Teng, and Xianbin Wang. A latency and reliability guaranteed resource allocation scheme for LTE V2V communication systems. *IEEE Transactions on Wireless Communications*, 17(6):3850–3860, 2018.

[33] Muhammad Ikram Ashraf, Chen-Feng Liu, Mehdi Bennis, and Walid Saad. Towards low-latency and ultra-reliable vehicle-to-vehicle communication. In *2017 European Conference on Networks and Communications (EuCNC)*, pages 1–5. IEEE, 2017.

[34] Lei Gao, Yanzhao Hou, Xiaofeng Tao, and Min Zhu. Energy-efficient power control and resource allocation for V2V communication. In *2020 IEEE Wireless Communications and Networking Conference (WCNC)*, pages 1–6. IEEE, 2020.

[35] J. B. Kenney. Dedicated short-range communications (dsrc) standards in the united states. *Proceedings of the IEEE*, 99(7):1162–1182, 2011.

[36] Elisabeth Uhlemann. Connected-vehicles applications are emerging [connected vehicles]. *IEEE Vehicular Technology Magazine*, 11:25–96, 03 2016.

[37] Akihito Kato, Katsuyoshi Sato, Masayuki Fujise, and Shigeru Kawakami. Propagation characteristics of 60-ghz millimeter waves for its inter-vehicle communications. *IEICE transactions on communications*, 84(9):2530–2539, 2001.

[38] Ryuichi Fukatsu and Kei Sakaguchi. Millimeter-wave v2v communications with cooperative perception for automated driving. In *2019 IEEE 89th Vehicular Technology Conference (VTC2019-Spring)*, pages 1–5. IEEE, 2019.

[39] Wada Tomotake, Maeda Makoto, Okata Minoru, Tsukamoto Katsutoshi, and Komaki Shozo. Theoretical analysis of propagation and network characteristics in millimeter waves inter-vehicle communication system. In *1998 IEEE Global Communications Conference (GLOBECOM)*, pages 910–915 vol.2. IEEE, 1998.

[40] Douglas W Harwood and John M Mason Jr. Horizontal curve design for passenger cars and trucks. *Transportation Research Record*, (1445), 1994.

[41] Transportation Officials. *A Policy on Geometric Design of Highways and Streets, 2011*. AASHTO, 2011.

[42] Andrea Goldsmith. *Wireless communications*. Cambridge university press, 2005.

[43] Gustavo A Siles, Jose Manuel Riera, and Padro Garcia-del Pino. Atmospheric attenuation in wireless communication systems at millimeter and thz frequencies [wireless corner]. *IEEE Antennas and Propagation Magazine*, 57(1):48–61, 2015.

[44] Makoto Nakamura, Hiroaki Nishiuchi, Konstantin Koslowski, Julian Daube, Ricardo Santos, Gia Khanh Tran, and Kei Sakaguchi. Performance evaluation of prefetching algorithm for real-time edge content delivery in 5g system. In *2019 IEEE 90th Vehicular Technology Conference (VTC2019-Fall)*, pages 1–5, 2019.

[45] ETSI TR 102 698 (V1.1.1). Intelligent Transport System (ITS); Vehicular Communications; C2C-CC Demonstrator 2008; Use cases and Technical Specifications. Technical Report (TR), ETSI, Jul 2009.

[46] Robert Schneider, Dirk Didascalou, and Werner Wiesbeck. Impact of road surfaces on millimeter-wave propagation. *IEEE Transactions on Vehicular Technology*, 49(4):1314–1320, 2000.

[47] Toyota. *Toyota 2020 Yaris specs*.

[48] Mathijs Mortimer. iperf3 documentation, 2018.

[49] Ryuichi Fukatsu and Kei Sakaguchi. Automated driving with cooperative perception using millimeter-wave V2V communications for safe overtaking. *Sensors*, 21(8), 2021.

[50] 3GPP. Service requirements for enhanced V2X scenarios. Technical Specification (TS) 22.186, 3rd Generation Partnership Project (3GPP), Jun 2019. Version 16.2.0.

[51] IEEE. P802.11-task group bd (ngv) meeting update. `https://www.ieee802.org/11/Reports/tgbd_update.htm`.

[52] Yang Yang, Zhen Gao, Yao Ma, Biao Cao, and Dazhong He. Machine learning enabling analog beam selection for concurrent transmissions in millimeter-wave V2V communications. *IEEE Transactions on Vehicular Technology*, 69(8):9185–9189, 2020.

[53] Yekaterina Sadovaya, Dmitrii Solomitckii, Wei Mao, Oner Orhan, Hosein Nikopour, Shilpa Talwar, Sergey Andreev, and Yevgeni Koucheryavy. Ray-based modeling of directional millimeter-wave V2V transmissions in highway scenarios. *IEEE Access*, 8:54482–54493, 2020.

[54] Yue Yin, Haoze Chen, Zongdian Li, Tao Yu, and Kei Sakaguchi. Zigzag antenna configuration for mmwave v2v with relay in typical road scenarios: Design, analysis and experiment. *IEICE Transactions on Communications*, advpub, 2021.

[55] Velodyne. *Velodyne VLP-16 specs*.

[56] Takahashi Kazuaki, Motozuka Hiroyuki, and Sakamomto Takenori. 60 GHz band Japanese Regulatory. Technical specification (TS), Panasonic Corp., May 2015.

[57] Sophocles J. Orfanidis. *Electromagnetic Waves and Antennas: Radiation from Apertures*, pages 800–843. ECE Department, Rutgers University, 94 Brett Road, Piscataway, NJ 08854-8058, 2016.